The dynamic modelling and simulation of a domestic air source heat pump system with integrated thermal energy storage and automatic mode switching functionality

Adam Thorburn
MEng

Submitted in fulfilment of the requirements for the
Degree of Master of Science (Research)

James Watt School of Engineering
College of Science and Engineering
University of Glasgow

March 2026

Abstract

Heat pump technologies are currently seen as crucial to the decarbonisation of the heating sector and the eventual phasing-out of fossil fuel-based heating systems. However, heat production using heat pumps only accounts for 10% of the total global heating demand in buildings, which is mainly due to their high upfront costs and poor performance in cold climates. The flexible heat pump concept is one such technology currently in development in collaboration between researchers at the University of Glasgow and the University of Liverpool which aims to improve the energy efficiency and performance of existing air source heat pump systems. This novel system incorporates a thermal energy storage tank into a standard Evans-Perkins vapour compression heat pump cycle in order to recover and store excess heat for later use during periods where standard operational modes would be unviable. The modelling and simulation of heat pump systems is often assessed while assuming constant steady-state conditions at the cost of constructing less accurate models, whereas dynamic modelling strategies allow for greater accuracy and complexity with regards to their real-life counterparts. In order to evaluate the realistic behaviours of a transient heat pump system, the flexible heat pump system with automatic mode switching functionality was constructed and simulated within a dynamic simulation environment based on the Modelica programming language. These models were primarily built using the Dymola software package and the TIL Suite component library, and were simulated for forty-nine iterations of the flexible heat pump system. Dynamic simulations of the modelled system demonstrated a potential coefficient of performance improvement of 25.2% in comparison to a standard, non-flexible heat pump system of equivalent size and scale. Furthermore, the performance of the modelled system was improved when the refrigerant choice, local climate, storage tank size and mode switching control scheme temperature setpoints were selected to fully leverage the flexible aspects of the system and to promote peak load shaving strategies.

Table of Contents

List of Tables

List of Figures

Acknowledgements

I would first like to thank my supervisors Prof Zhibin Yu, Dr Yiji Lu and Dr Yihuai Zhang for their collective knowledge, guidance and support throughout my PGR studies. It has been an incredible journey these past few years and I am proud to finally be presenting this work and demonstrating my skills as an engineer. Thank you for everything that you have done for me.

I would also like to thank Dr Zahra Hajabdollahi Ouderji for their technical knowledge and advice regarding the modelling of the flexible heat pump system and for their assistance when acquiring technical and component data for use in my models. This project would not have been possible without your help, and for that I am very grateful.

Thank you to the people at Claytex Services Ltd, especially to Alessandro Picarelli and Claire McGregor, for their assistance with acquiring and learning how to use Dymola and TIL Suite, which became the backbone of my project and my studies. I would never have been able to complete this project without your software and tutorage.

Thank you to the support staff at the University of Glasgow, especially to Prof Marc Sorel, Julia Deans, Kevin Crawford and Fiona Grey; for their help and support throughout my PGR studies. You have been a guiding light through some very tough times.

Thank you to the research development staff at the University of Glasgow, especially to Elaine Gourlay and Matthew Swayne, for their support and mentorship through the thesis mentoring programme. I am happy that I have been able to write a thesis that I am proud of and accurately represents both myself and my research.

To my family, who have continually supported me throughout my university endeavours no matter how hard times have been, you have my undying love and gratitude.

And finally, to my friends and to the university societies who have welcomed and supported me throughout my eight and a half years at university, thank you for all the good and fun times we've shared alongside our studies.

Author’s Declaration

The author would like to acknowledge the financial support received from the Engineering and Physical Sciences Research Council (EPSRC) (EP/R513222/1, EP/W524359/1, EP/T517896/1) in relation to their postgraduate studies.

The author declares no competing financial interests or personal relationships that may have influenced the contents of this thesis.

Nomenclature

Symbols

A	area [m^2]
c_p	specific heat capacity [kJ/kg.K]
h	enthalpy [J/kg]
k	thermal conductivity [W/m.K]
K_v	valve flow coefficient
m	mass [kg]
$\dot{m}$	mass flow rate [kg/s]
n	rotational speed [Hz, rps]
p	pressure [Pa, bar]
Q	heat energy [J]
$\dot{Q}$	heat transfer rate [W]
T	temperature [°C]
t	time [s]
V	volume [m^3, l]
W	compressor work [J]
$\dot{W}$	compressor power [W]

Subscripts

cha	charging
comp	compressor
cond	condenser
def	defrosting
dis	discharging
evap	evaporator
expT	expansion tank
expV	expansion valve
pump	circulation pump
sep	separator
sub	subcooler
tank	thermal storage tank
3V	three-way valve
4V	four-way valve

Greek letters

α	coefficient of performance improvement [%]
β	operational time ratio
γ	volumetric charging factor [s/l]
ρ	density [kg/m^3]
Δ	difference

Abbreviations

ASHP	air source heat pump
COP	coefficient of performance
DSM	demand side management
FHP	flexible heat pump
GSHP	ground source heat pump
GWP	global warming potential
HSPF	heating seasonal performance factor
HVAC	heating, ventilation and air conditioning
IHX	internal heat exchanger
ODP	ozone depletion potential
PCM	phase change material
TES	thermal energy storage
WSHP	water source heat pump

1 Introduction

1.1 Heat pump systems: overview, challenges and recent innovations

Heat pump technologies are currently seen as crucial to the decarbonisation of the heating sector and to reach net zero climate targets by 2050. Heat pump systems function using the same vapour compression cycles commonly found in refrigeration and cooling applications, but with the inverse goal of extracting and transferring heat from the ambient outdoor environment to increase the temperature of the desired indoor environment. The most common form of heat pumps are air source heat pumps (ASHPs), which extract heat from the surrounding air and elevate it to a higher temperature. Other common forms of heat pumps include water source heat pumps (WSHPs), which extract heat from bodies of water such as rivers, lakes, aquifers and various wastewater sources; and ground source heat pumps (GSHPs), which extract heat energy from the ground, rock or soil using underground or buried heat exchangers. In comparison to fossil fuel-based heating systems, heat pump systems can be ran entirely using electricity generated by renewable energy sources with significantly higher performance and energy efficiency up to 5 times greater than equivalent gas boiler systems [1].

In recent times, the growth and uptake of heat pump systems has continued to increase year-on-year. Reports have found that global sales of heat pump systems increased by 11% in 2022, with a 40% increase in sales in Europe alone and a 100% increase in some European countries such as Germany and Poland. Other areas, such as the United States and Japan, have experienced similar sales increases of 11% and 19% respectively [1]. The majority of these sales have been air source heat pump models, which have many advantages over other heat pump configurations due to their relative simplicity, ease of installation, compactness, lower capital and operational costs and environmentally friendly reputation [2-6]. It is estimated that if these trends continue to improve, heat pumps have the potential to reduce global carbon dioxide emissions by 500 million tonnes by 2030 [1].

Despite their continual market growth, heat production using heat pumps only accounts for 10% of the total global heating demand in buildings, with the current rate of deployment underperforming to meet net zero targets by 2050 [1]. This is primarily driven by a lack of consumer confidence with regards to their overall costs and their performance in cold climates. Heat pump systems require significantly higher upfront installation costs compared

to gas boiler systems, including additional retrofits to building insulation, windows and radiators; in order to achieve their most optimal energy efficient operation [7]. While a heat pump may be more efficient and financially beneficial to the consumer than a gas boiler system, the higher capital costs would demand a longer return on investment period before any beneficial financial savings could be realistically obtained. This also extends to its operating costs, as the electricity required to run the system is often more expensive than the cost of natural gas or other fossil fuels at peak times.

The performance of air source heat pump systems are largely dependent on the temperature difference between the ambient air heat source and the indoor environment heat sink. Larger temperature differences require significantly more compressor work to achieve the same setpoint temperature, which reduces the system's coefficient of performance (COP) [3]. Additionally, air source heat pump systems operating in cold and humid climates are very susceptible to frost and ice accumulation around the external surfaces of the evaporator. The thermal conductivity of the evaporator surfaces decreases with increasing ice buildup, hindering its heat transfer capabilities and reducing its coefficient of performance [8]. This requires the system to undergo regular defrosting operations using methods such as reverse cycle defrosting (RCD) or auxiliary resistance heating, further increasing the amount of energy they consume.

In response to these challenges, an increasing focus has been made into the development of heat storage technologies for use within heat pump systems. Heat pump systems can be integrated with thermal energy storage (TES) tanks to increase their flexibility in response to the fluctuating nature of renewable energy sources and end user demands. These storage tanks can recover and store excess heat energy for later use during periods where standard operational modes would be unviable, such as peak electricity demand or cold weather that would hinder the performance of the evaporator [9]. The energy density, thermal conductivity and overall size of the storage tank is dependent on the storage material used, and these properties can be optimised to provide the most cost-effective solution for different sized heat pump systems. Heat stored within thermal energy storage tanks can also be used to defrost the evaporator in the event of excessive ice formation while maintaining an acceptable level of indoor thermal comfort and either reducing or eliminating the need for an auxiliary backup heater.

1.2 Dynamic modelling and simulation: overview and challenges

In literature, the modelling and simulation of heat pump systems is often assessed while assuming steady state conditions where various system and environmental parameters remain fixed for the duration of the simulation run. This greatly reduces the complexity and computational time required to complete the simulation of the model but negatively affects the accuracy of the obtained results if the assumed values are too idealistic. While this can be very beneficial during the early development stage, relying on these simplistic models further into development can result in large inconsistencies between the simulated and real-life performances of the same heat pump system, as they are unable to account for various factors that are time-dependent. Roquet et al. (2024) [10] studied the performance of a six-building district heating network for a university campus in Uccle, Belgium. During the initial design process, the model was first constructed and simulated under nominal steady-state conditions before being simulated under dynamic conditions in order to study the true thermodynamic behaviour of the network during operation. Other studies conducted by Conte et al. (2024) [11], Wang et al. (2020) [12] and Cui et al. (2021) [13] followed a similar approach: first modelling a heat pump system under steady-state conditions before focusing on a dynamic version operating under realistic conditions.

In realistic scenarios, heat pump systems would be located within transient environments with conditions that vary according to the latitude and longitude of the location, local weather patterns, time of day, the presence of surrounding structures and urban areas, and other relevant factors. For example, heat pumps in cold and humid climates may be more prone to the effects of frosting and ice formation on outdoor components, particularly during the winter months. Similarly, the day-to-day operation of heat pump systems will vary significantly depending on the building type, the number of occupants and their daily schedules, and other human preferences or behaviours that may otherwise impact the system. For example, households where the occupants are families with young children may require a lower heating setpoint during weekday mornings and afternoons when the building is unoccupied, particularly during the standard 9-5 working day. Additionally, the transient behaviours of individual system components, subsystems and working fluids would also be implemented. As such, the dynamic modelling of heat pump systems is of key importance to understanding, analysing and predicting their behaviours to aid with the development, installation and operation of accurate systems.

As dynamic simulation models must be built using components utilising acausal non-linear systems of equations, the complexity of heat pump systems and their related control subsystems would be expected to steadily increase as development progresses. This would result in an increase in the computational time and resources required by the computer to complete a single simulation run, which may negatively impact development if this increases to unacceptable levels. A study conducted by Rasmussen et al. (2012) [14] found that for a 500 second simulation of a standard vapour compression heat pump cycle, the computational time required to complete this simulation increased depending on the modelling paradigms of the heat exchanger components. Nonlinearized models featuring a large number of finite control volumes required significantly more computational processing time relative to the 500s simulation runtime, with a real-time factor of up to 141.23 for complex component models featuring over 200 dynamic states (requiring 19.62 hours). Therefore, it is important to optimise simulation models to minimise the required computational time and resources while maintaining an acceptable level of accuracy in the results. Furthermore, the accuracy of the results obtained from dynamic simulations should be validated using some form of externally acquired and verifiable data in order to ensure that the model is functioning as intended by the user.

1.3 The flexible heat pump system

One such example of a heat pump system combined with thermal energy storage technologies is the flexible heat pump system described by Yu et al. (2022) [15] and developed in collaboration between researchers at the University of Glasgow [16] and the University of Liverpool [17]. The flexible heat pump system is a novel concept based on a modified Evans-Perkins vapour compression cycle utilising a thermal energy storage tank as a subcooling, heat recovery and energy storage device (figure 1 and 2). In comparison to a standard single stage heat pump system, the flexible heat pump system can recover, store and utilise heat through the charging and discharging of the storage tank. In charging mode, the storage tank recovers excess heat from warm refrigerant exiting the condenser, storing this thermal energy for later use and reducing throttling losses through the expansion valve to improve energy efficiency. In discharging mode, the storage tank is used as a high temperature heat source while isolating the evaporator from the rest of the system, allowing it to effectively function as the high stage of a two-stage heat pump system (defined as quasi-two-stage operation). An additional defrosting mode can also be utilised, where warm refrigerant exiting the condenser is instead rerouted through the evaporator to remove ice buildup during discharging. Unlike

other similar systems, this prevents the indoor environment from being utilised as a heat sink and allows for an acceptable level of thermal comfort to be maintained without the use of a backup heater.

The goal of this novel system architecture is to optimise the performance and energy efficiency of a standard Evans-Perkins vapour compression cycle for the purposes of providing low-cost renewables-based heat production for domestic space heating and hot water applications. Simulation models constructed early in development have estimated that this system can achieve a COP improvement of up to 20% over conventional systems, with a previously built prototype model demonstrating a COP improvement of 3.7-10% for a 35-65°C supply temperature [15]. However, these simulations and experiments were conducted under idealised, steady-state or simplistic laboratory conditions, during which a number of key factors were ignored: the temperature of the ambient environment that interacted with the evaporator remained constant throughout each test, mode switching was not considered with regards to the ambient temperature conditions, only a limited range of conditions and refrigerants were tested, and the thermal energy storage tank was not correctly sized for domestic heat storage purposes. Within the literature, other researchers have considered and explored heat pump systems incorporating individual elements shared by this system, such as thermal energy storage tanks, heat recovery devices, secondary/backup heat sources and defrosting modes; but have not considered the full flexible system in its entirety.

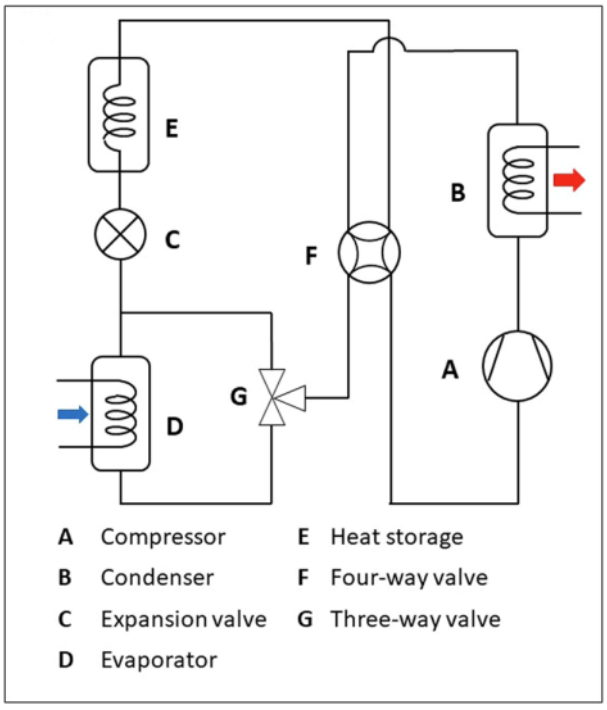

Figure 1: Schematic diagram of the flexible heat pump system [15].

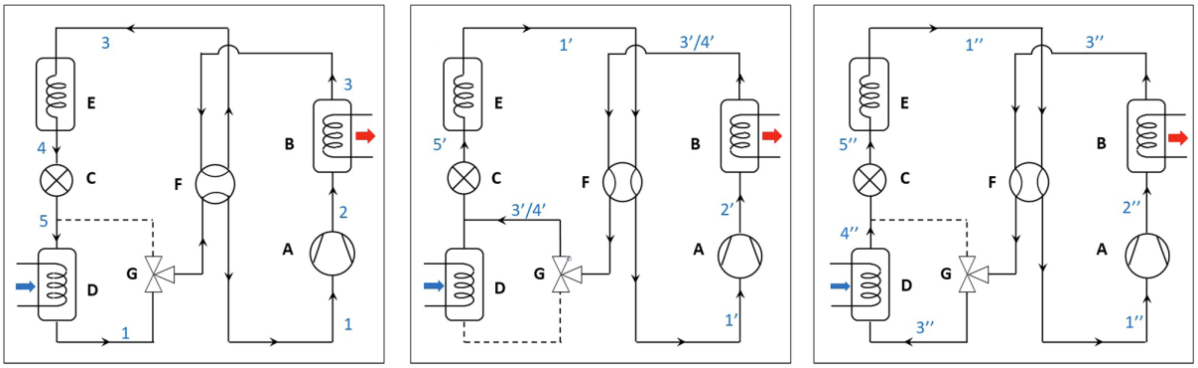

Figure 2: Schematic diagrams of the flexible heat pump system for the three configurable operational modes: TES charging with the thermal energy storage acting as a subcooler (left), TES discharging during quasi-two-stage operation (centre), TES discharging during quasi-two-stage operation with the additional defrosting of the evaporator (right) [15].

1.4 Research objective and knowledge gap

The research objective of this project is to develop a dynamic simulation model of the flexible heat pump system as originally described by Yu et al. (2022) [15], with the goal of accurately simulating its transient thermodynamic behaviour. The proposed research question can be summarised as follows: “How can the flexible heat pump system, wherein a standard Evans-Perkins vapour compression cycle is integrated with an in-cycle heat recovery-based thermal energy storage device and proper mode switching control systems, improve the energy efficiency of a domestic heat pump system for space heating and hot water applications?”. A knowledge gap has been identified in that the previous simulation models of this system were constructed using steady-state assumptions and currently do not reflect the expected dynamic behaviours that the system will experience during standard operation. While the flexible heat pump system shows great promise conceptually, this technology should be further reinforced and refined with accurate dynamic simulation models.

This research is conducted to demonstrate that the flexible heat pump system is capable of achieving significantly higher performance metrics in comparison to standard heat pump systems in terms of seasonal performance, energy efficiency and cost-effectiveness (when using mains grid electricity) under the same load conditions. The optimisation of the thermodynamic performance of the flexible heat pump system will also be considered with regards to refrigerant choices, thermal energy storage tank sizing and potential control methods in order to minimise energy usage and costs while maintaining a consistent supply temperature for the end user. Therefore, this study aims to prove that this novel system architecture provides realistic, long-term benefits to the end user in addition to the already

established eco-friendly benefits of decarbonising home heating through the use of heat pumps over fossil fuel-based systems.

With regards to the research objective, the research question and the identified knowledge gap, the dynamic simulation model of the flexible heat pump system was constructed with regards to the following transient behaviours:

- **Operational conditions** such as the ambient air heat source temperature and heating load patterns that vary according to the time of day, local weather conditions and end user demands.
- **Environmental effects** such as frosting and ice accumulation on the evaporator surfaces that affect the performance and power consumption of the heat pump during cold and humid periods.
- **Mode switching and transitioning between modes**, where the configuration of the heat pump valves and refrigerant flow directions must be altered to shift between multiple modes of operation, such as the normal heating and defrosting modes, when required.
- **The state of the thermal energy storage**, where sensible and latent storage materials experience temperature and phase changes respectively as heat is absorbed or extracted over time.

Furthermore, alternative system configurations and control methods out with the original scope defined by the associated patent documentation [16] may also be considered, modelled and compared to the baseline flexible heat pump model.

1.5 Dynamic modelling software packages

The steady-state modelling and simulation of the flexible heat pump system as described by Yu et al. (2022) [15] was previously conducted using Aspen. Studies utilising the Aspen series of modelling and simulation software packages primarily focus on chemical industry fields that share many common theoretical bases with the thermodynamic fields that relate to heat pumps and refrigeration systems, which allows heat pump systems to be simulated using the relevant fundamental equations of state, transfer equations and constitutive equations of matter [18, 19]. While Aspen is suitable for domestic-sized heat pump systems, recent studies

in literature primarily focus on waste heat recovery in industrial plants as opposed to the domestic heating sector, which were found to be difficult to fully implement during early simulation models. As such, it was recommended that future transient simulations should be conducted using the Modelica programming language.

Modelica is an equation-based, object-oriented modelling language that supports both causal and acausal modelling [20, 21]. This allows for the development of complex models using a graphical and hierarchical approach, allowing models to be constructed from standard form physical equations with separate, automatically generated simulation code. Many commercially available and open-source libraries exist for Modelica that contain a vast array of model components and blocks for constructing or improving new dynamic models [22, 23]. In literature, the Modelica language has been used to accurately simulate transient heat pump systems [24], in addition to large scale district heating and cooling networks [25, 26] or individual heat pump components such as compressors [27, 28]. As Modelica is its own proprietary language, can be used to simulate systems across a wide range of technical domains and does not require the user to have extensive prior knowledge of other programming languages, Modelica was chosen for the dynamic modelling and simulation of the flexible heat pump system.

After conducting a preliminary exploration into potential options, it was identified that Dymola and OpenModelica are the two most common software packages utilising the Modelica language for the dynamic modelling and simulation of domestic heating systems. Dymola (Dynamic Modeling Laboratory) is a commercially available modelling and simulation environment developed by Dassault Systèmes [29], whereas OpenModelica is a freely available and open-sourced modelling and simulation environment developed by the Open Source Modelica Consortium (OSMC) [30]. In comparison to OpenModelica, Dymola features a more robust and user-friendly interface in addition to better user documentation and support services through the supplier company Claytex Technica. Additionally, the number of recorded studies conducted using Dymola significantly outweighs the number of those conducted using OpenModelica. As such, Dymola was used to model the flexible heat pump system while utilising publicly available training resources for OpenModelica and the Modelica programming language in general. Additional component libraries obtained from a variety of sources were also utilised in these models. For the flexible heat pump system, the dynamic simulation models will be validated using data obtained from an experimental test rig setup currently in use at the University of Liverpool (figure 3), data obtained from other research

papers for similar heat pump systems of comparable size and function, and datasets of historical weather data and operational load patterns.

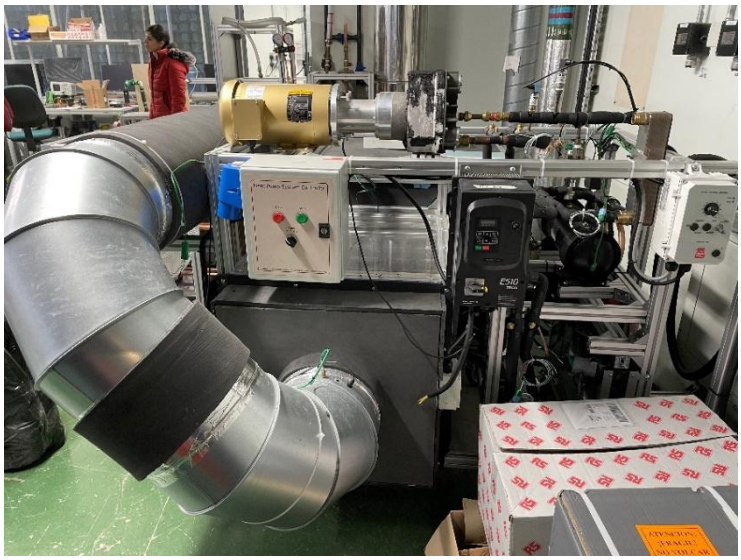

Figure 3: Image of the experimental test rig setup based on the flexible heat pump system.

2 Literature Review & Background

2.1 Heat pump systems

Heat pump systems are an innovative form of heating, ventilation and air conditioning (HVAC) technologies that function by extracting heat energy from a designated heat source (usually an outdoor medium such as the ambient air, accessible bodies of water or underground bodies of earth) and elevating this heat to a higher temperature before rejecting it to a designated heat sink (usually an enclosed indoor environment). These systems operate with significantly higher performance and energy efficiency up to 5 times greater than that of equivalent gas boiler systems [1]. In comparison to fossil fuel-based heating systems that generate heat energy through the combustion of non-renewable fuels such as coal, oil or natural gas; heat pump systems can be ran entirely using a mains electricity supply from nationwide scale energy grids. If these technologies were to be implemented alongside renewable energy sources such as wind or solar power, heat pump systems have the potential to decarbonise the domestic heating sector by significantly reducing the amount of greenhouse gas emissions produced annually by domestic heating systems. On a global scale, heat pump systems have the potential to meet more than 60% of the global space heating and hot water demand while producing fewer carbon dioxide emissions than if condensing gas boilers were used, but currently still only meet around 10% of this demand as of 2023 [1].

A standard heat pump system operating on a typical Evans-Perkins single-stage vapour compression cycle usually consists of four main components: a compressor, a condenser, an expansion valve and an evaporator. As shown in figure 4, the system operates on a fixed cycle from state points 1-2-3-4-1 in order, restarting at state point 1 (before the compressor inlet). For domestic space heating and hot water production, one complete vapour compression cycle can be summarised as follows:

Compressor (1-2): The hot vapourised refrigerant exiting the evaporator enters the compressor, where it is then compressed to increase its temperature and pressure, causing it to become superheated. This stage requires some form of external input energy to be completed, usually in the form of electricity required to power the compressor motor.

Condenser (2-3): The superheated vapourised refrigerant entering the condenser rejects heat energy to the heat sink, causing it to cool down and condense into a liquid state.

Expansion Valve (3-4): The cooler liquid refrigerant exiting the condenser enters the expansion valve, where it is then throttled to reduce its pressure and temperature, returning it to its initial cold liquid state.

Evaporator (4-1): The cold liquid refrigerant entering the evaporator absorbs heat energy from the heat source, causing it to increase in temperature and vaporise.

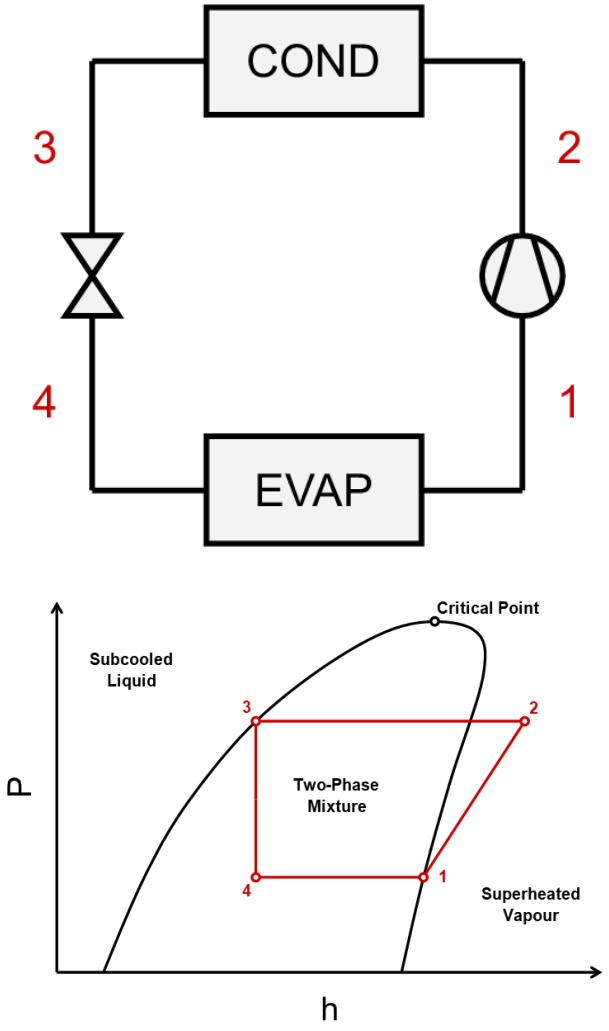

Figure 4: Schematic and pressure-enthalpy (p-h) diagrams of a single-stage heat pump system.

The choice of refrigerant fluid employed within the refrigerant loop of a heat pump system has a significant impact on its performance, complexity and costs. Fluid properties such as viscosity, thermal conductivity, specific heat capacity, heat of vaporisation, critical pressure, critical temperature, density and volumetric heating capacity all directly affect the coefficient of performance (COP) value of the system during operation [31]. The most important values to consider are the critical pressure and critical temperature of the refrigerant fluid, which designate the point in which the liquid-vapour phase boundaries

vanish and fluid within the subcritical (subcooled liquid) region starts to behave within the supercritical (superheated vapour) region. This is often represented by the “critical point” value of the refrigerant, which can be observed in the pressure-enthalpy diagram of figure 4 as the apex of the curve where the liquid saturation line and the vapour saturation line intersect. Heat pump systems such as the flexible heat pump system utilise subcritical cycles, whereby the system operates at a pressure that is consistently below the critical pressure value of the refrigerant and prioritises maximising its performance by having a condensing temperature that is considerably lower than the critical temperature value. Other systems, such as the ones discussed in section 2.1.3, instead employ transcritical cycles that elevate the refrigerant to a higher pressure and temperature that is significantly higher than its critical point values during the compression stage in order to achieve a lower gas cooler outlet temperature during heat rejection [31].

In terms of their impacts on the environment, refrigerants with low global warming potential (GWP) and ozone depletion potential (OPD) values are generally more desirable than environmentally damaging ones such as chlorofluorocarbons (CFCs), hydrochlorofluorocarbons (HCFCs) and hydrofluorocarbons (HFCs) [32, 33]. Furthermore, refrigerants should ideally be non-toxic and non-flammable in order to ensure safe operation at all times [31]. Common refrigerants such as R134a are currently in the process of being phased out of active use due to their poor environmental friendliness and high global warming potential values, significantly limiting their uptake in future heat pump systems. As such, natural refrigerants such as propane (also known as R290), carbon dioxide (CO_2) and ammonia (also known as R717) are becoming increasingly widespread in modern heat pump systems due to their good thermodynamic properties, environmental friendliness and natural abundance. Some examples of potential high-temperature refrigerant fluids, as well as their fluid properties, can be found in table 1.

Table 1: Properties of potential high-temperature refrigerant fluids [31].

Refrigerant	Type	P_{Crit} (kPa)	T_{Crit} (°C)	GWP	ODP	Safety group
R1224yd(Z)	HFCO	3337	155.5	1	minimal	A1
R1233zd(E)	HFCO	3624	166.5	1	minimal	A1
R1234-yf	HFO	3382	94.7	<1	0	A1
R1234ze(E)	HFO	3635	109.4	6	0	A2L
R1234ze(Z)	HFO	3531	150.1	<1	0	A2L
R1243zf	HFO	3518	103.8	<1	0	A2
R1336mzz(Z)	HFO	2903	171.4	2	0	A1
Ammonia	Natural	11,363	132.4	0	0	B2L
CO_2	Natural	7377.3	31.0	1	0	A1
Water	Natural	22,064	374.0	0	0	A1
Propane	Natural	4251.2	96.7	3	0	A3
Isobutane	Natural	3629	134.7	4	0	A3
Butane	Natural	3796	152.0	4	0	A3
Isopentane	Natural	3378	187.2	5	0	A3
Pentane	Natural	3368	196.6	5	0	A3
R245fa	HFC	3651	153.9	1030	0	B1
R365mfc	HFC	3266	186.9	794	0	A2
R410a	HFC	5782	78.1	675	0	A1
R134a	HFC	4059.2	101.1	1430	0	A1
R227ea	HFC	2925	101.8	3220	0	A1

2.1.1 Air, water and ground source heat pump systems

Standard heat pump systems can be categorised into three main types depending on the nature of the heat source:

Air source heat pumps (ASHPs) extract heat energy from the outdoor ambient air or from exhaust air sources such as industrial waste steam [34, 35] and waste heat rejected by the compressor [36]. Air source heat pumps are highly efficient systems that can be up to five times more efficient than electric resistance heaters, and are the most commonly adopted form of heat pump system in the domestic heating sector [37]. Air source heat pump systems have many advantages over other forms of heat pump systems, such as their relative simplicity, ease of installation, compactness, lower capital and operational costs and environmentally friendly reputation [2-6]. However, their performance is greatly dependent on the temperature difference between the heat source and the heat sink, and are particularly susceptible to frosting and ice accumulation in cold and humid climates [4, 38, 39].

Water source heat pumps (WSHPs) extract heat energy from bodies of water such as ponds, lakes, rivers, oceans and aquifers; as well as wastewater sources such as sewers and

industrial plants [40]. Water source heat pumps utilising heat sources such as groundwater benefit from a greatly reduced temperature fluctuation range in comparison to the ambient air, allowing for highly efficient systems with a reliable, consistent and steady heat supply [2, 41]. Additionally, bodies of water such as aquifers have shown further promise by functioning as naturally-occurring thermal energy storage devices at a district heating level [42, 43]. However, water source heat pump systems are limited by the availability of suitably-large water sources (especially in dense urbanised areas) and certain environmental regulations [41]. Furthermore, systems utilising water sources containing seawater are subjected to corrosion and fouling that may result in component wear or breakage, reducing the overall performance and operational lifespan of the system [44].

Ground source heat pumps (GSHPs) extract heat energy from the ground, rock or soil using underground or buried heat exchangers. Ground source heat pumps are highly efficient systems with a stable and reliable heat supply but often incur high initial costs due to the need for extensive ground excavation and the drilling of boreholes [2, 45, 46]. Additionally, ground source heat pump systems are often unsuitable in cold regions where ground temperature imbalances greatly affect their long-term operation [45, 47]. Horizontal heat exchanger arrangements are typically laid and buried in trenches at a depth of up to 20m, depending on the local frost line, which eliminates the need for extensive deep drilling. While this arrangement is very area-intensive (requiring up to twice the area for the heat source compared to the area of the heating space), straight sections of piping can be substituted for sections of coiled loops in order to maximise the cost-effectiveness and space-efficiency of the system [48]. Similarly, vertical heat exchangers are typically installed in the form of boreholes containing long U-shaped tubes with a total length of up to 100m, operating independently from the ambient climate conditions observed at surface level [48]. These boreholes can also be utilised as thermal energy storage devices by storing heat energy within thermally stable sections of rock located deep underground, providing an efficient and cost-effective solution for long-term seasonal thermal energy storage [49-51].

Heat pump systems can also be supplied heat energy through other methods such as solar thermal collectors [46, 52-56] and thermal energy storage devices, but these are often used in combination with a primary air-, water- or ground-based heat source. A summary of these different heat pump technologies can be found in table 2.

Table 2: Summary of heat pump technologies [41].

Technology	Installation Cost	Average COP	Environmental Impacts	Pros	Cons
Air Source Heat Pump	+	3	• Highest environmental impact in cold regions • Leakage of refrigerant can cause pollution • Causes noise pollution	• Less or no pollution concerns • Simple operation • Low maintenance cost • High COP • Low primary energy consumption	• Frost formation on outer units • COP varies with ambient temperature • May need supplemental heat system for better performance
Water Source Heat Pump	++	4.5	• Can cause water pollution, stratum settlement and trigger geological disasters	• Highly efficient • Not affected by ambient conditions • Can utilise heat from rivers and lakes	• Requires water bodies or storage tanks in vicinity • Needs regulatory permission for installation
Ground Source Heat Pump	+++	3.5-4	• Unchecked heat transfer fluids are hazardous • Surface water can enter borehole • Can perturb groundwater temperature • Reduces emissions with low payback period	• Highly efficient and shows great energy saving potential • High COP • Utilises vast source of heat • Very reliable source of heat • Can operate in regions with extreme winters	• Needs careful assessment of local geology and requirements • COP may decrease over heating season due to saturation of soil temperature
Sorption Heat Pump	++++	1.8	• Working fluids do not cause ozone depletion	• Waste heat utilisation from sewage and brine	• Low COP
Solar Assisted Heat Pump	++ to +++++	Higher than individual HP COP	• Significant environmental benefits • Can reduce emissions by 50%	• Financially and energetically viable solution • Solar helps HPs in achieving higher COP • Lowers grid electricity consumption	• Needs additional control mechanisms for optimal operation • Highly location and application specific

2.1.2 Two-stage and cascade cycles

Two-stage heat pump cycles (figure 5) are an alternative configuration for refrigerant compression that utilises multiple compressors to complete a series of successive, smaller compression stages across one full vapour compression cycle. In this configuration, the refrigerant fluid is first compressed from an initial low pressure state to an intermediary pressure in the first compression stage, and then from the intermediary pressure to the required high pressure state in the second compression stage. This results in lower compression work across each compressor component in the cycle, but significantly increases the mechanical complexity and costs associated with the overall system [31].

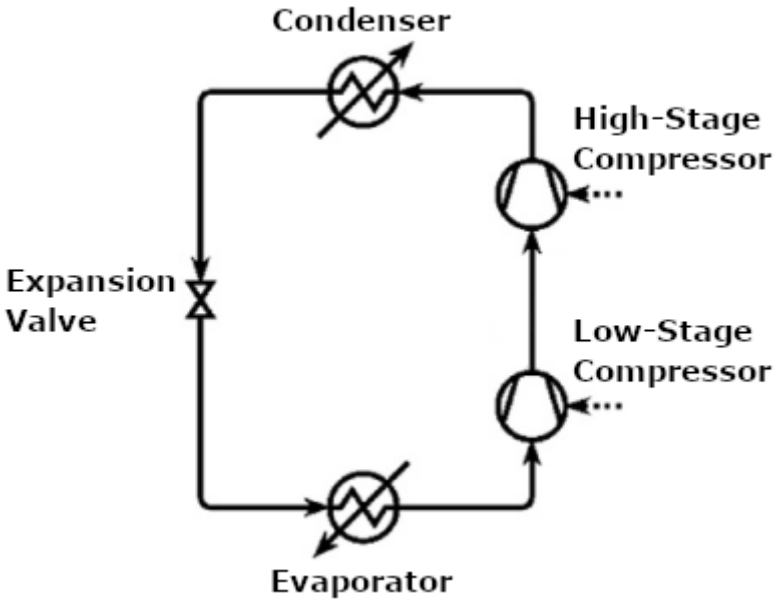

Figure 5: Schematic diagram of a two-stage heat pump cycle [31].

Bertsch & Groll (2008) [3] studied the implementation of two-stage air source heat pump systems for residential heating and cooling application in northern US climates. A series of simulation models for various heating systems were initially developed for two-stage heat pump cycles (with intercoolers or economisers) and cascade heat pump cycles at a design point of -20°C ambient air temperature and 50°C hot water supply temperature. Following this, an experimental test setup for the two-stage cycle with closed economiser and R410a refrigerant was constructed and analysed in order to assess its performance for ambient air temperatures ranging from -30°C to 10°C in both the heating and cooling modes. The results of this study found that for the same ambient air temperature, the setup operating as a two-stage cycle approximately doubles the heating capacity of the system in comparison to the same setup operating as a single-stage cycle. Furthermore, second law efficiency values of 39-46% were measured across the whole operating range, which outperformed most commercially available single-stage air source heat pump systems at the time. While the authors emphasised that the installation costs for this system were considerably higher than those for single-stage systems due to the need for additional components and control systems, the costs were less than those required for an equivalent ground source heat pump system (considering the costs for drilling and ground preparation).

Another variation of the two-stage concept is the cascade heat pump cycle (figure 6), which uses an intermediary heat exchanger to combine two or more closed loop vapour compression cycles to form a full heat pump system that operates over multiple compression stages. The

intermediary heat exchanger acts as the evaporator component in the high temperature cycle and as the condenser component in the low temperature cycle, transferring thermal energy from one cycle to the other. In comparison to the two-stage cycle, some additional thermal losses are incurred due to the temperature difference across the intermediary heat exchanger, and multiple sets of expansion valves and heat exchangers are required for each cycle utilised. However, this configuration allows for different refrigerant fluids to be used for each temperature cycle, resulting in better and more optimal performance in comparison to an equivalent single stage cycle if the refrigerant choices are calibrated to the conditions of each temperature cycle [31].

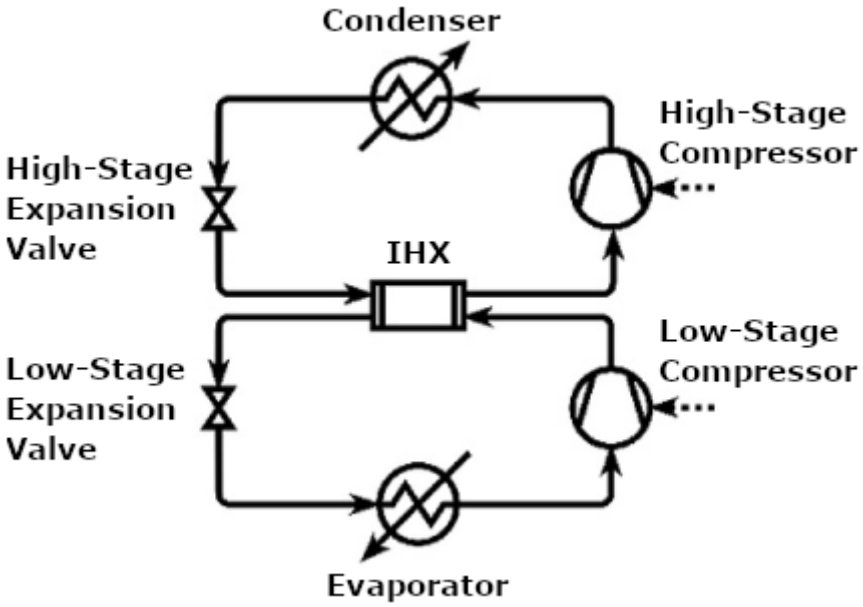

Figure 6: Schematic diagram of a cascade heat pump cycle [31].

Bai et al. (2023) [57] studied the thermal performance of an experimental high temperature heat pump system with a double heat source cascade cycle configuration to facilitate efficient heat recovery using industrial waste steam. In addition to the low temperature heat source at the evaporator, a secondary medium temperature heat source was utilised through the intermediary heat exchanger where the two compression cycles interconnect, allowing the system to absorb heat energy from both low and medium temperature heat sources simultaneously. An experimental test setup was constructed, and the results of this study found that the working mode utilising the dual heat sources had a significant impact on the performance of the cascade system, increasing the heating capacity and coefficient of performance values by 18.6% and 8.9% respectively, with an 8.7% increase in power consumption.

The design of the flexible heat pump system bears many similarities to the architectures of both the two-stage cycle and the cascade cycle. As described by Yu et al. (2022) [15], the flexible heat pump system functions using a “quasi-two stage cycle”. In the charging mode, the system functions as a single-stage cycle, which can also be interpreted as the single compressor component operating as both the high stage and low stage compressors in a two-stage cycle simultaneously. In the discharging and defrosting modes, the system instead functions as the high stage of a two-stage cycle, as the refrigerant fluid enters the compressor at a higher pressure and temperature due to the high temperature thermal energy storage being used as a heat source. This functionality is what denotes the flexible system as “quasi two-stage”, as the single-stage system periodically acts as the high stage of an equivalent two-stage system. Similarly, the architecture of the thermal energy storage tank and how it is integrated into the heat pump cycle could be interpreted as a form of cascade system, as the storage tank and the fluid loop that it inhabits is used to transfer heat energy between itself and the main refrigerant loop during operation.

2.1.3 Transcritical CO_2 cycles

In the field of working fluids for heat pump systems, carbon dioxide (CO_2) currently exhibits excellent potential for use in transcritical vapour compression heat pump cycles operating at low ambient air temperatures or in situations where a high temperature water supply is required by the system [44]. CO_2 is a natural refrigerant fluid and competitive replacement for most common CFC and HCFC refrigerants due to its excellent thermal properties and low environmental impact. Of key importance to transcritical cycles are its high critical pressure and low critical temperature values of 7.38 MPa and 31.1°C respectively, which allow air source heat pump system utilising this refrigerant fluid to operate within the supercritical region at naturally occurring ambient air temperatures [58]. Additionally, its low global warming potential (GWP) and ozone depletion potential (ODP) values of 1 and 0 respectively validates its reputation as an environmentally friendly refrigerant fluid and as a potential option to further the decarbonisation of the heating sector. Furthermore, CO_2 exists as an abundant, low-cost, non-flammable and non-toxic material with high thermal conductivity and a large thermal capacity, making it an ideal option for domestic heating and refrigeration systems [59].

In comparison to conventional vapour compression cycles that operate with both heat rejection and heat absorption in the subcritical region, transcritical cycles operate with

supercritical heat rejection and subcritical heat absorption [33]. Furthermore, the condenser component used in the subcritical cycle arrangement is replaced with a gas cooler in the arrangement for the transcritical cycle, which functions identically to the condenser as the indoor heat exchanger albeit without requiring the superheated vapourised refrigerant to condense back to a liquid state during the heat rejection process. As the subcritical CO_2 refrigerant is compressed through the compressor, the pressure and temperature of the refrigerant fluid increases above its respective critical point values and the refrigerant becomes supercritical. In this state, the supercritical CO_2 refrigerant behaves with the fluid density of the liquid phase and the fluid viscosity of the vaporous phase. This improves the flowability and heat transfer properties of the refrigerant fluid, and allows the receiving water in the gas cooler to reach higher supply temperatures [60]. An example of the pressure-enthalpy (p-h) diagram for a single-stage transcritical heat pump system utilising CO_2 can be found in figure 7.

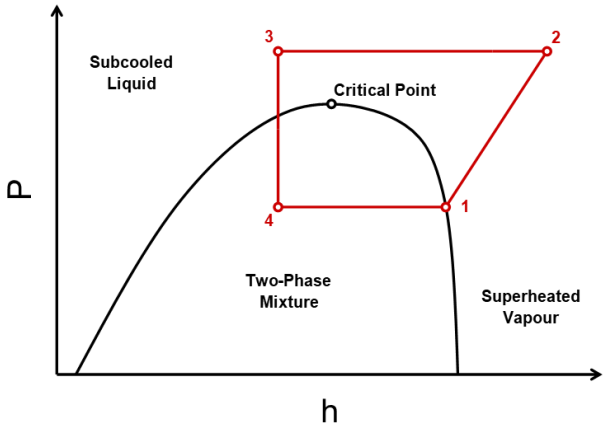

Figure 7: Pressure-enthalpy (p-h) diagram of a single-stage transcritical heat pump system.

Wang et al. (2021) [59] studied the performance of a transcritical CO_2 air source heat pump system combined with radiators and radiant floor coils for the space heating of buildings located in different climate zones in China. A representative single-family house with a total space heating area of $100m^2$ was modelled using TRNSYS and the thermal performance of the transcritical heat pump system was analysed for five different climate zones comprising of two cold zones (Yinchuan and Xi'an) and three severe cold zones (Haliar, Qiqihar and Shenyang). The inlet water temperature through the gas cooler was also analysed in detail, as the thermophysical properties of CO_2 operating in the supercritical region are particularly sensitive to large temperature changes which would negatively impact its performance. The results of this study found that the transcritical CO_2 air source heat pump system was

sufficiently capable of meeting the levels of thermal comfort desired by the building's occupants. Additionally, the arrangement of the space heating terminals provided a lower inlet water temperature in comparison to a benchmark system without radiant floor coils, further improving the performance of the transcritical system by reducing throttling losses. For the severely cold region of Shenyang, the coefficient of performance (COP) and heating seasonal performance factor (HSPF) values of the transcritical system were 17-28% and 9-22% higher respectively when compared to the benchmark system. Previous studies conducted by the same author on the subject of integrating transcritical CO_2 air source heat pump systems with thermal energy storage devices further reinforce these conclusions, reiterating that transcritical CO_2 systems are an effective solution for providing energy efficient and high performance space heating at low ambient air temperatures [58, 61].

2.2 Thermal energy storage methods

Thermal energy storage (TES) devices, such as storage tanks or vessels, are another key technology used alongside heat pump systems to further improve the decarbonisation of the domestic heating sector by enabling flexible operation strategies. Thermal energy storage devices can be categorised into three main types depending on the nature of the storage medium and their method of heat release: sensible, latent and thermochemical storage materials (which can all be described as active storage methods); and these types can be further supported by passive storage methods (which are related to and complement pre-existing active storage devices).

During standard operating procedures, domestic heat pump systems absorb heat energy from an outdoor heat source and elevate it to a higher temperature through the compressor, where it is then immediately rejected to the indoor environment through the condenser. If a portion of this energy is not required to maintain the desired setpoint temperature as specified by the end user, total heat transfer does not occur, and this excess heat energy is instead wasted when the refrigerant fluid undergoes the subsequent throttling process through the expansion valve. This results in a reduction in the energy efficiency of the system, as a portion of the compressor work is essentially used to no end. Furthermore, the inverse is also true. If the system is unable to meet the desired setpoint temperature due to a lack of transferrable heat energy (primarily due to the presence of a low temperature heat source), this also results in a reduction in the energy efficiency of the system, as the system requires more compressor work in order to meet the same setpoint temperature.

Thermal energy storage devices allow for heat energy absorbed by the system to be captured and stored for later use, where it can then be rejected to the indoor environment when required. If a thermal energy storage tank were to be placed within the thermodynamic cycle of the heat pump system between the condenser and the expansion valve, such as the one found in the flexible heat pump system, the excess heat energy exiting the condenser could instead be recovered and stored within the storage tank instead of being wasted. Similarly, the heat pump system could also be rearranged in such a way as to instead transfer heat energy directly into the storage tank without providing heat to the indoor environment. Once the thermal energy storage tank becomes fully charged with heat energy, this charge could then be utilised as a secondary or auxiliary heat source, often at a higher temperature in comparison to the primary outdoor heat source. This allows domestic heat pump systems to operate during conditions that would otherwise negatively affect the end user, such as periods of low outside temperatures or periods where the cost of electricity is sold at a premium, therefore improving the overall performance of the system.

2.2.1 Sensible storage materials

In sensible thermal energy storage devices, energy is stored by changing the temperature of the storage material without changing its phase. This process involves transferring heat energy directly from the heat supply to the storage medium, where it increases in temperature as it gradually gains heat energy over time. Common materials for sensible thermal energy storage systems include water [62-66], natural rock or soil [67-69] and man-made materials such as brick or concrete; as well as other less common materials such as metals and oils. This method is classified as an active storage method, as the charging and discharging of the thermal energy storage tank is directly controlled by the system and the end user.

Sensible thermal energy storage systems typically exhibit a temperature difference in the range of 5-10°C between its fully charged and fully discharged states [70]. The amount of heat energy that is able to be stored within a sensible thermal energy storage device is proportional to the density, specific heat capacity, necessary storage volume and temperature of the storage material, while other important properties surrounding their implementation include material costs and heat transfer rate [71]. Water is the most commonly adopted material for sensible thermal energy storage devices, as it is an abundant, low-cost and chemically stable material choice with a relatively high thermal conductivity

value [8]. Thermally stratified storage tanks using water as the storage medium are commonly used in domestic heating applications, as the thermal stratification of the water above the thermocline ensures a stable hot water supply can be provided with the minimal mixing of the different temperature volumes present inside the storage tank [71]. However, water-based thermal energy storage tanks are greatly limited by their low energy density in comparison to latent storage materials, requiring a significantly larger storage volume in order to provide a similar level of energy storage [8]. Some examples of potential sensible thermal energy storage materials, as well as their material properties, can be found in table 3.

Table 3: Properties of potential sensible thermal energy storage materials [67].

Storage Material	Type	ρ (kg/m^3)	c_p (kJ/kg.K)	k (W/m.K) (at 20°C)	Maximum Storage Temperature (°C)
Brick	Solid	1600	0.84	1.20	70
Concrete	Solid	2240	1.13	0.9-1.3	70
Granite	Solid	2650	0.900	2.90	70
Marble	Solid	2500	0.880	2.00	70
Sandstone	Solid	2200	0.712	1.83	70
Aluminium	Solid	2707	0.896	204	160
Copper	Solid	8954	0.383	385	160
Stone, granite	Solid	2640	0.82	1.7-3.98	160
Stone, sandstone	Solid	2200	0.71	1.83	160
Water	Liquid	1000	4.19	0.58	100
Ethanol	Liquid	790	2.4	0.171	78
Butanol	Liquid	809	2.4	0.167	118
Engine oil	Liquid	888	1.88	–	160

2.2.2 Latent storage materials

In latent thermal energy storage devices, energy is stored by changing the phase of the storage material without changing its temperature. This process is achieved by utilising phase change materials (PCMs) as the storage medium, which operate with a melting point temperature within the operating range of the heat pump system. Common materials for latent thermal energy storage systems include ice [72], paraffin waxes [73-77] and salt hydrates [9, 38, 78]; and these materials can be further classified into organic, inorganic and eutectic types. Similar to sensible storage materials, this method is classified as an active storage method.

Latent thermal energy storage systems make use of the storage material's high heat of fusion (for solid-liquid phase transitions) or heat of vaporisation (for liquid-vapour transitions) that

allow latent storage materials to store large amounts of heat energy within a relatively small volume [44, 71]. This higher level of energy density allows for significantly smaller and more compact tank designs in comparison to sensible storage materials. The thermal performance of latent storage systems varies significantly with the characteristics and classification of the storage medium used. Organic materials, such as paraffin waxes and fatty acids, are characterised by their good thermal and chemical stability, but have low thermal conductivity, high volumetric expansion and are often flammable. Inorganic materials, such as salt hydrates and metallic alloys, are characterised by their high thermal conductivity and greater phase change enthalpy, but suffer from complications involving supercooling, phase separation and corrosion. Eutectic materials are not their own form of material, but instead comprise of two or more organic or inorganic materials (organic-organic, inorganic-inorganic or inorganic-organic), which often exhibit good thermal properties but are very expensive to manufacture [79]. A summary of different phase change materials can be found in table 4, and some examples of commercially-available latent thermal energy storage materials, as well as their material properties, can be found in table 5.

Table 4: Summary of phase change materials [79].

Types of PCMs	Advantages	Disadvantages
Organic PCMs	• No supercooling • No phase segregation • Chemically stable • Availability in large temperature range • Compatibility with other materials • Low vapor pressure	• Low thermal conductivity • Flammability • Low phase change enthalpy • More expensive • Low heat capacity • High volumetric expansion
Inorganic PCMs	• High thermal conductivity • Greater phase change enthalpy • Less costly • Lower volumetric expansion • Compatibility with other materials • Non-flammable	• High supercooling • Phase segregation • Corrosive • Chemical instability • Low heat capacity
Eutectic PCMs	• Sharp melting temperature • High volumetric thermal storage density • No phase segregation • Low supercooling	• Lack of thermophysical properties • Low total latent heat capacity • Costly

Table 5: Properties of commercial latent thermal energy storage materials [71].

Product	Type	Melting Temperature (°C)	Heat of Fusion (kJ/kg)	Thermal conductivity (W/m.K)	Source
RT 20	Paraffin	22	172	0.88	Rubitherm Gmbh
Climsel C23	Salt hydrate	23	148	–	Climator
E23	Salt hydrate	23	155	0.43	EPS Ltd
Climsel C24	Salt hydrate	24	108	1.48	Climator
TH 24	Salt hydrate	24	45.5	0.8	TEAP
RT 26	Paraffin	25	131	0.88	Rubitherm Gmbh
RT25	Paraffin	26	232	–	Rubitherm Gmbh
STL 27	Salt hydrate	27	213	1.09	Mitsubishi Chemical
S27	Salt hydrate	27	207	–	Cristopia
AC 27	Salt hydrate	27	207	1.47	Cristopia
RT 27	Paraffin	28	179	0.87	Rubitherm Gmbh
RT 30	Paraffin	28	206	–	Rubitherm Gmbh
E28	Salt hydrate	28	193	0.21	EPS Ltd

One potential solution to the problems surrounding the low thermal conductivity of phase change materials are hybrid thermal energy storage systems. These systems utilise both sensible and latent thermal energy storage materials, leveraging the higher thermal conductivity of sensible materials (often sensible water) to support the higher energy density of latent materials (often in the form of encapsulated PCM inclusions within the water storage tank) [54, 80-82]. In combination with storage tank designs that are optimised to facilitate higher levels of heat transfer, hybrid storage systems have the potential to perform better than either material individually, at the cost of greater system complexity.

2.2.3 Thermochemical storage materials

In thermochemical thermal energy storage devices, energy is stored by inducing a chemical reaction within the storage material itself. This process first involves utilising heat energy transferred from the heat supply to excite an endothermic chemical reaction within the storage medium, causing it to absorb heat energy into the storage device. This can then be reversed as an exothermic chemical reaction, allowing the storage device to release this stored heat energy back to the environment when desired [71].

In comparison to sensible and latent storage materials, thermochemical storage materials exhibit higher energy storage density and longer storage duration, requiring a significantly lower volume of storage medium with regards to the amount of energy capable of being stored. However, the development of thermochemical storage devices is limited with regards to domestic heat pump applications, and these technologies lack the widespread deployment of more commonly utilised sensible and latent storage devices [72, 83, 84].

2.2.4 Passive storage methods

In passive thermal energy storage methods, the structural mass and interior of the building itself is used as the storage medium, which both stores and releases heat energy in a non-controlled fashion [85]. The maximum amount of heat that can be retained by a particular building is dependent on the effective heat capacity of the overall structure, including walls, ceilings, floors, windows and doors; as well as the presence of any interior furnishings [86]. In comparison to active sensible or latent thermal energy storage methods, no additional costs or space is required to install passive storage methods, as the storage medium is effectively built into the structure of the building during its initial construction. As such, passive storage methods can be employed alongside active storage devices in order to increase the total amount of sensible mass that can be utilised to store heat energy. This compatibility can also be extended to latent storage materials by introducing hybrid thermal energy storage systems into the building's structure. Most structures with passive storage capabilities can be enhanced further by retrofitting pre-existing buildings with interior, internal or external insulation materials. However, these retrofitting processes may be limited, difficult or expensive for buildings that are legally protected due to their special architectural or historical significance.

Hedegaard et al. (2012) [87] studied the effects of different heat storage options to support the integration of variable renewable wind power alongside individual heat pump systems for non-district domestic heat in Denmark. A selection of detached houses based on the existing Danish building stock were modelled using an EnergyPLAN model to optimise the hour-by-hour operation of air source or ground source heat pump systems alongside various sizes of heat accumulation tanks and different levels of passive heat storage capabilities. The results of this study found that buildings with low to high levels of passive heat storage capabilities resulted in larger reductions in excess electricity production and fuel consumption in comparison to those utilising heat accumulation tanks. While the replacement of oil boilers

and electric heating systems with energy efficient heat pump systems was identified as the most important factor to reducing fuel consumption overall, passive heat storage methods were found to be a very cost-effective method to further reducing fuel costs relative to its initial investment costs.

Similarly, Reynders et al. (2013) [88] studied the potential of structural thermal mass to support electrical grid stability and demand-side management strategies for a domestic single family dwelling in Uccle, Belgium. A typical two-storey, ten room detached house equipped with an air source heat pump and supporting photovoltaic systems was modelled using Modelica and the IDEAS library. The effects of the structural thermal storage capacity were analysed for three different levels of insulation and two different lightweight and heavyweight variants of the structural mass of the construction, and was evaluated alongside predictive and non-predictive demand-side management strategies. The results of this model found that passive storage methods using the structural thermal storage capacity of the building were able to significantly reduce the electricity usage of the heat pump system during peak demand periods, with the highest reductions obtained using the non-predictive control strategy alongside high levels of insulation and the heavyweight building construction. However, this study also recommended the implementation of active control methods for regulating the temperature of the indoor environment, as using passive storage methods alone limited the thermal comfort boundaries of the building due to their inherently uncontrolled heat release mechanisms.

2.3 Renewable energy technologies and peak load shaving

Alongside heat pump and thermal energy storage technologies, renewable energy technologies are important to the decarbonisation of the domestic heating sector and the phasing out of fossil fuel-based heating systems. One of the main benefits of heat pump technologies is its ability to run entirely off of an electricity supply, which if generated using renewable energy sources could drastically reduce the total amount of CO_2 emissions produced annually on an individual or global scale [41, 89]. However, the nature of renewable energy sources such as wind and solar are inherently dependent on the current weather conditions and time of day to be effective. Wind power cannot be generated if the current windspeed is unable to rotate a turbine or so high as to potentially cause damage to the turbine’s structure or internal machinery. Solar power cannot be generated when the sun is absent during nighttime or when sufficient cloud cover or shade is present during daytime as

to obscure or block a solar panel from viewing direct sunlight. Other forms of renewable energy sources such as hydroelectric and geothermal rely on natural resources that greatly depend on their physical location, and as such are used less frequently. This problem also extends to electrical supply grids on a nationwide scale, as renewables-based energy sources are often unable to fully meet the demands of end users during peak periods, requiring additional electricity generation using non-renewable resources. As such, peak electricity tariffs are often more expensive than those available during off-peak periods. Furthermore, the performance of air source heat pump systems are largely dependent on the temperature of the surrounding air and typically experience reduced performance during nighttime or wintertime, further limiting the timeframe in which renewables-based electricity can be properly utilised. Therefore, additional control strategies and methods to regulate the supply and demand relationship between renewable energy sources and domestic heating systems must be implemented for heat pump technologies.

Peak load shaving is a form of demand side management (DSM) in which the electrical load of an appliance or dwelling is made consistent and near-constant by flattening load peaks and troughs over a specified period of time. This is achieved through the use of storage units, tanks or batteries to shift electrical or thermal loads from off-peak periods when the load demand is minimal to peak periods when the load demand is greatest. In the case of domestic heat pump systems, energy is most commonly stored in the form of heat in thermal energy storage tanks or other such storage mediums. The primary goals of peak load shaving are to create a uniform load profile that is easy to generate and predict for national energy providers and meets the full demands of the end users while also providing benefits to system performance, efficiency and running costs. Many examples of peak load shaving strategies for domestic heat pump systems can be found in literature, and representations of electricity usage and load patterns omitting and incorporating peak load shaving strategies can be found in figure 8.

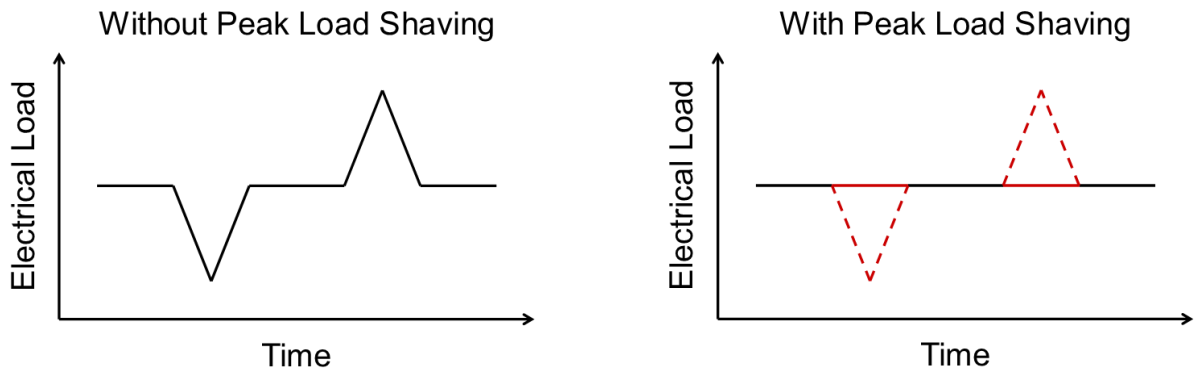

Figure 8: Representations of electricity usage and load patterns omitting (left) and incorporating (right) peak load shaving strategies.

Hedegaard and Balyk (2013) [86] studied an energy system investment model using heat pumps incorporating thermal energy storage in the form of storage tanks, active floor heat storage and passive building heat storage using the internal structure and furnishings. The Balmorel investment model was used to assess the impacts of how potential heat storage options could enable flexibility in order to optimise system investments and efficient operation. The model was demonstrated to be well suited for analysing the flexibility of heat pump systems, and found that prioritising heat pump operation during hours with lower electricity tariffs combined with peak load shaving strategies resulted in a reduction in the need for larger peak and reserve capacity investments.

Jin et al. (2023) [9] studied the energy and economic performance of an air source heat pump integrated with a latent heat thermal energy storage for peak demand shifting. An experimental air source heat pump latent heat thermal energy storage (ASHP LHTES) heating system was developed and iterated upon with regards to the volume fraction, setpoint temperature and phase-change temperature of the phase change material, in addition to various seasonal operation strategies. Simulation models found that the phase change material with a melting range of 40-50°C resulted in the best performance with regards to its energy efficiency and cost savings benefits, and the storage unit with a volume fraction of 75% PCM noticeably shifted heating loads to off-peak periods during wintertime. Furthermore, nighttime heating strategies successfully resulted in the flattening of peak loads, reducing running costs and minimising carbon emissions by 52.2%.

Agyenim and Hewitt (2010) [74] studied the development of a finned phase change material storage unit to take advantage of off-peak electricity tariffs for improving the cost of heat

pump operation. A longitudinally finned RT58 PCM storage unit was developed and experimentally tested to evaluate the heat transfer characteristics of RT58 (paraffin) within a domestic air source heat pump system. The results of this study showed a quadratic relationship between the heat transfer coefficient and the inlet heat transfer fluid temperature. Increasing the temperature of the heat transfer fluid at the inlet of the storage unit by 21.9% during charging resulted in increases to the heat transfer coefficient of 45.3% and 16.6% during charging and discharging respectively. The study concluded by stating that with sufficient improvements to the heat transfer of the storage unit, the size of the storage unit required for the flexible heating of common residential buildings in the UK could be reduced by up to 30%.

Cabrol and Rowley (2012) [78] studied the implementation of low carbon homes using building-integrated air source heat pump systems. A modern air source heat pump with a floor-embedded heating system was modelled using TRNSYS for various UK locations, and the effects of heat pump control during off-peak electricity tariff periods were analysed. The results of this model found that using a concrete floor slab as a heating system and thermal energy storage unit, in combination with external wall insulation, allowed for acceptable levels of thermal comfort during the heating season while operating solely during off-peak tariff periods, with better performance attainable using embedded phase change materials. For all cases assessed in this study, the implementation of an air source heat pump system in addition to peak load shaving control strategies was found to be highly efficient and cost-effective, significantly reducing operating costs and CO_2 emissions in comparison to an equivalent condensing gas boiler heating system.

In the flexible heat pump system, the integration of the thermal energy storage tank into an Evans-Perkins vapour compression cycle allows for the implementation of peak load shaving control strategies. By operating the heat pump system during off-peak tariff periods during daytime, the storage tank can be fully charged at a lower cost in comparison to charging it during peak tariff periods or during periods where more energy would be required to power the compressor due to low ambient air temperatures. This low-cost heat can then be stored for later use during these peak tariff or cold temperature periods in order to reduce the energy consumption of the system (and improve its overall performance in the case of the low temperature periods). This would result in a significant reduction in the long-term operating costs for the end user, as well as additional benefits in allowing for more consistent and stable electricity generation for national energy providers if the adoption of renewables-based heat pump systems becomes more widespread.

3 Methodologies

3.1 System overview and model development

The development of the flexible heat pump system was undertaken within the dynamic modelling and simulation package Dymola, developed by Dassault Systèmes [29]. This software and its component libraries, such as the Modelica standard library, are based on the Modelica language: an equation-based, object-oriented modelling language that supports both causal and acausal modelling. This allows for the development of complex models using a graphical and hierarchical approach, allowing models to be constructed from standard form physical equations with separate, automatically generated simulation code. Additional thermodynamic and data interpretation components were obtained from the TIL Suite component library developed by TLK-Thermo [90, 91] and the ExternData component library developed by Modelica 3rd Party Libraries [92, 93].

The main assumptions for the simulation of the flexible heat pump system are as follows:

1. The heat exchangers and the thermal energy storage tank operate under isothermal heat transfer conditions.
2. The compressor operates with 100% isentropic efficiency.
3. No heat or pressure losses occur through any pipes or heat exchangers.
4. The condenser operates with near-constant heating capacity, with minor variations due to mode switching fluctuations.
5. The thermal energy storage tank operates with 100% round trip efficiency, with minor heat losses to the surrounding environment when the storage tank is idle.

The development lifespan of the flexible heat pump model for model versions V1 through V9 can be described as follows:

V1 (figure 9) is a standard heat pump model comprising of a compressor, an expansion valve and two heat exchangers (an evaporator and a condenser). An additional separator component has been added directly after the evaporator to improve the fluid flow characteristics of the system and to eliminate any incompressible phases from entering the compressor. This model represents the absolute minimum number of components required to simulate a heat pump system within a dynamic simulation environment.

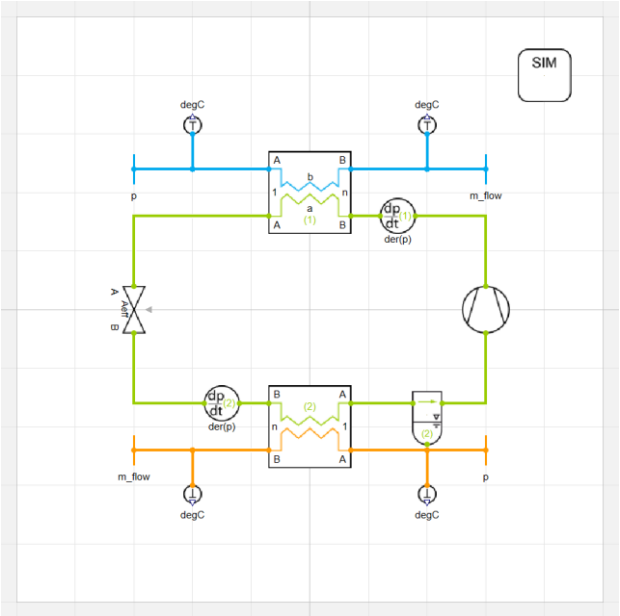

Figure 9: Diagram view of the FlexHeatPump_V1 model within Dymola.

V2 (figure 10) is a standard heat pump model and an extension of the V1 model. This model incorporates a compressor control system that automatically modifies the rotational speed of the compressor with regards to the measured and desired values of the condenser outlet water temperature. This allows the compressor to automatically vary its operation in order to meet the desired condenser outlet water temperature as specified by the parameter cond_setpoint, which would be specified by the end user through an external thermostatic control interface.

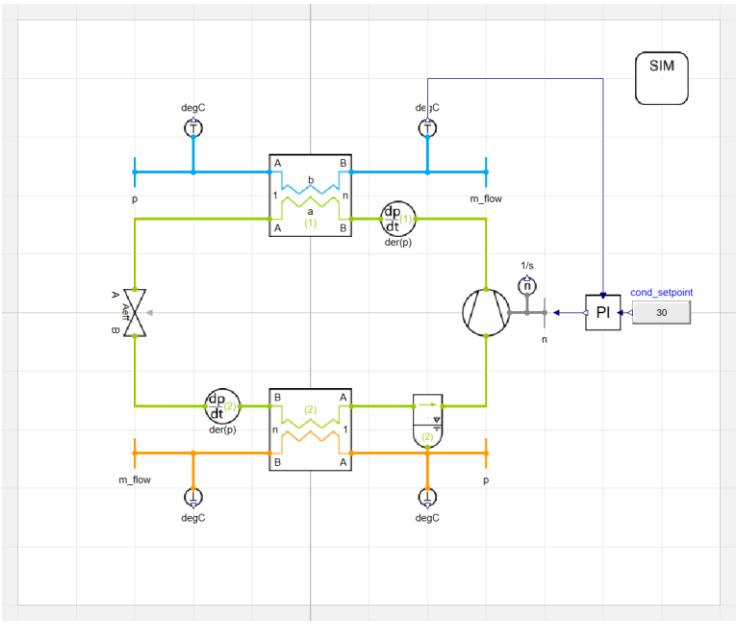

Figure 10: Diagram view of the FlexHeatPump_V2 model within Dymola.

V3 (figure 11) is a standard heat pump model and an extension of the V2 model. This model incorporates an additional third heat exchanger (a subcooler) directly after the condenser to facilitate heat recovery from the warm refrigerant exiting the condenser.

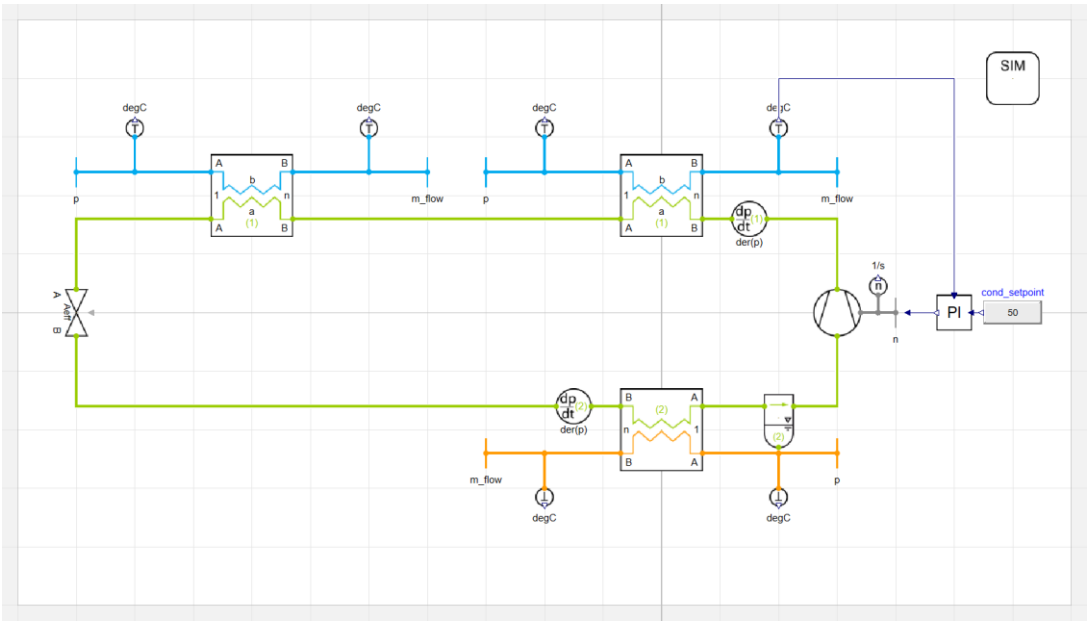

Figure 11: Diagram view of the FlexHeatPump_V3 model within Dymola.

V4 (figure 12) is a standard heat pump model and an extension of the V3 model. This model replaces the two liquid boundaries at the water side inlet and outlet ports of the subcooler with a subsystem representing the thermal energy storage tank. The volume of the thermal energy storage tank is represented by a fluid volume connected alongside an expansion tank and a circulation pump to facilitate continuous heat transfer between the refrigerant loop and the storage loop via the subcooler. This allows the heat pump model to recover and store excess thermal energy before it is lost through the expansion valve, and in effect simulates the default charging mode of the flexible heat pump system.

Additionally, V4_altTank (figure 13) is an alternative version of the standard V4 model that utilises a tube component fluidly and thermodynamically connected in place of the fluid volume component to isolate the fluid volume from the storage loop. This allows the system to utilise different fluid mediums for the thermal energy storage and the storage loop, allowing the heat transfer rate and energy density of the thermal energy storage to be varied and optimised across a variety of different fluid selections.

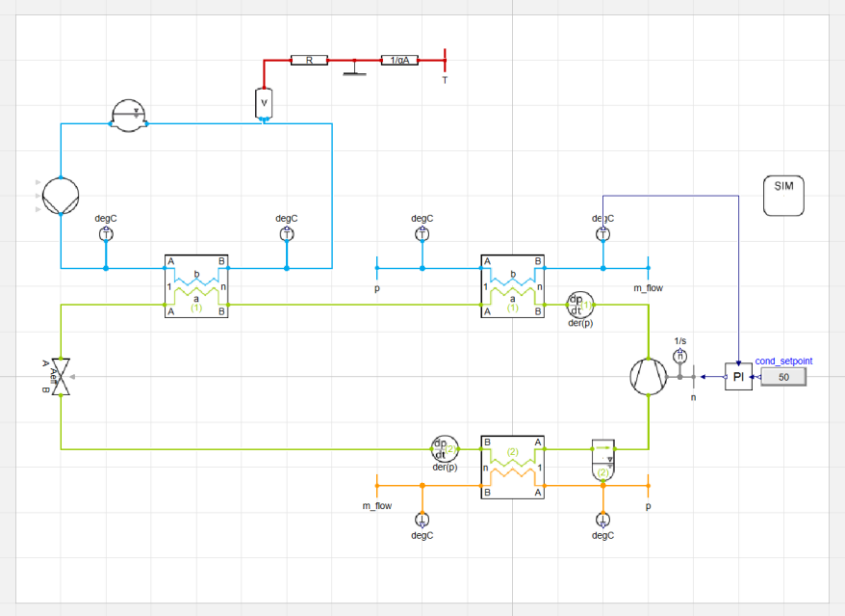

Figure 12: Diagram view of the FlexHeatPump_V4 model within Dymola.

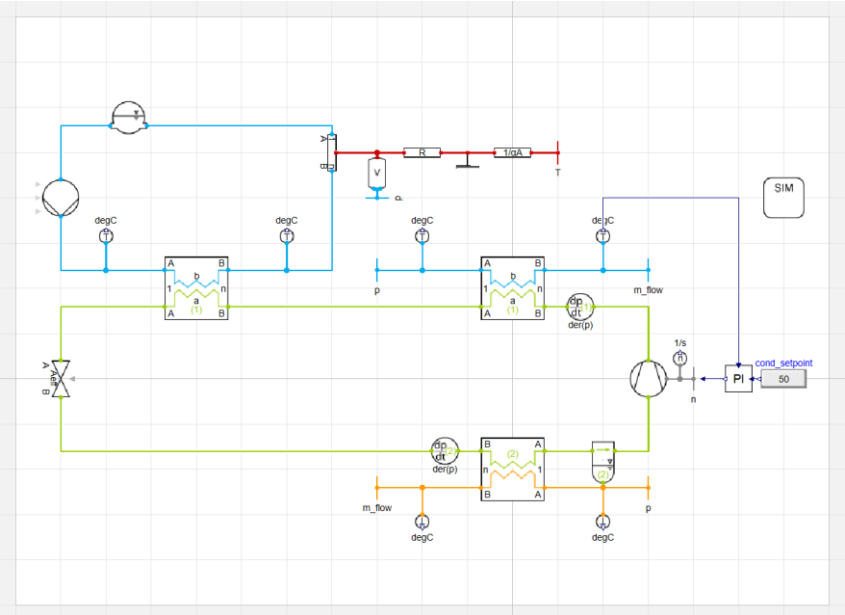

Figure 13: Diagram view of the FlexHeatPump_V4_altTank model within Dymola.

V5 is the first iteration of the flexible heat pump model and an extension of the V4 model. This model enables the mode switching functionality of the flexible heat pump system and has been subdivided into two smaller models due to the significant number of adaptations required: V5a (which included only the four-way valve) (figure 14) and V5b (which included both the four-way valve and the three-way valve) (figure 15). Depending on the manually selected input signals supplied to the four-way and three-way valves, the model can switch between the charging, discharging and defrosting modes required by the flexible heat pump system during operation.

Additionally, V5b_altValve (figure 16) is an alternative version of the standard V5b model that replaces the singular three-way valve component with a pair of three-way valves at each fluid junction surrounding the evaporator. In doing so, this completely isolates the evaporator during discharging mode operations and prevents simulation errors from occurring due to undesired fluid flows entering valve ports that have otherwise been disabled. This model was found to have significantly improved performance over the standard V5b model and it was decided that this model would be carried forward into the later development stages.

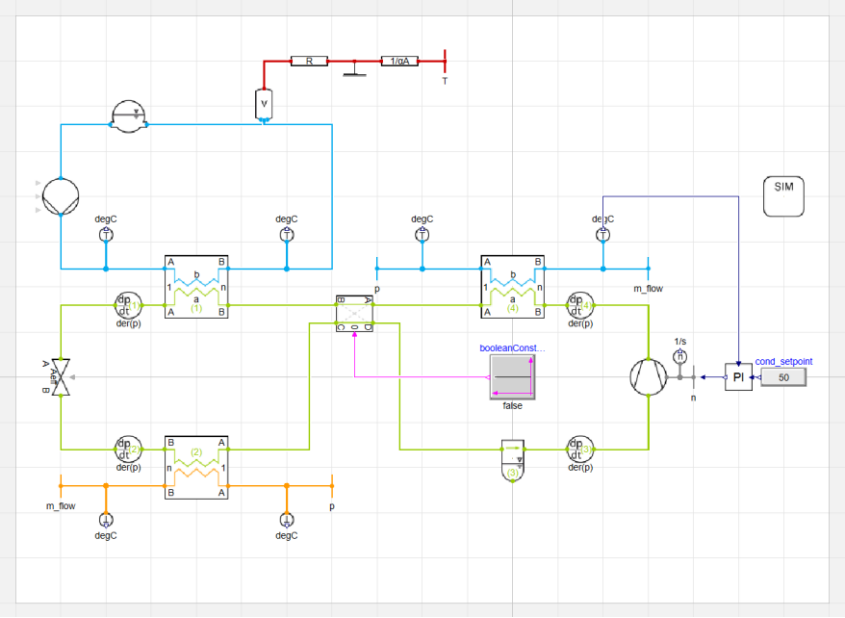

Figure 14: Diagram view of the FlexHeatPump_V5a model within Dymola.

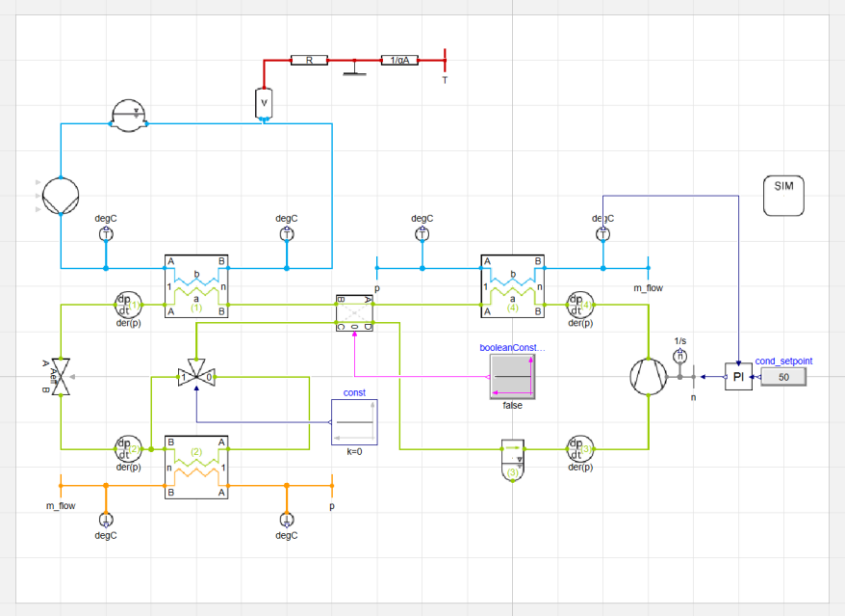

Figure 15: Diagram view of the FlexHeatPump_V5b model within Dymola.

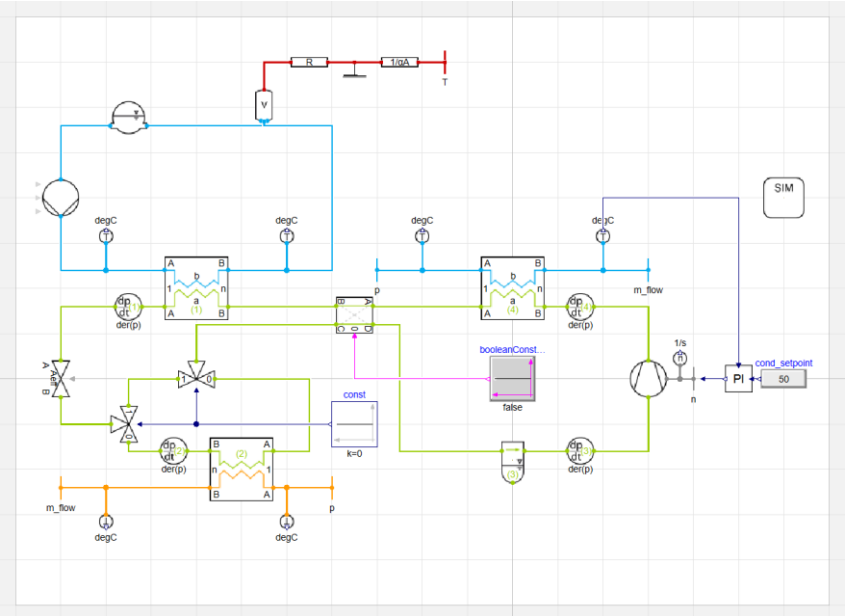

Figure 16: Diagram view of the FlexHeatPump_V5b_altValve model within Dymola.

V6 (figure 17) is the second iteration of the flexible heat pump model and an extension of the V5b_altValve model. This model expands upon the flexible mode switching functionality of the previous model by implementing a temperature-based control system to automatically switch between the three operational modes of the heat pump without requiring any external user input. This model also implements a secondary temperature-based control system for the thermal energy storage tank to prevent any unnecessary discharging or overcharging during

operation. For the purposes of model development, the V6 and V6_tempControl (figure 18) models represent the systems using manual and automatic (temperature-based) mode switching functionality respectively.

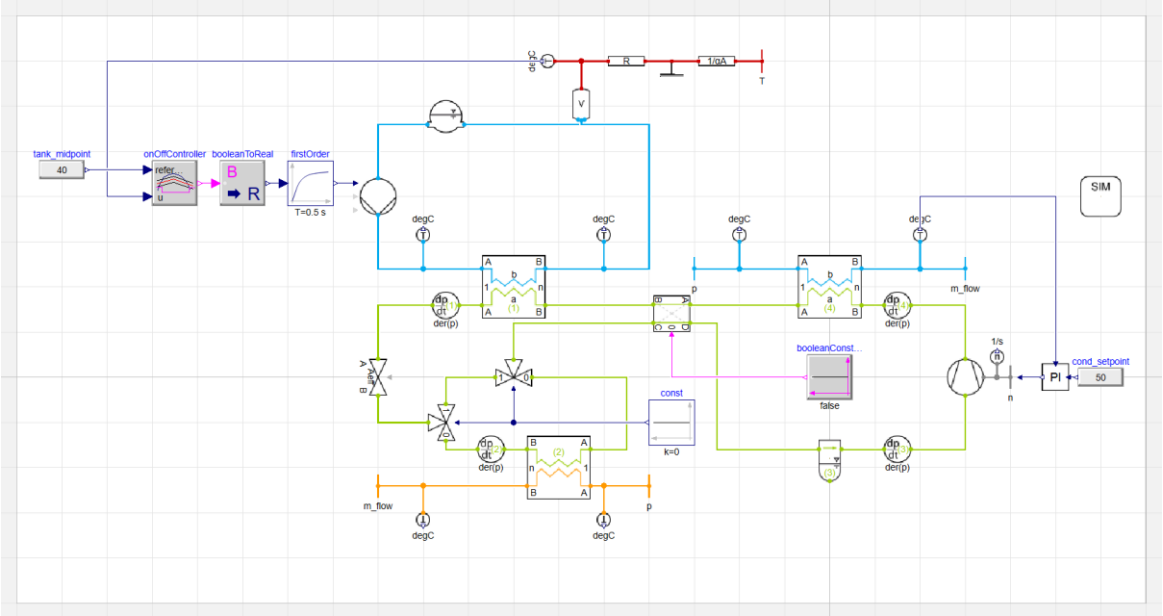

Figure 17: Diagram view of the FlexHeatPump_V6 model within Dymola.

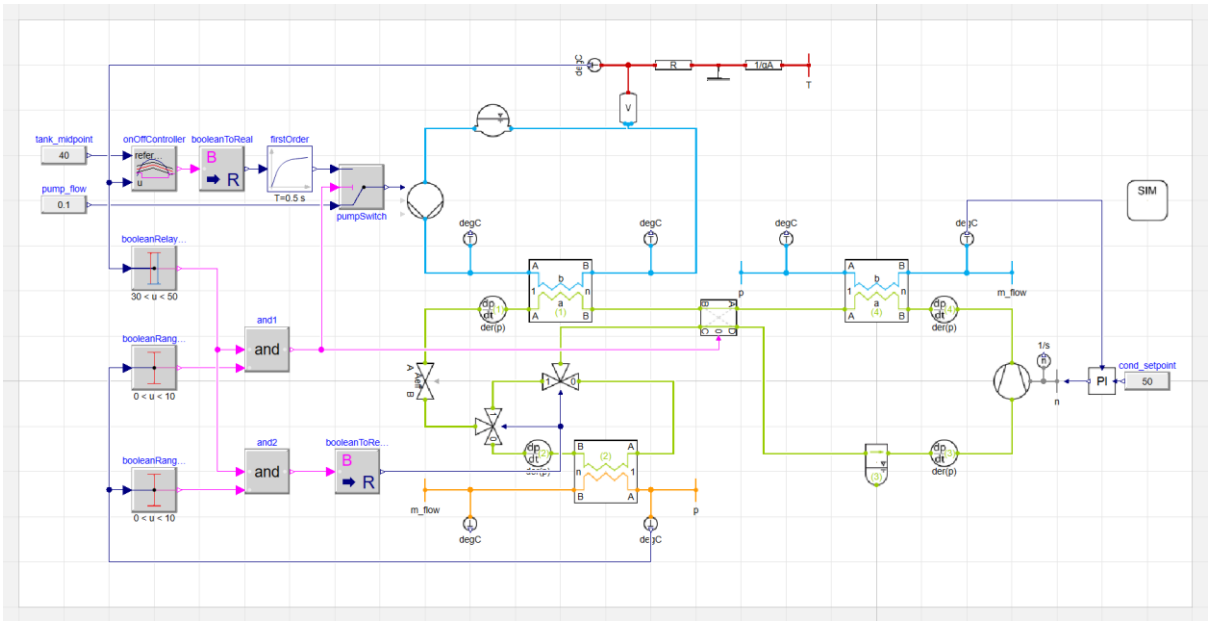

Figure 18: Diagram view of the FlexHeatPump_V6_tempControl model within Dymola.

V7 (figure 19) is the third iteration of the flexible heat pump model and an extension of the V6_tempControl model. This model replaces the prescribed fixed temperature value of the evaporator inlet air boundary with temperature inputs from an external data table. These inputs can be delivered in a variety of file formats, such as comma-separated delimited values (.csv) and Excel spreadsheets (.xls / .xlsx), and can be interpreted, extrapolated and smoothened by the system before being properly utilised. This allows the flexible heat pump model to operate under realistic ambient temperature profiles based on historical weather data records, as opposed to an idealised model operating under constant laboratory conditions.

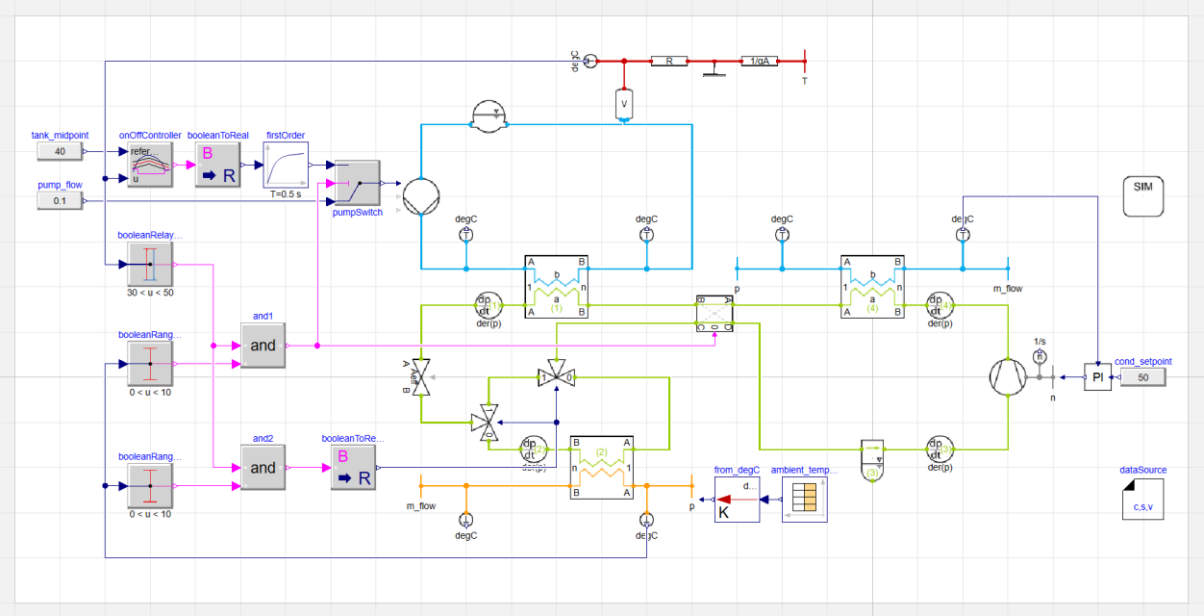

Figure 19: Diagram view of the FlexHeatPump_V7 model within Dymola.

V8 (figure 20) is the fourth iteration of the flexible heat pump model and an extension of the V7 model. This model replaces the example parameters and geometries of the compressor, the expansion valve, the three heat exchangers (the evaporator, the condenser and the subcooler) and the fluid volume with manufacturers data for components normally found and in use within current domestic air source heat pump systems. As such, this model more accurately reflects the realistic performance of the flexible heat pump system in comparison to previous models.

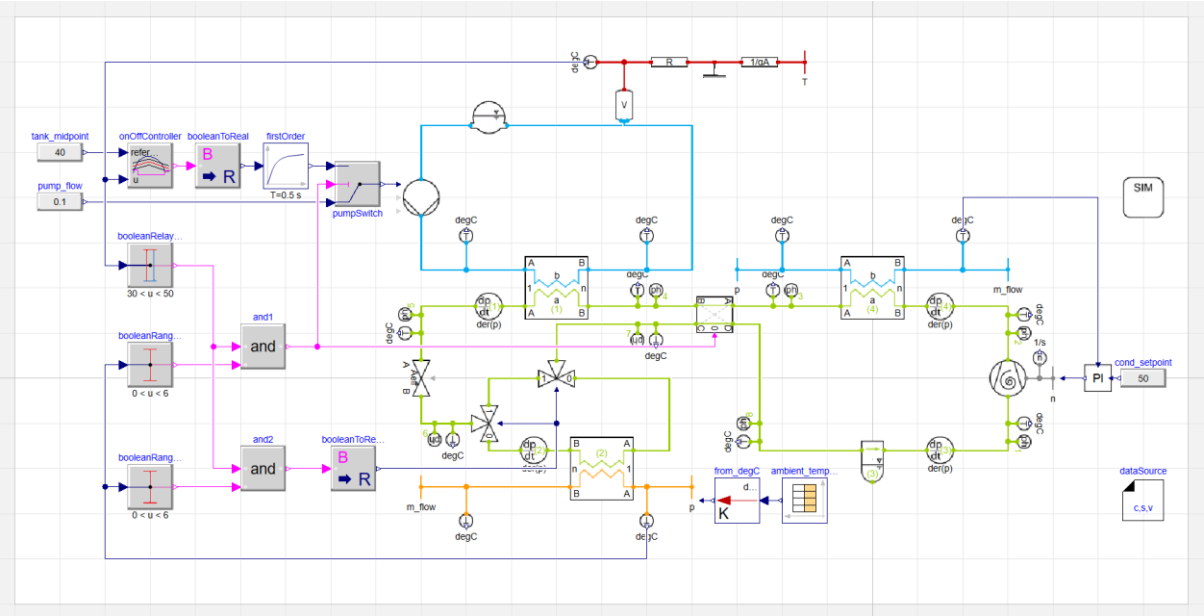

Figure 20: Diagram view of the FlexHeatPump_V8 model within Dymola.

V9 (figure 21) is the fifth iteration of the flexible heat pump model and an extension of the V8 model. This model further improves upon the previous iteration by introducing a series of pipe components of negligible effect and size in order to improve the initialisation of the fluid pressure states within the refrigerant loop. Two of these pipe components have been implemented in this model: one between the first three-way valve and port C of the four-way valve for the fluid path that is utilised during all three operational modes, and one between the two three-way valves for the fluid path that is utilised only during the discharging mode to bypass the evaporator. In doing so, this improves the computation of the pressure states between each set of valve components and prevents simulation errors from occurring due to two valves components directly neighbouring each other. This is the final and most recent version of the flexible heat pump model currently in development and this model will be used and iterated upon for all simulations mentioned in this report hereafter. The complete Modelica code for this model can be found in appendix 1.

Additionally, two alternative versions of the V9 model, V9_altCompressor (which included a geometry-based scroll compressor model) (figure 22) and V9_altTank (which included the alternative tank charging configuration previously explored in the V4_altTank model) (figure 23) were also considered during development. These models may be redeveloped and iterated upon in the future, but are otherwise not included in the analysis of the flexible heat pump system at this time.

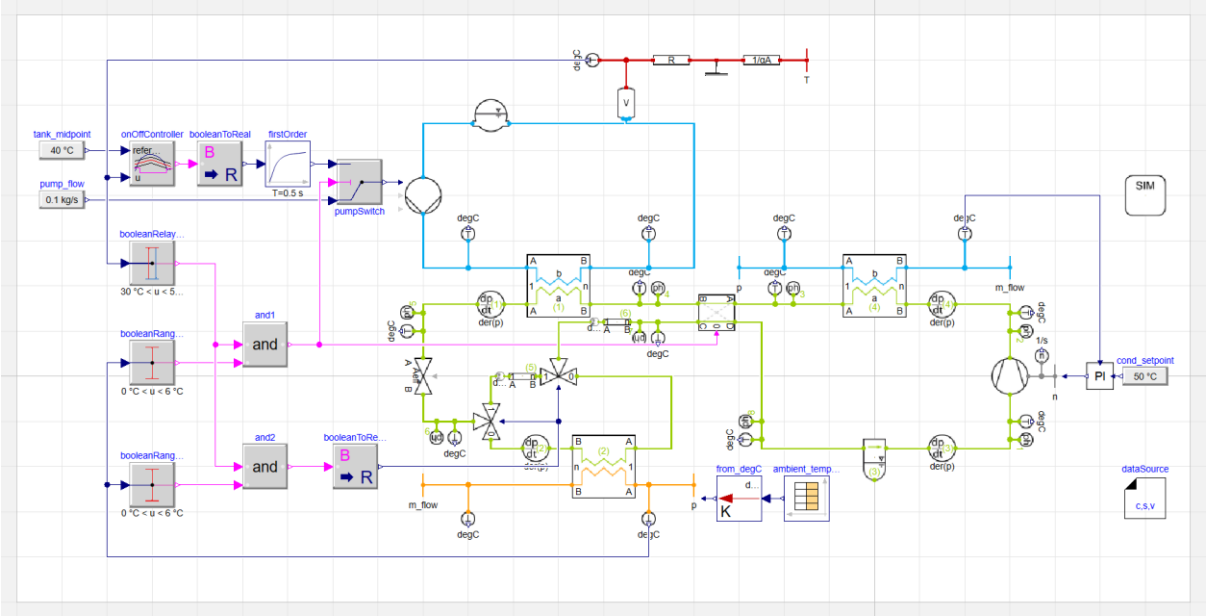

Figure 21: Diagram view of the FlexHeatPump_V9 model within Dymola.

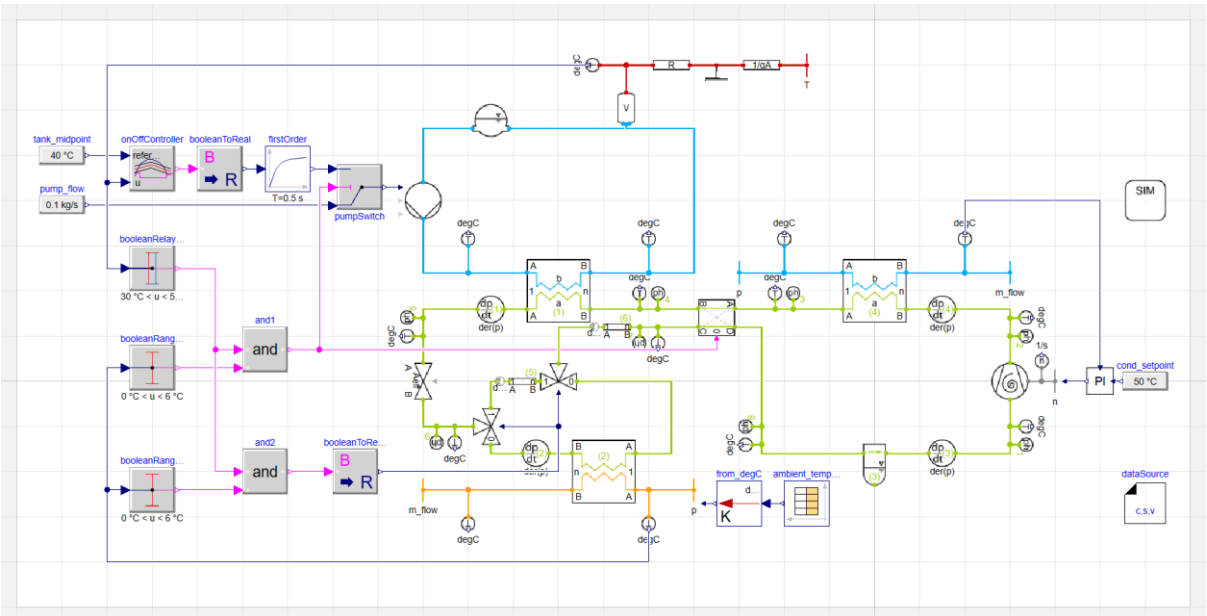

Figure 22: Diagram view of the FlexHeatPump_V9_altCompressor model within Dymola.

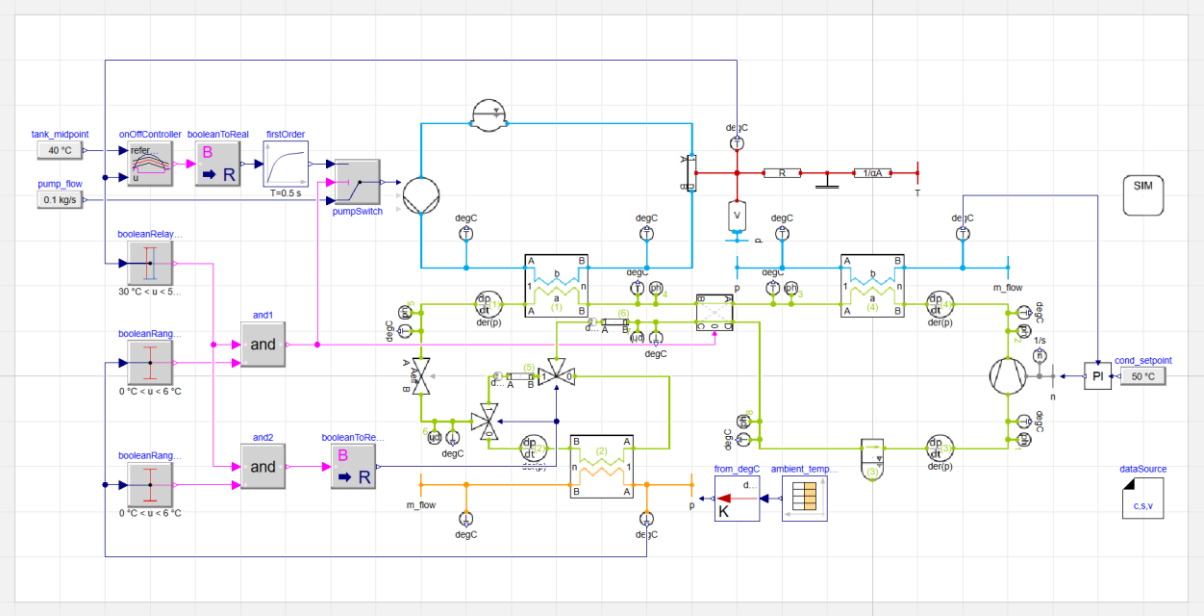

Figure 23: Diagram view of the FlexHeatPump_V9_altTank model within Dymola.

3.2 Components

3.2.1 Evaporator

The air-refrigerant evaporator has been modelled as a fin and tube heat exchanger component and was obtained from the TIL Suite component library. This component was arranged in a counterflow arrangement to increase heat transfer between the ambient air stream and the refrigerant loop. During initialisation, the initial wall temperature of the fin and tube heat exchanger was set equal to the initial value of the ambient air source boundary in order to improve heat transfer and simulate an initial state of thermal equilibrium. The geometries and parameterisations of this component for the Dymola simulation models were based on the manufacturer's specifications for the C16x16 heat exchanger model by VEVOR [94] and can be found in table 6.

Table 6: Parameters of the fin and tube evaporator heat exchanger defined within Dymola.

Parameter	Value
Length of finned tubes (m)	0.406
Number of serial tubes	3
Distance between serial tubes (m)	0.02159
Number of parallel tubes	16
Distance between parallel tubes (m)	0.02391
Thickness of fins (m)	0.00109
Distance between fins (m)	0.00212
Inner diameter of tube (m)	0.009525
Thickness of tube walls (m)	0.000889
Number of parallel tube side flows	4
Number of discretisation cells	5
Tube side heat transfer model	Constant Alpha (α = 2000 K/W)
Tube side pressure drop model	Zero Pressure Drop
Wall material	Copper
Wall heat conduction model	Geometry Based Conduction
Fin material	Aluminium
Fin efficiency model	Constant Fin Efficiency
Fin side heat transfer model	Constant Alpha (α = 2000 K/W)
Fin side pressure drop model	Zero Pressure Drop

3.2.2 Condenser

The refrigerant-water condenser has been modelled as a plate heat exchanger component and was obtained from the TIL Suite component library. This component was arranged in a counterflow arrangement to increase heat transfer between the refrigerant loop and the water supply stream. During initialisation, the initial temperature all liquid cells in the plate heat exchanger were set equal to the initial value of the water supply source boundary in

order to improve heat transfer and simulate an initial state of thermal equilibrium. The geometries and parameterisations of this component for the Dymola simulation models were based on the manufacturer's specifications for the B8LAS heat exchanger model by SWEP [95] and can be found in table 7.

Table 7: Parameters of the plate condenser heat exchanger defined within Dymola.

Parameter	Value
Total number of plates	70
Plate length (m)	0.278
Plate width (m)	0.0762
Plate angle (°)	31
Wall thickness (m)	0.75×10^{-3}
Pattern amplitude (m)	2×10^{-3}
Pattern wavelength (m)	12.6×10^{-3}
Number of discretisation cells	5
Side A heat transfer model	Constant Alpha (α = 2000 K/W)
Side A pressure drop model	Zero Pressure Drop
Side B heat transfer model	Constant Alpha (α = 2000 K/W)
Side B pressure drop model	Zero Pressure Drop
Wall material	Stainless Steel
Wall heat conduction model	Geometry Based Conduction

3.2.3 Subcooler

The refrigerant-water subcooler has been modelled as a tube and tube heat exchanger component and was obtained from the TIL Suite component library. This component was arranged in a counterflow arrangement to increase heat transfer between the refrigerant loop and the water storage loop. During initialisation, the initial temperature all liquid cells in the tube and tube heat exchanger were set equal to the initial value of the thermal energy storage tank in order to improve heat transfer and simulate an initial state of thermal equilibrium. The geometries and parameterisations of this component for the Dymola simulation models were based on the manufacturer's specifications for a component provided by the University of Liverpool and can be found in table 8.

Table 8: Parameters of the tube and tube subcooler heat exchanger defined within Dymola.

Parameter	Value
Length A (m)	0.6
Number of parallel tubes A	70
Inner diameter of circular tube A (m)	0.005
Length B (m)	0.6
Number of parallel tubes B	70
Inner diameter of circular tube B (m)	0.005
Number of discretisation cells	5
Tube side heat transfer model A	Constant Alpha (α = 2000 K/W)
Tube side pressure drop model A	Zero Pressure Drop
Tube side heat transfer model B	Constant Alpha (α = 2000 K/W)
Tube side pressure drop model B	Zero Pressure Drop
Thermal resistance (K/W)	6×10^{-5}
Mass of wall (kg)	6
Wall material	Copper

3.2.4 Compressor

The compressor has been modelled as an efficiency-based compressor component and was obtained from the TIL Suite component library. The variable speed of the compressor is dictated by the compressor control system during operation, and the displacement of the compressor was declared to be a constant fixed value of 2.1×10^{-5} m^3. The parameterisations of this component for the Dymola simulation models were based on the manufacturer's specifications for the EDTN210D32EFZ Hermetic Rotary DC Inverter model by Area Cooling Solutions [96], which was provided by the University of Liverpool and can be found in table 9.

Table 9: Parameters of the efficiency-based compressor defined within Dymola.

Parameter	Value
Speed (Hz)	Variable (12-120)
Displacement (m^3)	2.1×10^{-5}
Effective flow area for pressure loss at suction port (m^2)	1.309×10^{-4}
Effective flow area for pressure loss at discharge port (m^2)	5.15×10^{-5}
Effective flow area for internal leakage (m^2)	0.7×10^{-7}
Volume of suction chamber (m^3)	4.2×10^{-5}
Volume of discharge chamber (m^3)	3.15×10^{-5}
Volumetric efficiency	1
Isentropic efficiency	1
Effective isentropic efficiency	1

3.2.5 Expansion Valve

The expansion valve has been modelled as an orifice valve component and was obtained from the TIL Suite component library. The effective flow area of the valve was declared to be a constant fixed value of 0.7×10^{-6} m^2 and calculates the correlation between the mass flow rate and the pressure drop of the refrigerant fluid using the Bernoulli flow principle:

$$\dot{m}_r = A_{eff}\sqrt{\Delta p \cdot 2\rho_r} \tag{51}$$

$$A_{eff} = K_v \sqrt{\frac{\rho_{nominal}}{2\Delta p_{nominal}}} \tag{52}$$

Where $\dot{m}_r$ is the mass flow rate of the refrigerant fluid (kg/s), A_{eff} is the effective flow area of the valve (m^2), Δp is the fluid pressure difference between the inlet and outlet of the valve (Pa), ρ is the fluid density (kg/m^3) and K_v is the flow coefficient of the valve.

As the fluid flow within the refrigerant loop reverses in direction during the discharging and defrosting modes, this model was also parameterised to allow fluid flow in either direction (A-B or B-A).

3.2.6 Thermal Energy Storage

The thermal energy storage has been modelled as a fluid volume component and was obtained from the TIL Suite component library. Additionally, a subsystem of other TIL Suite components consisting of a heat resistor, a heat capacitor, a convective resistor and a thermal boundary connected in series were utilised in order to simulate the heat conduction through the walls of the storage tank casing, the thermal mass of the storage tank casing, the heat convection to the ambient air and the ambient air thermal sink respectively (figure 24). The parameterisations of these components for the Dymola simulation models were based on the manufacturer's specifications for the Megaflo Eco Indirect 210i tank model by Heatrae Sadia [97] and can be found in table 10.

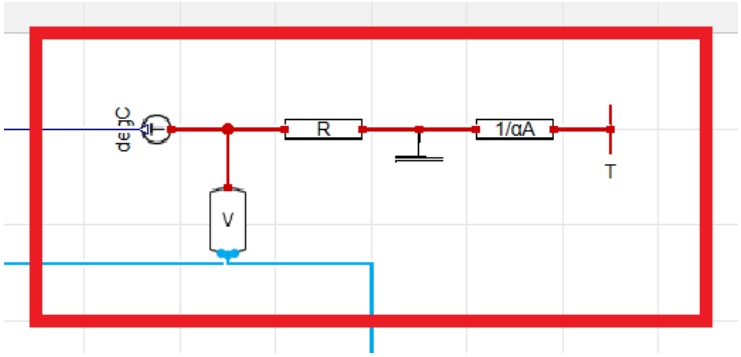

Figure 24: Diagram view of the storage tank fluid volume and thermal subsystem from the FlexHeatPump_V9 model within Dymola.

Table 10: Parameters of the storage tank fluid volume and thermal subsystem (for the default 210i configuration) defined within Dymola.

Parameter	Value
Size of fluid volume (l)	210
Length of cylinder (m)	1.486
Inner diameter of cylinder (m)	0.579
Wall material	Stainless Steel with Polyurethane Foam insulation
Mass of tank casing (kg)	47
Thickness of tank casing (m)	0.06
Thermal conductivity of the tank casing (W/(m.K))	0.03
Convection heat transfer model	Cylinder Forced Convection Cross Flow
Fixed flow velocity for forced convection (m/s)	0.1

In addition to the default configuration, a series of model iterations that focus on the performance and behaviours of the flexible heat pump model using a variety of different storage tank sizes (ranging from 70l to 300l in internal volume) were also considered as part of this research. The manufacturer's specifications for the different storage tank sizes included in this product range can be found in table 11.

Table 11: Parameters of the storage tank fluid volume and thermal subsystem (for the model iterations varying the tank size) defined within Dymola.

Parameter	**Value**						
Model	**70i**	**125i**	**145i**	**170i**	**210i**	**250i**	**300i**
Size of fluid volume (l)	70	125	145	170	210	250	300
Length of cylinder (m)	0.802	1.102	1.229	1.384	1.486	1.738	2.053
Inner diameter of cylinder (m)	0.579						
Wall material	Stainless Steel with Polyurethane Foam insulation						
Mass of tank casing (kg)	25	31	35	43	47	54	60
Thickness of tank casing (m)	0.06						
Thermal conductivity of the tank casing (W/(m.K))	0.03						
Convection heat transfer model	Cylinder Forced Convection Cross Flow						
Fixed flow velocity for forced convection (m/s)	0.1						

3.3 Control systems

3.3.1 Compressor controls

The scroll compressor used in the refrigerant loop of the heat pump system is controlled through a single PI controller used to adjust the compressor speed (measured in Hz or rps) and, by extension, the mass flow rate of the refrigerant fluid. The PI controller accepts a setpoint input signal u_s from the real expression cond_setpoint and a measurement input signal u_m from a temperature sensor measuring the condenser outlet water temperature. The real expression cond_setpoint represents the desired condenser outlet water temperature as specified by the end user, which in this instance has been designated as 50°C. The proportional gain of the PI controller k was set to 0.06, with a time constant Ti of 0.1s. In line with the specifications of the compressor model, the upper and lower limits of the PI controller output yMax and yMin were set to 120 Hz and 12 Hz respectively, with an initial output yInitial of 25 Hz during initialisation. This control system (figure 25) allows the heat pump to automatically adapt to any changes in the supply temperature of the refrigerant fluid entering the compressor from the evaporator (or from the subcooler in the cases of the discharging and defrosting modes) in order to continuously meet the desired condenser outlet water temperature.

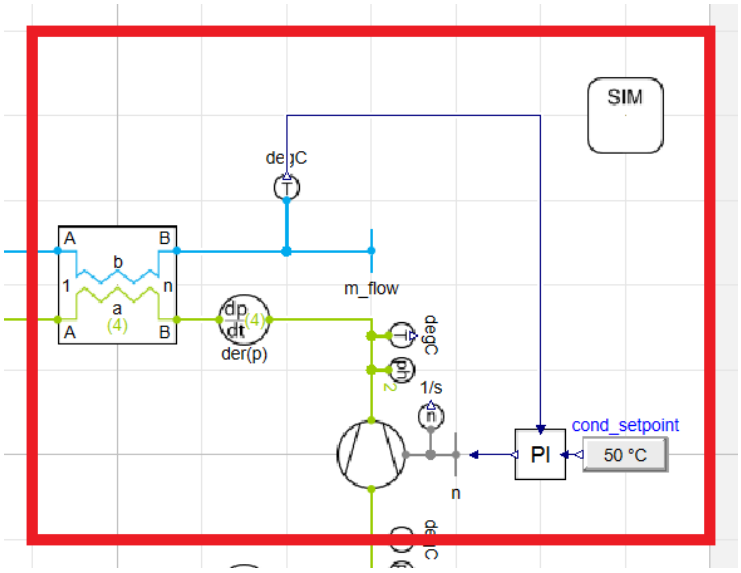

Figure 25: Diagram view of the compressor control system from the FlexHeatPump_V9 model within Dymola.

3.3.2 Mode switching

In these simulation models, the operational modes of the flexible heat pump system are controlled through altering the positions of the four-way and three-way valves as originally described by Yu et al. (2022) [15]. This control system is shown in figure 26.

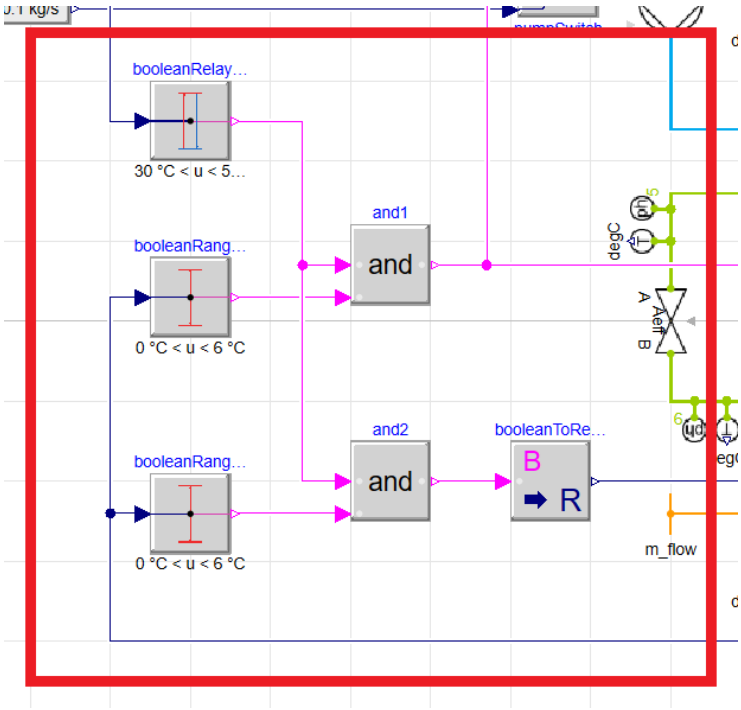

Figure 26: Diagram view of the temperature-based mode switching control system from the FlexHeatPump_V9 model within Dymola.

The four-way valve component fourWayValve was obtained from the TIL Suite component library (figure 27). This model consists of four fluid ports A, B, C and D that are fluidly connected to each other depending on the value of the boolean input signal crossedConnection_in. If the value of the input signal crossedConnection_in is equal to TRUE, port A and port C are fluidly connected to one another, as are port B and port D. Otherwise, if the value of the input signal crossedConnection_in is equal to FALSE, port A and port B are fluidly connected to one another, as are port C and port D. This allows the fluid flow entering port A from the outlet of the condenser to become reversed through the evaporator, the subcooler and the expansion valve depending on the currently active fluid connections to either port B (in charging mode) or port C (in discharging and defrosting modes). Furthermore, it is impossible to fluidly connect ports A and D and ports B and C together in any configuration.

Similarly, the three-way valve component linearDirectionalControlValve was also obtained from the TIL Suite component library (figure 28). This model consists of three fluid ports A, B and C that are fluidly connected to each other depending on the value of the real input signal switchingPosition_in. If the value of the input signal switchingPosition_in is equal to one, port A and port C are fluidly connected to one another, and port B is disabled. Otherwise, if the value of the input signal switchingPosition_in is equal to zero, port A and port B are fluidly connected to one another, and port C is disabled. This allows the fluid flow entering port A from either of the two interconnected three-way valves to either enter (in charging or defrosting modes) or bypass (in discharging mode) the evaporator, connecting or isolating it from the rest of the system respectively. Furthermore, it is impossible to fluidly connect ports B and C together in any configuration.

As the three-way valve is unable to accept an external input signal that is boolean in nature, a boolean-to-real component from the Modelica standard library has been used as an intermediary to convert these signals into a format that can be read by the three-way valve components. For this intermediary system, a boolean input of TRUE produces a real output value of one, whereas a boolean input of FALSE produces a real output value of zero. Additionally, the three-way valve components can also be controlled internally through the parameter switchingPositionFixed if the connection to the external input signal is disabled.

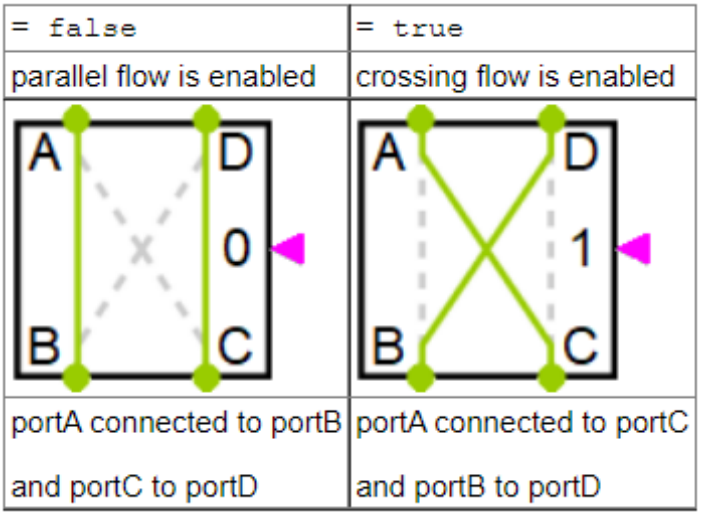

Figure 27: Component icon and diagram detailing the function of the four-way valve component from the TIL Suite component library within Dymola.

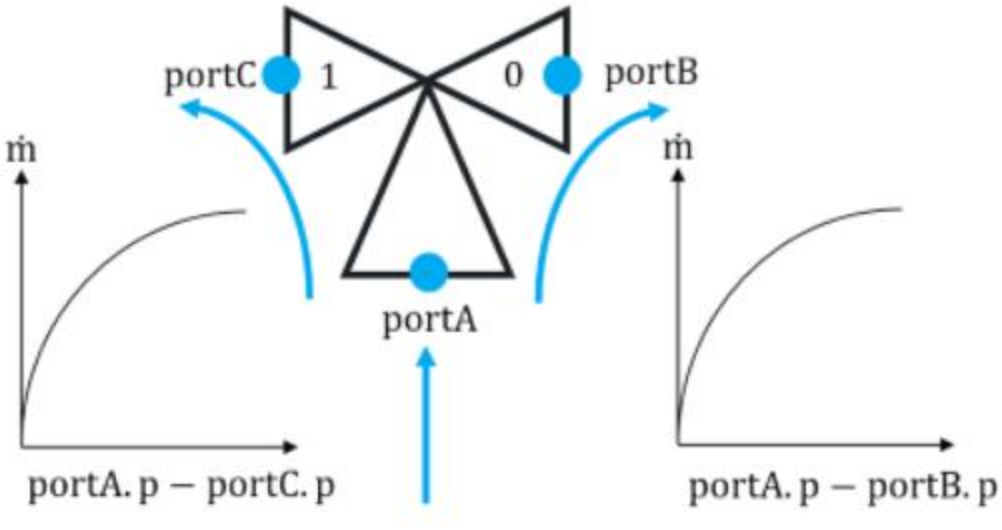

Figure 28: Component icon and diagram detailing the function of the three-way valve component (using a pressure drop model based on Bernoulli's flow correlation) from the TIL Suite component library within Dymola.

In order to facilitate the desired mode switching functionality of the flexible heat pump system, two custom components were created and implemented as part of the temperature-based control system: RangeSwitch and RelaySwitch. These components were created using the Modelica language and exist as individual component models that can be utilised, duplicated or extended in future simulation models. More in-depth information about how these components work can be found in section 3.3.4, as well as in each component's documentation view within Dymola.

The component booleanRangeSwitch1 accepts a measurement input signal from a temperature sensor measuring the evaporator inlet air temperature and produces output signal values of FALSE, TRUE and TRUE for hot, cold and freezing ambient air temperatures respectively. In these simulation models, a hot environment is considered to be any environment with an ambient air temperature of 6°C or higher, whereas a freezing environment is considered to be any environment with an ambient air temperature of 0°C or lower (which is equal to the freezing point of liquid water). Therefore, a cold environment is considered to be any environment with an ambient air temperature greater than 0°C and lower than 6°C. Similarly, the component booleanRangeSwitch2 also uses this same input from the evaporator inlet air temperature and produces outputs signal values of FALSE, TRUE and FALSE for the same set of environmental conditions. For the thermal energy storage tank, the component booleanRelaySwitch accepts a measurement input signal from a temperature sensor measuring the thermal storage tank temperature and outputs a signal value of TRUE for a storage tank temperature greater than 50°C (or when the tank is discharging from 50°C to 30°C) and a signal value of FALSE for a storage tank temperature lower than 30°C (or when the tank is charging from 30°C to 50°C) The output signals from these three logical components are then inputted into a set of two AND blocks to determine the correct signal values to be sent to the multi-directional valves. This results in six possible unique temperature profiles that could be used to dictate the required arrangements and flow directions of components within the system.

Details of the control logic required for the temperature-based mode switching control system can be found in table 12-14.

Table 12: Table detailing the control logic and intended operating conditions for the temperature-based mode switching and pump switching control systems.

	$T_{evap} \geq 6°C$	$0°C < T_{evap} < 6°C$	$T_{evap} \leq 0°C$
$T_{tank} \geq 50°C$	IDLE CHARGING • Ambient air is hot • TES is charged • Ambient air is used over the TES • TES uses the on/off charging controls	DISCHARGING • Ambient air is cold • TES is charged • TES is used over the ambient air • TES is discharged at a constant rate	DEFROSTING • Ambient air is freezing • TES is charged • TES is used over the ambient air • TES is discharged at a constant rate
$T_{tank} \leq 30°C$	OPTIMAL CHARGING • Ambient air is hot • TES is discharged • Ambient air is used over the TES • TES uses the on/off charging controls	SUBOPTIMAL CHARGING • Ambient air is cold • TES is discharged • TES cannot be used, defaults to ambient air • TES uses the on/off charging controls	DETRIMENTAL CHARGING • Ambient air is freezing • TES is discharged • TES cannot be used, defaults to ambient air • TES uses the on/off charging controls

Table 13: Table detailing the control logic for the temperature-based mode switching and pump switching control systems for the four-way valve and the circulation pump.

	$T_{evap} \geq 6°C$ FALSE		$0°C < T_{evap} < 6°C$ TRUE		$T_{evap} \leq 0°C$ TRUE	
$T_{tank} \geq 50°C$ TRUE	FALSE	TRUE	TRUE	TRUE	TRUE	TRUE
	FALSE (CHARGING)		TRUE (DISCHARGING)		TRUE (DEFROSTING)	
$T_{tank} \leq 30°C$ FALSE	FALSE	FALSE	TRUE	FALSE	TRUE	FALSE
	FALSE (CHARGING)		FALSE (CHARGING)		FALSE (CHARGING)	

Table 14: Table detailing the control logic for the temperature-based mode switching and pump switching control systems for the three-way valves.

	$T_{evap} \geq 6°C$ FALSE		$0°C < T_{evap} < 6°C$ TRUE		$T_{evap} \leq 0°C$ FALSE	
$T_{tank} \geq 50°C$ TRUE	FALSE	TRUE	TRUE	TRUE	FALSE	TRUE
	FALSE = 0 (CHARGING)		TRUE = 1 (DISCHARGING)		FALSE = 0 (DEFROSTING)	
$T_{tank} \leq 30°C$ FALSE	FALSE	FALSE	TRUE	FALSE	FALSE	FALSE
	FALSE = 0 (CHARGING)		FALSE = 0 (CHARGING)		FALSE = 0 (CHARGING)	

3.3.3 Pump switching

In addition to the primary mode switching control system, a secondary pump switching control system (figure 29) was also implemented to enable or disable heat transfer between the refrigerant loop and the storage loop depending on the currently required operational mode. The circulation pump used in the storage loop of the heat pump system is controlled through a subsystem consisting of an on-off controller, a boolean-to-real component, a first order controller and a switch component in series. These components were obtained from the Modelica standard library and are used to adjust the mass flow rate of the circulation pump (measured in kg/s).

The on-off controller accepts a reference input signal reference from the real expression tank_midpoint and a measurement input signal u from a temperature sensor measuring the thermal storage tank temperature. If the value of the input signal u is less than the value of the reference signal minus half the bandwidth, the output signal y is set equal to TRUE.

Otherwise, if the value of the input signal u is greater than the value of the reference signal plus half the bandwidth, the output signal y is set equal to FALSE. The bandwidth of the on-off controller was set to 20, resulting in an allowable temperature range of tank_midpoint ± 10°C when implemented alongside the real expression tank_midpoint. Additionally, an initial output pre_y_start of TRUE was used during initialisation. The boolean-to-real component then converts this boolean signal to a real number representing the desired mass flow rate of the circulation pump. For this subsystem, a boolean input of TRUE produces a real output value of 0.1 kg/s, whereas a boolean input of FALSE produces a real output value of 0 kg/s, indicating that heat transfer between the refrigerant loop and the storage loop is enabled and disabled respectively. The first order controller then interprets and smoothens this signal before it is used as the input to the circulation pump.

The switch component pumpSwitch alters the desired control signal of the circulation pump depending on the current operational mode as dictated by the mode switching control system. This component shares a boolean input signal u2 with the four-way valve component in the mode switching control system. If the value of the input signal u2 is equal to TRUE, the output signal y is set equal to input signal u1, which in this instance is defined as the real expression pump_flow with a value of 0.1 kg/s. Otherwise, if the value of the input signal u2 is equal to FALSE, the output signal y is set equal to input signal u3, which is the real output value of the temperature-based control system for the circulation pump as previously described. This allows the circulation pump to operate at a constant mass flow rate when the thermal storage tank would need to be continuously utilised during the discharging and defrosting modes, and allows a variable mass flow rate to be used during the charging mode in order to prevent any unnecessary discharging or overcharging during operation.

Details of the control logic required for the temperature-based pump switching control system can be found in table 12-13.

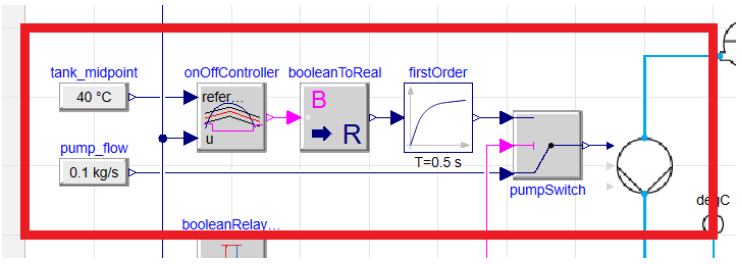

Figure 29: Diagram view of the temperature-based pump switching control system from the FlexHeatPump_V9 model within Dymola.

3.3.4 Custom components

3.3.4.1 RangeSwitch

The custom components RangeSwitch and BooleanRangeSwitch (figure 30 and 31) are designed to switch between three specified output values for a given range of input values. Within a Modelica environment, these blocks provide an output signal y depending on the value of the input signal u and the parameters rangeUpper and rangeLower.

If the value of the input signal u is greater than or equal to the value of parameter rangeUpper, the output signal y is set equal to parameter outputUpper. If the value of the input signal u is less than or equal to the value of parameter rangeLower, the output signal y is set equal to parameter outputLower. Otherwise, if the value of the input signal u is greater than the value of parameter rangeLower and less than the value of parameter rangeUpper, the output signal y is set equal to parameter outputMiddle. The output signal y and the three output parameters outputUpper, outputMiddle and outputLower are declared as either real or boolean values for the RangeSwitch and BooleanRangeSwitch components respectively.

$$\begin{aligned} y \; = \; & if \; u \; \geq \; rangeUpper \; then \; outputUpper \\ & elseif \; u \; \leq \; rangeLower \; then \; outputLower \\ & else \; outputMiddle \end{aligned} \tag{53}$$

If the input signal u is declared to be the evaporator inlet air temperature, this allows the system to detect the three ambient temperature regions (hot, cold and freezing) and supply different predetermined controls signals for the charging, discharging and defrosting valve positions of the flexible heat pump system respectively. In comparison to other similar components found within the Modelica standard library, these components can supply a larger range of potential output values without any external limitations or additional inputs beyond the required input signal u.

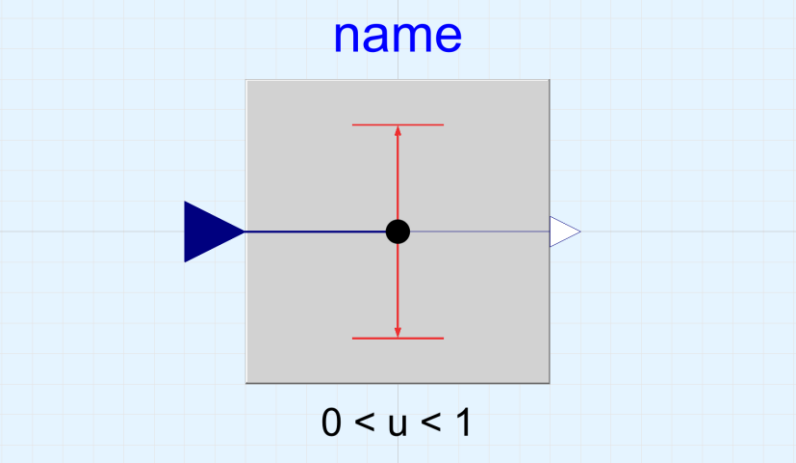

Figure 30: Component icon of the RangeSwitch component within Dymola.

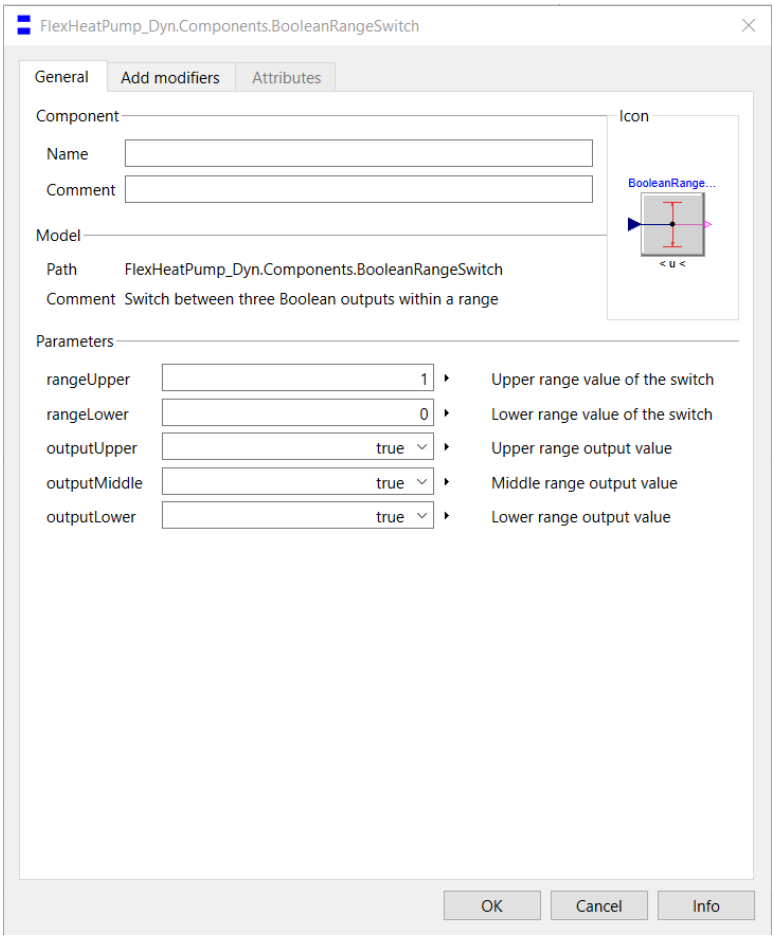

Figure 31: Parameter dialogue box of the BooleanRangeSwitch component within Dymola.

3.3.4.2 RelaySwitch

The custom components RelaySwitch and BooleanRelaySwitch (figure 32 and 33) are designed to relay between two specified output values for a given range of input values. Within a Modelica environment, these blocks provide an output signal y depending on the value of the input signal u and the parameters rangeUpper and rangeLower.

If the value of the input signal u is greater than or equal to the value of parameter rangeUpper, the output signal y is set equal to parameter outputUpper. If the value of the input signal u is less than or equal to the value of parameter rangeLower, the output signal y is set equal to parameter outputLower. Otherwise, if the value of the input signal u is greater than the value of parameter rangeLower and less than the value of parameter rangeUpper, the output signal y is set equal to the last declared value of y used in this simulation. For the purposes of preventing errors during initialisation, if the value of the input signal u is greater than the value of parameter rangeLower and less than the value of parameter rangeUpper when the current simulation time is equal to zero, the output signal y is set equal to parameter yInitial. The output signal y and the three output parameters outputUpper, outputLower and yInitial are declared as either real or boolean values for the RelaySwitch and BooleanRelaySwitch components respectively.

$$\begin{aligned} y = \; & if\ u \geq rangeUpper\ then\ outputUpper \\ & elseif\ u \leq rangeLower\ then\ outputLower \\ & elseif\ time \leq 0\ then\ yInitial \\ & else\ y \end{aligned} \tag{54}$$

If the input signal u is declared to be the thermal storage tank temperature, this allows the system to detect if the tank is fully charged, partially charged or empty and adjust the current operating mode of the flexible heat pump system accordingly. In this way, the value of the output signal y only changes once the value of the input signal u crosses the boundary thresholds specified by the parameters rangeUpper and rangeLower and maintains a constant output signal while ascending or descending within the middle region towards the next boundary threshold (equivalent to the parameter outputMiddle in the RangeSwitch components).

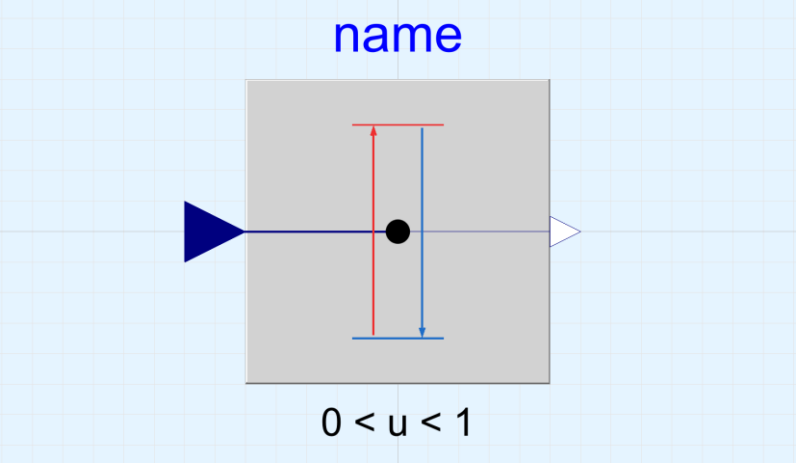

Figure 32: Component icon of the RelaySwitch component within Dymola.

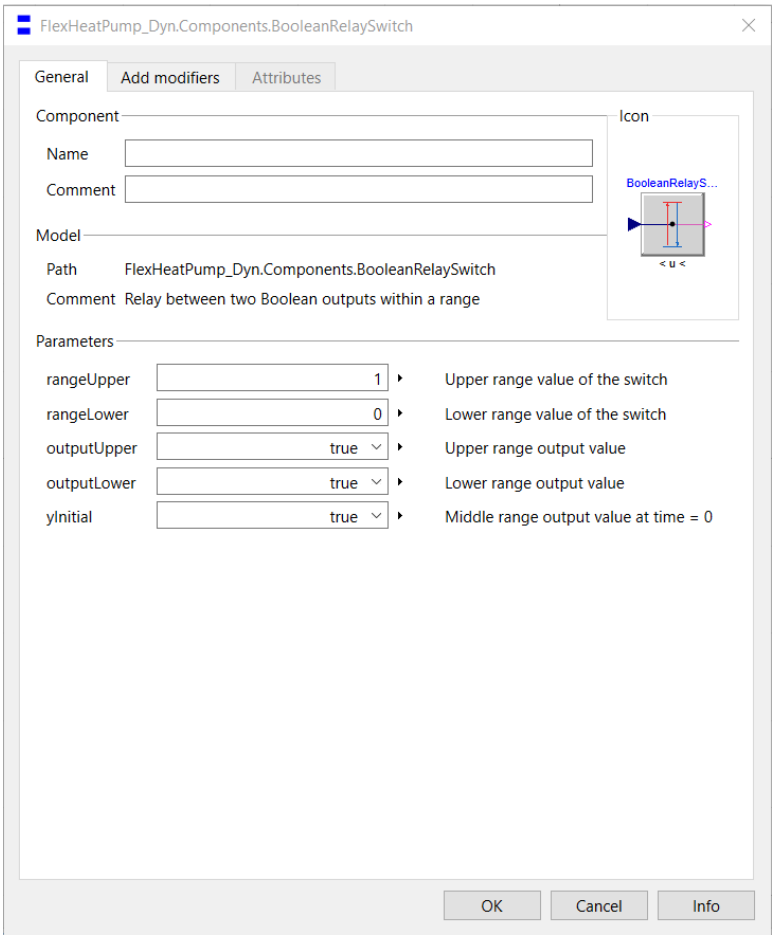

Figure 33: Parameter dialogue box of the BooleanRelaySwitch component within Dymola.

3.4 Thermodynamic equations

For the simulation of the flexible heat pump system, the dynamic model is governed by the thermodynamic equations of heat transfer associated with the general behaviours of most standard vapour compression heat pump cycles.

As shown in figure 34, for the charging mode of the flexible heat pump system, the system operates on a fixed cycle from state points 1-2-3-4-5-6-7-8-1 in order, restarting at state point 1 (before the compressor inlet). For the discharging and defrosting modes, due to the altered flow path through the four-way valve, the system instead operates on a modified cycle from state points 1-2-3-7-6-5-4-8-1 in order based on their physical locations within the configuration of the system. Relative to the charging mode, state points 4 and 7 are inverted in the discharging and defrosting modes, as are state points 5 and 6.

For the thermodynamic equations presented in the following subsections, the number of the state point refers to the order in which they are encountered in the vapour compression cycle for each operational mode (ie. h_4, $h_{7'}$ and $h_{7''}$ share the same physical location but differ in their order in the vapour compression cycle). The corresponding pressure-enthalpy (p-h) diagrams for the three operational modes can also be found in figure 34.

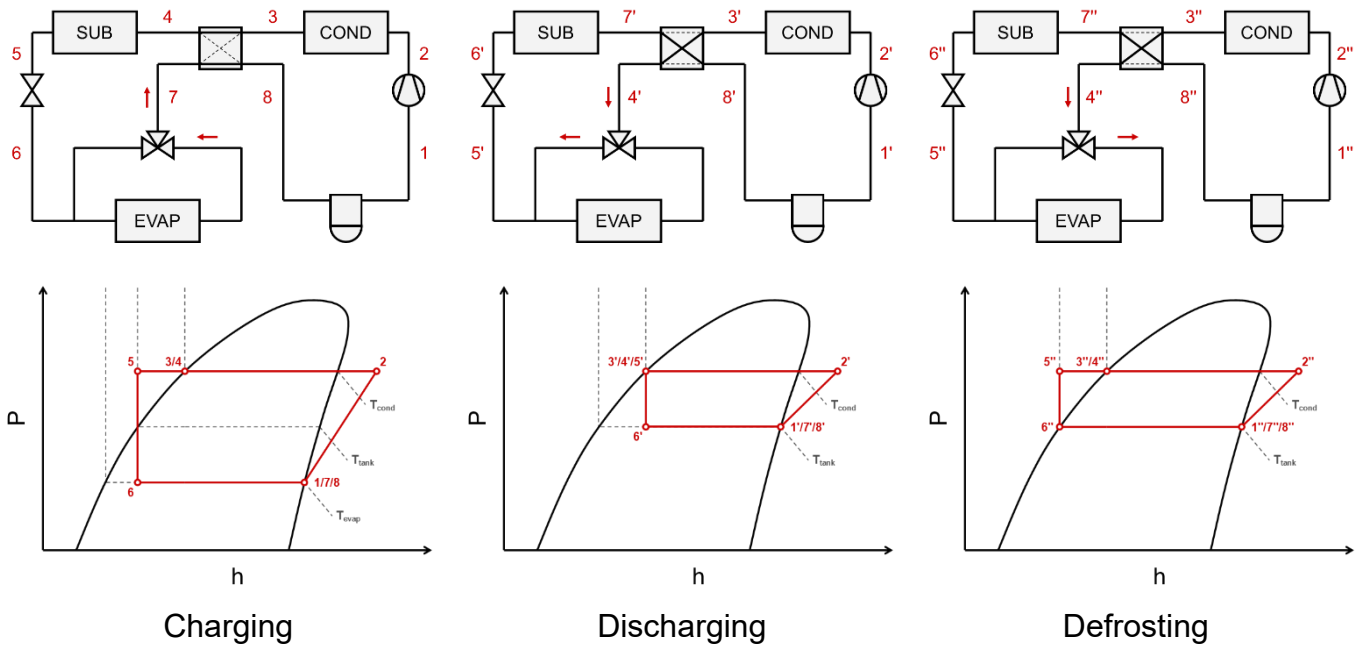

Figure 34: Schematic and pressure-enthalpy (p-h) diagrams of the flexible heat pump system, detailing the state points of the vapour compression cycle for each operational mode: charging (left), discharging (centre) and defrosting (right).

3.4.1 Charging mode

During the charging mode, the evaporator is used as the heat source to supply heat to the condenser (primary heat sink for domestic heating) and subcooler (heat recovery using the thermal energy storage tank).

The heat transfer through the condenser between the refrigerant loop and the water supply stream can be written as:

$$\dot{Q}_{cond,cha} = \dot{m}_r(h_2 - h_3) \quad (1)$$

$$Q_{cond,cha} = \dot{m}_r(h_2 - h_3)\Delta t_{cha} \quad (2)$$

Where $\dot{Q}$ is the heat transfer rate (W), Q is the amount of heat transferred (J), $\dot{m}_r$ is the mass flow rate of the refrigerant fluid (kg/s), h is the fluid enthalpy (J/kg) and Δt is the time spent in the operational mode (s).

The heat transfer through the evaporator between the ambient air stream and the refrigerant loop can be written as:

$$\dot{Q}_{evap,cha} = \dot{m}_r(h_7 - h_6) \quad (3)$$

$$Q_{evap,cha} = \dot{m}_r(h_7 - h_6)\Delta t_{cha} \quad (4)$$

The heat transfer through the subcooler between the refrigerant loop and the water storage loop can be written as:

$$\dot{Q}_{sub,cha} = \dot{m}_r(h_4 - h_5) \quad (5)$$

$$Q_{sub,cha} = \dot{m}_r(h_4 - h_5)\Delta t_{cha} \quad (6)$$

In this system, the subcooler and the thermal energy storage tank are fluidly connected by the water storage loop. As the water contained within the water storage loop is circulated between the subcooler and the thermal energy storage tank, it can be assumed that the

amount of heat stored within the tank is equal to the amount of heat transferred into the water storage loop through the subcooler.

Therefore:

$$\dot{Q}_{sub} = \dot{Q}_{tank} \tag{7}$$

$$Q_{sub} = Q_{tank} \tag{8}$$

Given that a small amount of heat transfer occurs between the storage tank and the surrounding environment, the amount of heat lost while the storage tank is idle can be approximated as:

$$Q_{tank} = Q_{tank,initial} - \dot{Q}_{loss}\Delta t_{loss} \tag{9}$$

The shaft power required to operate the compressor can be calculated as:

$$\dot{W}_{comp,cha} = \dot{m}_r(h_2 - h_1) \tag{10}$$

$$W_{comp,cha} = \dot{m}_r(h_2 - h_1)\Delta t_{cha} \tag{11}$$

Where $\dot{W}$ is the compressor power (W), and W is the compressor work (J).

3.4.2 Discharging mode

During the discharging mode, the thermal energy storage tank and subcooler are used as the heat source to supply heat to the condenser for domestic heating only.

The heat transfer through the condenser between the refrigerant loop and the water supply stream can be written as:

$$\dot{Q}_{cond,dis} = \dot{m}_{r'}(h_{2'} - h_{3'}) \tag{12}$$

$$Q_{cond,dis} = \dot{m}_{r\prime}(h_{2\prime} - h_{3\prime})\Delta t_{dis} \quad (13)$$

Where the subscript ′ denotes the discharging mode of the flexible heat pump system.

As the evaporator is isolated from the rest of the system and bypassed during the discharging mode, no heat transfer occurs through this component.

As such:

$$\dot{Q}_{evap,dis} = 0 \quad (14)$$

$$Q_{evap,dis} = 0 \quad (15)$$

The heat transfer through the subcooler between the water storage loop and the refrigerant loop can be written as:

$$\dot{Q}_{sub,dis} = \dot{m}_{r\prime}(h_{7\prime} - h_{6\prime}) \quad (16)$$

$$Q_{sub,dis} = \dot{m}_{r\prime}(h_{7\prime} - h_{6\prime})\Delta t_{dis} \quad (17)$$

The total heat produced by the storage tank during the discharging mode is equal to the amount of heat transferred into it during the charging mode.

Therefore:

$$Q_{sub,cha} = Q_{sub,dis} \quad (18)$$

$$\dot{m}_r(h_4 - h_5)\Delta t_{cha} = \dot{m}_{r\prime}(h_{7\prime} - h_{6\prime})\Delta t_{dis} \quad (19)$$

Furthermore, the total heat production during one charging-discharging cycle is:

$$Q_{total} = Q_{cha} + Q_{dis} \quad (20)$$

$$Q_{total} = \dot{Q}_{cha}\Delta t_{cha} + \dot{Q}_{dis}\Delta t_{dis} \quad (21)$$

The shaft power required to operate the compressor can be calculated as:

$$\dot{W}_{comp,dis} = \dot{m}_{r,}(h_{2,} - h_{1,}) \quad (22)$$

$$W_{comp,dis} = \dot{m}_{r,}(h_{2,} - h_{1,})\Delta t_{dis} \quad (23)$$

3.4.3 Defrosting mode

During the defrosting mode, the thermal energy storage tank and subcooler are used as the heat source to supply heat to the condenser (primary heat sink for domestic heating) and evaporator (secondary heat sink for defrosting operations).

The heat transfer through the condenser between the refrigerant loop and the water supply stream can be written as:

$$\dot{Q}_{cond,def} = \dot{m}_{r,,}(h_{2,,} - h_{3,,}) \quad (24)$$

$$Q_{cond,def} = \dot{m}_{r,,}(h_{2,,} - h_{3,,})\Delta t_{def} \quad (25)$$

Where the subscript ′′ denotes the defrosting mode of the flexible heat pump system.

The heat transfer through the evaporator between the ambient air stream and the refrigerant loop can be written as:

$$\dot{Q}_{evap,def} = \dot{m}_{r,,}(h_{4,,} - h_{5,,}) \quad (26)$$

$$Q_{evap,def} = \dot{m}_{r}(h_{4,,} - h_{5,,})\Delta t_{def} \quad (27)$$

The heat transfer through the subcooler between the water storage loop and the refrigerant loop can be written as:

$$\dot{Q}_{sub,def} = \dot{m}_{r,,}(h_{7,,} - h_{6,,}) \quad (28)$$

$$Q_{sub,def} = \dot{m}_{r,,}(h_{7,,} - h_{6,,})\Delta t_{def} \quad (29)$$

The total heat produced by the storage tank during the defrosting mode is equal to the amount of heat transferred into it during the charging mode.

Therefore:

$$Q_{sub,cha} = Q_{sub,def} \quad (30)$$

$$\dot{m}_r(h_4 - h_5)\Delta t_{cha} = \dot{m}_{r,,}(h_{7,,} - h_{6,,})\Delta t_{def} \quad (31)$$

Furthermore, the total heat production during one charging-defrosting cycle is:

$$Q_{total} = Q_{cha} + Q_{def} \quad (32)$$

$$Q_{total} = \dot{Q}_{cha}\Delta t_{cha} + \dot{Q}_{def}\Delta t_{def} \quad (33)$$

During periods wherein all three operational modes are utilised (ie. the storage tank is first charged before initiating defrosting operations and later transitions to the discharging mode once completed), the total heat production can be defined as:

$$Q_{total} = Q_{cha} + Q_{dis} + Q_{def} \quad (34)$$

$$Q_{total} = \dot{Q}_{cha}\Delta t_{cha} + \dot{Q}_{dis}\Delta t_{dis} + \dot{Q}_{def}\Delta t_{def} \quad (35)$$

The shaft power required to operate the compressor can be calculated as:

$$\dot{W}_{comp,def} = \dot{m}_{r,,}(h_{2,,} - h_{1,,}) \quad (36)$$

$$W_{comp,def} = \dot{m}_{r,,}(h_{2,,} - h_{1,,})\Delta t_{def} \quad (37)$$

3.4.4 Coefficient of performance

In general terms, the coefficient of performance (COP) of a heat pump is the ratio of the heat output delivered by the system to the power input supplied to the compressor in order to achieve this output:

$$COP = \frac{Q_{cond}}{W_{comp}} \tag{38}$$

As the performance of the flexible heat pump system is dependent on the configuration of the operational modes and the desired heat sinks, the coefficient of performance equation must be adapted to include the additional heat sinks used in the charging and defrosting modes.

Therefore, the three coefficients of performance for the charging, discharging and defrosting modes can be calculated as:

$$COP_{cha} = \frac{Q_{cond,cha} + Q_{sub,cha}}{W_{comp,cha}} \tag{39}$$

$$COP_{dis} = \frac{Q_{cond,dis}}{W_{comp,dis}} \tag{40}$$

$$COP_{def} = \frac{Q_{cond,def} + Q_{evap,def}}{W_{comp,def}} \tag{41}$$

Furthermore, the average coefficient of performance of the flexible heat pump system across all three operational modes can be defined as:

$$\overline{COP} = \frac{COP_{cha} + COP_{dis} + COP_{def}}{Number\ of\ distinct\ modes} \tag{42}$$

Where the number of distinct modes refers to the number of operational modes required by the system to function over a specified period of time.

For systems that utilise all three operational modes, the number of distinct modes equals three. For systems that utilise the charging and discharging modes but do not require the defrosting mode, the number of distinct modes equals two. For systems that only operate in the charging mode, the number of distinct modes equals one and thus $\overline{COP} = COP_{cha}$.

3.4.5 Improvement metrics

In order to analyse the performance of the flexible heat pump system in relation to a conventional single-stage heat pump system, the coefficient of performance values for each system must be compared.

An example of a conventional single-stage heat pump system and its corresponding pressure-enthalpy (p-h) diagram can be found in figure 35.

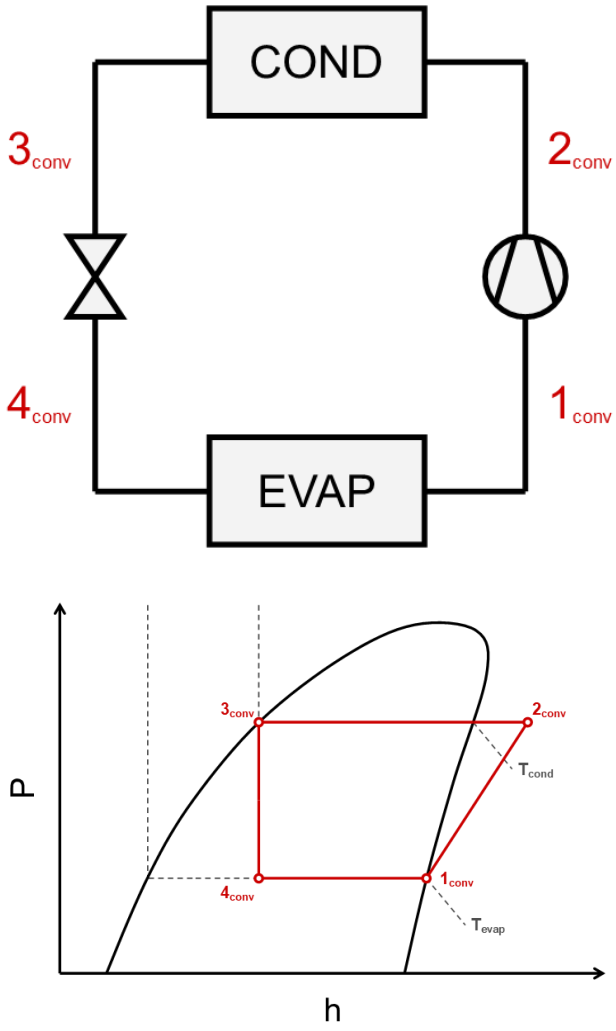

Figure 35: Schematic and pressure-enthalpy (p-h) diagrams of a conventional single-stage heat pump system.

As the conventional system omits the thermal energy storage tank and subcooler found in the flexible system, it essentially functions only in the “charging” mode.

For the conventional system, the heat transfer through the condenser can be written as:

$$Q_{cond,conv} = \dot{m}_{r,conv}(h_{2,conv} - h_{3,conv})\Delta t \quad (43)$$

Similarly, the shaft power required to operate the compressor can be calculated as:

$$W_{comp,conv} = \dot{m}_{r,conv}(h_{2,conv} - h_{1,conv})\Delta t \quad (44)$$

Therefore, based on equation 38, the coefficient of performance for the conventional system can be calculated as:

$$COP_{conv} = \frac{Q_{cond,conv}}{W_{comp,conv}} \quad (45)$$

As described by Yu et al. (2022) [15] and Essadik et al. (2024) [17], the coefficient of performance improvement α is defined as the potential improvement to a heat pump system's coefficient of performance while operating under a flexible configuration compared to a conventional one and can be calculated as:

$$\alpha = \frac{\overline{COP} - COP_{conv}}{COP_{conv}} \times 100\% \quad (46)$$

In order to analyse the characteristics and thermodynamic performance of the thermal energy storage tank during the charging, discharging and defrosting modes, the operational time ratio and volumetric charging factor can be calculated using data obtained from the dynamic simulation models.

The operational time ratio β is defined as the ratio between the time required to fully charge and fully discharge the storage tank over the course of a single charging-discharging or charging-defrosting cycle and can be calculated as:

$$\beta_{dis} = \frac{\Delta t_{dis}}{\Delta t_{cha}} \quad (47)$$

$$\beta_{def} = \frac{\Delta t_{def}}{\Delta t_{cha}} \quad (48)$$

During periods wherein all three operational modes are utilised, such as that described in equations 34 and 35, the operational time ratio can instead be calculated as:

$$\beta_{total} = \frac{\Delta t_{dis} + \Delta t_{def}}{\Delta t_{cha}} \quad (49)$$

The volumetric charging factor γ is defined as the time required to charge or discharge one litre of sensible fluid within the thermal energy storage tank and can be calculated as:

$$\gamma = \frac{\Delta t}{V_{tank}} \quad (50)$$

Where V_{tank} is the internal volume of the storage tank (l) and Δt is the total time required to fully charge or discharge the storage tank over the course of a single cycle in any operational mode (s).

3.5 Simulation parameters

3.5.1 Refrigerant fluid

The experimental test rig setup for the flexible heat pump system prototype described by Yu et al. (2022) [15] used R134a (1,1,1,2-tetrafluoroethane) as the primary refrigerant fluid, which is a mainstream refrigerant for most heat pump systems and applications. As such, the refrigerant fluid used within the dynamic simulation model was declared as being R134a from the TILMedia fluid library in order to remain consistent with its real-life counterpart. However, as R134a is more recently being phased out of active use in heating and refrigeration applications due to its high global warming potential (GWP) value, alternative refrigerants for domestic heat pump applications are currently being explored within the literature.

Rehman et al. (2023) [63] conducted a study into the development of a solar-assisted water-to-water reversible heat pump system utilising thermal and electrical energy storage mediums and R1234ze (trans-1,3,3,3-tetrafluoropropene) refrigerant for domestic heating applications. Simulations were carried out for three different European climates (Athens, Greece; Marseille, France; and Stuttgart, Germany) to determine the interaction between the heat pump and the storage mediums in order to maximise the self-sufficiency and self-

consumption of the system. R1234ze is considered to be a low-GWP replacement for R134a due to its similar thermodynamic and fluid properties, low flammability and environmentally friendly characteristics. This refrigerant is suitable for high temperature or organic Rankine cycles and can be immediately substituted into a R134a-based cycle with minimal system changes. This study proved that using R1234ze, despite being an unconventional refrigerant choice in residential-sized heat pump applications, resulted in reduced electricity costs and better performance for this heat pump system in comparison to a reference gas boiler heating system.

Similarly, Huang et al. (2024) [72] conducted a study into the development of a cascade heat pump system utilising integrated latent phase change material (PCM) thermal energy storage and R290 (propane) and CO_2 (carbon dioxide) refrigerants for domestic heating applications. Simulations were carried out for three different PCM mediums (ice, tetradecane and SP9) and compared to a baseline system excluding the thermal energy storage to determine the effects of thermal capacity and PCM transition temperature on the performance of the system, with the goal of reducing electricity costs and implementing peak-shaving control strategies using off-peak electricity. R290 was used in the outdoor refrigerant loop in order to charge the PCM thermal energy storage, which was then discharged at a slower rate by the indoor refrigerant loop using CO_2, thus improving the thermal storage's ability to build up and maintain a thermal charge. Both of these refrigerants exhibit low GWP values, and can be seen as more environmentally friendly alternatives to mainstream refrigerants such as R134a. This study proved that using R290 and CO_2, in combination with the cascaded system architecture and PCM thermal energy storage, resulted in reduced electricity costs and electricity use during peak periods where the benefits of the thermal energy storage could be leveraged.

Therefore, R1234ze and R290 were also chosen alongside R134a for the simulations of the flexible heat pump system within Dymola, with R290 being chosen as the default configuration. The thermodynamic and fluid properties of R134a and R290 were obtained directly from TILMedia, whereas the properties of R1234ze were obtained using NIST REFPROP and then later exported into Dymola.

3.5.2 Weather data

In these simulation models, historical weather data consisting of the maximum and minimum recorded air temperature values for three winter months during 2021-22 (table 15) were used as the temperature input of the ambient air source boundary.

Values for five locations across the UK (Glasgow, Edinburgh, Kirkwall, Liverpool and London) were obtained from the HadUK-Grid dataset, which are a collection of gridded climate variables derived from the network of UK land surface observations collated and maintained by the UK Met Office [98]. This data is interpolated from meteorological station data onto a uniform grid at a 1km by 1km scale to provide complete and consistent coverage across the UK [99]. These datasets are available online using the network common data form (NetCDF) file format (.nc), which is a file format commonly used in climatology and atmospheric research applications. These files can then be viewed, mapped and exported into other file formats using climatology software packages such as the Sentinel Application Platform (SNAP) by the European Space Agency (ESA) (figure 36) [100].

Additionally, three locations in Germany (Aachen, Berlin and Kempten) and two locations in Italy (Rome and Parma) were also selected to include historical weather data for mainland European countries. These datasets were obtained from gridded climate maps maintained by the DWD (Deutscher Wetterdienst) (figure 37) [101] and the SCIA (Sistema Nazionale per l'Elaborazione e Diffusione di Dati Climatici) (figure 38) [102] respectively. These interactive climate maps allowed for this data to be viewed and exported online without the use of external software packages and allowed for individual weather stations to be identified and selected for the purpose of acquiring datasets for each location [103, 104].

A time period ranging from 1st December 2021 to 28th February 2022 was selected in order to represent an accurate depiction of the cold winter months where the flexible heat pump and the thermal energy storage tank would be used frequently and to their fullest potential. This resulted in a selected period of 90 days, equivalent to 7,776,000s of simulation time. The maximum and minimum recorded air temperature values for each day were assumed to take place at 12pm noon and 12am midnight respectively, with other temperature values located between these predetermined points being interpreted, extrapolated and smoothened by the system before being properly utilised as inputs. The final temperature datapoint of each dataset, equivalent to 28th February 2022 at 11:59pm, was acquired using the monthly average air temperature value for the same time and location in order to allow the simulation

to end without requiring the use of extrapolations that would produce potentially unrealistic input values. Weather profiles for all ten locations can be found in appendix 2.

Table 15: Table summarising the historical weather datasets for ten locations across Europe, including geographic co-ordinates, temperature profiles and the number of datapoints within each temperature threshold.

Location	Latitude	Longitude	T_{Avg} (°C)	T_{Max} (°C)	T_{Min} (°C)	#Hot	#Cold	#Freeze
Glasgow, Scotland	55.8703	-4.2936	6.1	14.3	-3.4	97	75	8
Edinburgh, Scotland	55.9488	-3.1931	5.4	14.3	-4.1	80	90	10
Kirkwall, Scotland	58.9785	-2.9655	5.2	11.6	-1.2	76	99	5
Liverpool, England	53.4071	-2.9704	6.7	15.2	-1.9	104	71	5
London, England	51.5081	0.1338	7.2	16.2	-1.8	114	60	6
Aachen, Germany	50.7983	6.0244	4.6	14.1	-4.8	69	88	23
Berlin, Germany	52.4676	13.4020	3.7	14.2	-10.8	56	84	40
Kempten, Germany	47.7233	10.3348	1.3	16.8	-13.4	41	66	73
Rome, Italy	41.9206	12.5236	9.8	20.2	0.1	124	56	0
Parma, Italy	44.8170	10.2830	4.6	20.0	-5.0	74	56	50

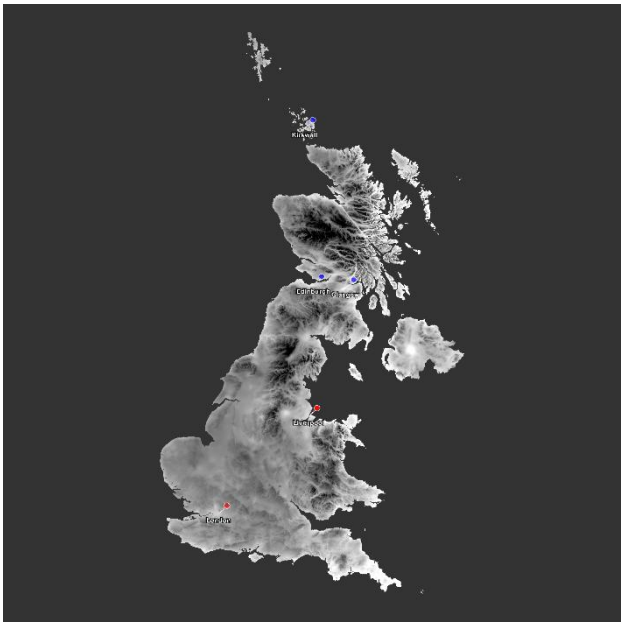

Figure 36: Image of the Met Office HadUK-Grid dataset viewed within ESA SNAP.

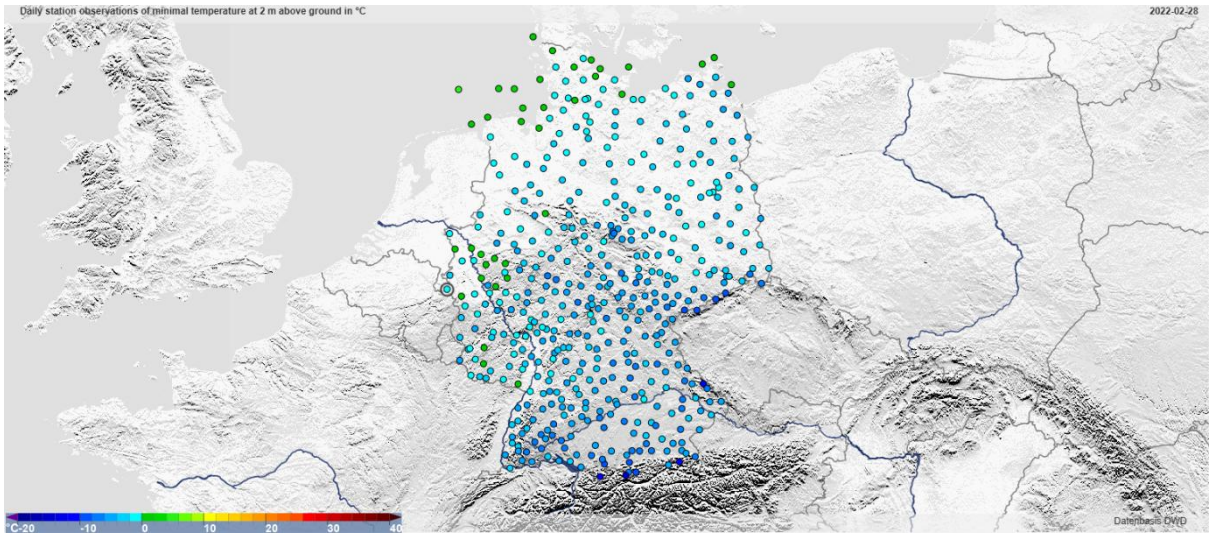

Figure 37: Image of the online climate map dataset for Germany maintained by the DWD (Deutscher Wetterdienst) [103].

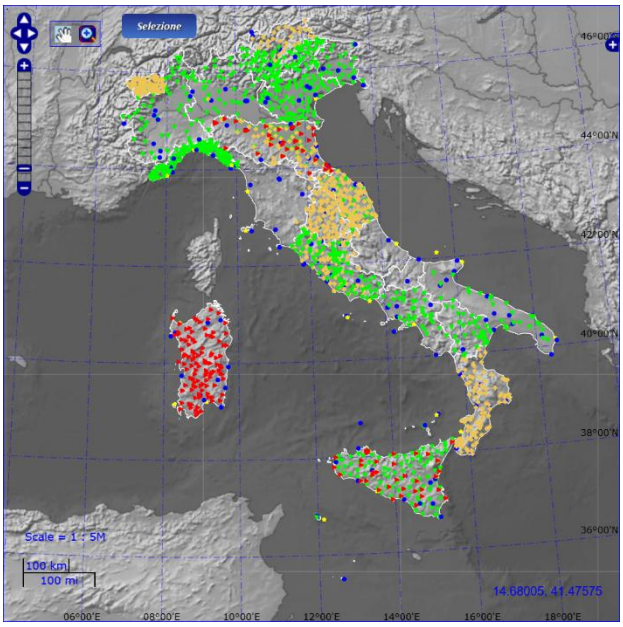

Figure 38: Image of the online climate map dataset for Italy maintained by the SCIA (Sistema Nazionale per l'Elaborazione e Diffusione di Dati Climatici) [104].

3.5.3 System outputs and model setup

In order to investigate the relationships between the thermodynamic behaviours and characteristics of the flexible heat pump system, forty-nine iterations of the flexible heat pump model were simulated within a dynamic simulation environment:

- The baseline flexible heat pump model, the standard heat pump model used for comparison against a non-flexible configuration, and the modified flexible heat pump model used for validation against data obtained from Lyu et al. (2022) [105].
- Three model iterations where the refrigerant fluid used in the refrigerant loop changed between iterations. (R134a, R1234ze and R290)
- Ten model iterations where the historical weather dataset used for the ambient air source boundary changed between iterations. (Glasgow, Edinburgh, Kirkwall, Liverpool, London, Aachen, Berlin, Kempten, Rome and Parma)
- Seven model iterations where the size and internal volume of the thermal energy storage tank changed between iterations. (70l, 125l, 145l, 210l, 250l and 300l)
    - Additionally, a subset of these iterations focusing on the storage tank charging-discharging and charging-defrosting times for constant ambient air temperatures of 10°C and 0°C respectively were also carried out for each tank size.
- Five model iterations where the hot/cold air temperature threshold used to control the operational modes of the flexible heat pump system changed between iterations. (4°C, 5°C, 6°C, 7°C and 8°C)
- Seven model iterations where the maximum/minimum tank temperature thresholds used to control the temperature bounds of the water inside the thermal energy storage tank changed between iterations. (30-50°C, 25-55°C, 20-60°C, 30-55°C, 30-60°C, 25-50°C and 20-50°C)

This series of dynamic simulations were completed on a Dell Latitude 5431 laptop running the Windows 10 Enterprise operating system with 12th Gen Intel(R) Core(TM) i7-1270P processor and 16.0 GB of installed ram (15.2 GB useable). Each model iteration was simulated for 77,760 timesteps over a simulation runtime of 7,776,000s, equivalent to one timestep every one hundred seconds (or every 1.67 minutes), and integrated using the Dassl or Radau (5^{th} order stiff) integration algorithms. All forty-nine simulations were completed over a total computational processing time of 11.28 hours.

The initial values of the system were selected in order to mirror the parameters of the flexible heat pump system as described by Yu et Al (2022) [15] as closely as was feasibly possible. The evaporator inlet temperature and the initial temperature of the evaporator walls were set equal to the initial value of the external temperature input from the historical weather dataset, which starts at a predetermined value and varies dynamically over time. The condenser was configured to output a constant supply temperature of 50°C, which was chosen based on the values used in the experimental test rig setup for the flexible heat pump system prototype for both space heating and domestic hot water heating. The return temperature of the water re-entering the condenser was chosen to be 45°C. Minor variations to these initial values were made depending on the model iteration where required.

Results for the individual components of the system for each simulation run were recorded and analysed before being collated into a larger dataset for parametric comparison. The coefficient of performance values of the flexible heat pump system were then calculated externally using equations 39-42 and 45 to measure the overall efficiency of the system.

4 Results & Discussion

4.1 Model validation

For the validation of the dynamic simulation model, the results of the flexible heat pump system were compared to those obtained in the literature for another heat pump system of similar size, configuration and function.

Lyu et al. (2022) [105] studied the effects of different air source heat pump and thermal energy storage tank sizes on the performance of an energy storage heating system for clean heating in Beijing, China. The energy storage heating system (figure 39) extracts heat from the surrounding air and elevates it to a higher temperature before delivering it to an air handling unit through a hot water loop for the space heating of an indoor environment. A sensible water storage tank was installed in the hot water loop in order to store excess heat for use during low ambient conditions without running the heat pump. A detached family home with a maximum heating load of 5.97kW was modelled in the dynamic modelling software package TRNSYS and simulated for a typical heating season between November 15th and March 15th. Thirty-three potential system configurations were investigated, with heat pump sizes ranging from 80-100% of the building's design heating load and storage tank sizes ranging from 0.06-4.5m^3 in internal volume. This study found that the implementation of the water storage tank reduced stop-start losses from 12.5% without a storage tank to 0.2% with a tank size of 1.0m^3, with diminishing returns for tanks of a greater size. The energy savings benefits achieved by operating the air source heat pump only during high ambient conditions were found to be significant, with total energy saving rates of 13.3% and 18.6% for tank sizes of 1.0m^3 and 4.0m^3 respectively. The effects of the size of the air source heat pump were found to be minimal, with an energy saving rate variation of 1% between the heat pump sizes for 80% and 100% of the building's design heating load.

As can be seen in figure 40, the configuration of the energy storage heating system described by Lyu et al. (2022) [105] resembles the configuration of the flexible heat pump system. In both systems, an air source heat pump extracts energy from the ambient air through the evaporator and elevates the hot vapourised refrigerant to a higher pressure and temperature through the compressor. In the flexible heat pump system, the superheated refrigerant exiting the compressor is then used to supply heat to the indoor environment through the condenser before facilitating heat recovery through the subcooler. This recovered heat is then used to charge the water storage tank and can later be discharged back into the

refrigerant loop during the discharging and defrosting modes. In the energy storage heating system, the superheated refrigerant instead transfers all of its heat energy into the hot water loop through an internal heat exchanger. This heat is then used to charge the water storage tank before entering the air handling unit to supply heat to the indoor environment. In both cases, heat energy is first transferred from the ambient air to the refrigerant loop and secondly from the refrigerant loop to a hot water storage loop before entering a fluidly connected thermal energy storage tank. As such, the overall charging and discharging mechanisms of the water storage tank in each model are identical and therefore comparable for the purposes of model validation.

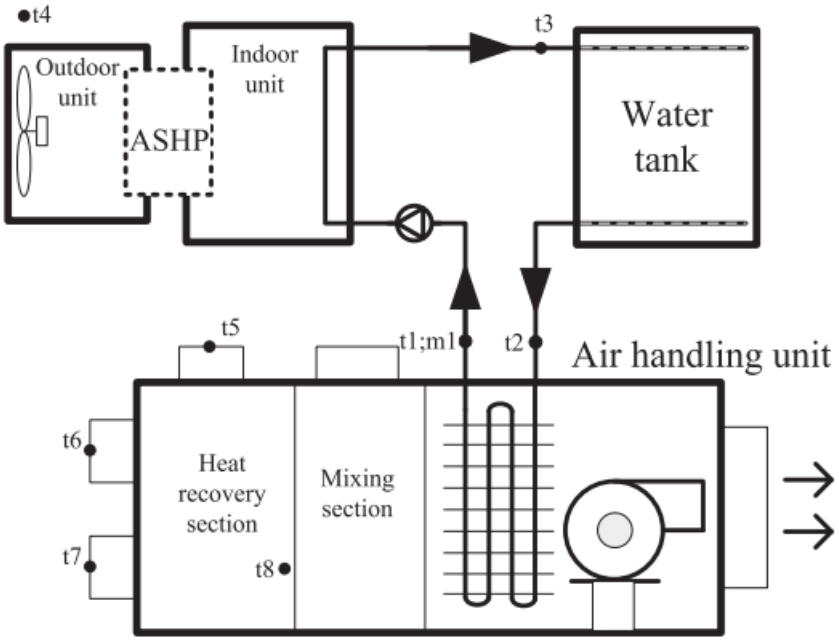

Figure 39: Schematic diagram of the energy storage heating system described by Lyu et al. (2022) [105].

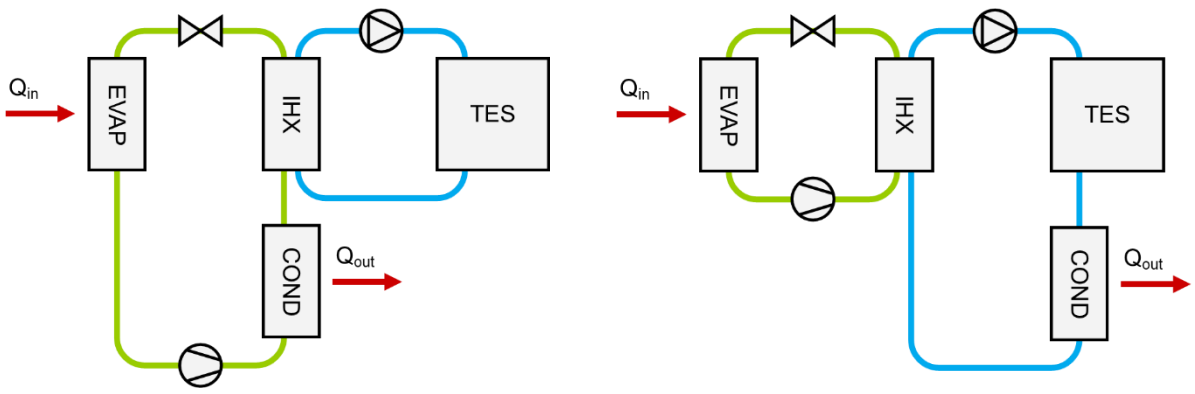

Figure 40: Schematic diagrams comparing the layout of the flexible heat pump system (left) to the energy storage heating system described by Lyu et al. (2022) (right).

The validation of the flexible heat pump system in relation to the system described by Lyu et al. (2022) [105] is shown in figure 41, which shows the temperature changes of the water storage tank over time for a total simulation runtime of 48 hours. For the purposes of model validation, the parameters of the flexible heat pump system were reconfigured to mirror the parameters of the energy storage heating system as closely as was feasibly possible. For the first ten hours of operation, both systems discharge the storage tank at a near identical rate from an initial temperature of 45°C to the minimum allowable tank temperature of 32°C. As the storage tank is then considered to be fully discharged, both systems change their operating modes in order to recharge the storage tank to the maximum allowable tank temperature of 52°C. In contrast to the energy storage heating system, the flexible heat pump system recharges its thermal energy storage tank at a significantly slower rate and requires approximately 80% longer in order to fully charge the storage tank under the same set of ambient air conditions. These behaviours can be explained by the configuration of each system, as the flexible heat pump system focuses on charging the tank through heat recovery over charging it directly through the internal heat exchanger arrangement found in the energy storage heating system. The systems then change their operating modes back to discharging the storage tank and repeating this cycle of charging and discharging. While minor differences between the two systems are identifiable, these instances are explainable and the thermodynamic mechanisms of charging and discharging in each system are identical. Therefore, the flexible heat pump system was validated to be functioning correctly and as intended by design.

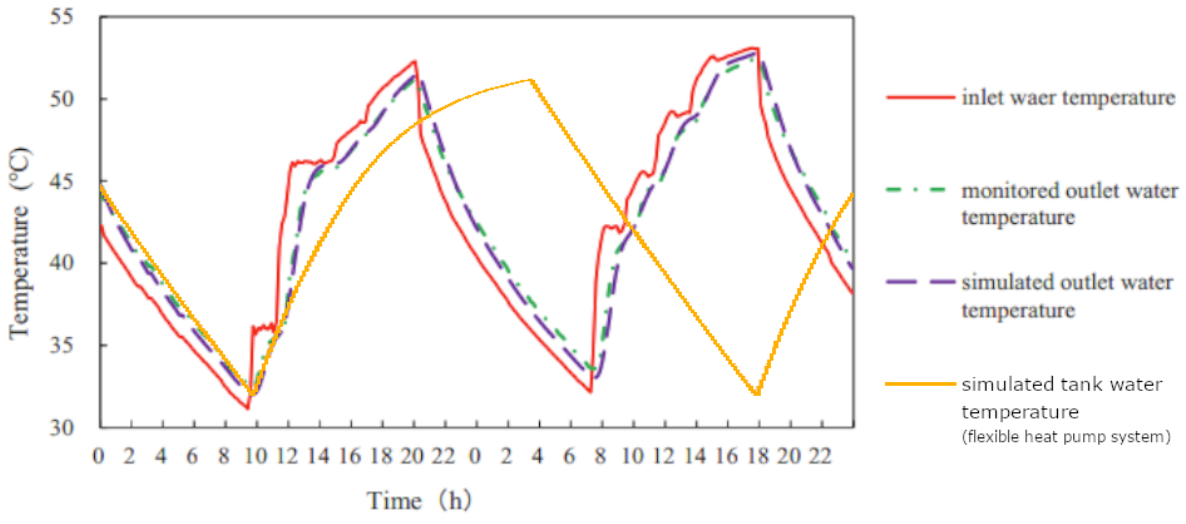

Figure 41: Validation of the thermal energy storage tank comparing the results of the flexible heat pump system to the energy storage heating system described by Lyu et al. (2022) [105].

4.2 Performance of the baseline system

Figure 42-44 show the ambient air temperature, the water outlet temperature and the storage tank temperature of the flexible heat pump system respectively. These figures represent the performance of the default (baseline) model configuration, wherein the historical weather data for Glasgow, Scotland was used (figure 42) and the components of the control systems were calibrated against an average air temperature of approximately 6°C.

The outlet water temperature (figure 43) confirms that the system is able to meet the desired condenser outlet water temperature of 50°C for the majority of its operational runtime. Minor fluctuations can be observed during periods where the operational mode of the flexible heat pump system changes, and these were either upwards (positive) or downwards (negative) in nature. Upwards fluctuations occurred when the thermal energy storage tank becomes fully charged and the system changes to either the discharging or defrosting modes. As the system adjusts to using a heat source with a higher temperature than that of the outside air, the system briefly supplies too much heat energy to the condenser before it gradually readjusts the speed of the compressor to accommodate this. These fluctuations have a maximum magnitude of +2.6°C and typically last no longer than a few minutes. Similarly, downwards fluctuations occurred when the thermal energy storage tank becomes fully discharged and the system changes back to the charging mode. As the system readjusts to a heat source with a lower temperature than that of the storage tank, the system requires a longer period of time to recover and for the outlet water temperature to return to its designated setpoint value. These fluctuations have a maximum magnitude of -6.6°C and typically last no longer than forty-five to sixty minutes, up to a maximum of two hours if the system was previously operating in the defrosting mode and the ambient air temperature was considered to be “freezing”. Overall, the system was deemed to be working very well with regards to providing the desired outlet water temperature over the course of a traditional cold winter heating season in Scotland.

The storage tank temperature (figure 44) shows the pattern of the thermal energy storage tank as it completes each charging, discharging and defrosting cycle. In the charging mode, the storage tank is gradually charged up to the maximum tank temperature threshold of 50°C. The rate in which the storage tank is charged is non-linear and gradually starts to slow as the temperature of the storage tank increases over time. If the storage tank is fully charged and the ambient air temperature is considered to be too low for efficient operation, the flexible heat pump system then immediately transitions into the discharging mode (or the defrosting

mode if the defrosting of the evaporator is required). If the storage tank is not required, the flexible heat pump system holds the thermal charge stored in the tank by deactivating the circulation pump, preventing heat transfer through the subcooler between the refrigerant loop and the water storage loop. While the storage tank remains “idle”, stored heat is gradually lost to the surrounding environment and would result in the storage tank fully discharging over a period of approximately 18 days for the default 210l tank size. In the discharging and defrosting modes, the storage tank is discharged at a near-constant rate until it reaches the minimum tank temperature threshold of 30°C, upon which it is considered to be fully discharged. In comparison to the discharging mode, the defrosting mode discharges the tank at a significantly faster rate due to the greater thermal load required, up to approximately three times faster than the discharging mode. Furthermore, the discharging of the storage tank in the discharging and defrosting modes is independent of the temperature of the outside air.

A pressure-enthalpy (p-h) diagram for the flexible heat pump system during the charging, discharging and defrosting modes, as well as an additional “standard” mode for the charging mode while the storage tank is fully charged and idle, can be found in figure 45.

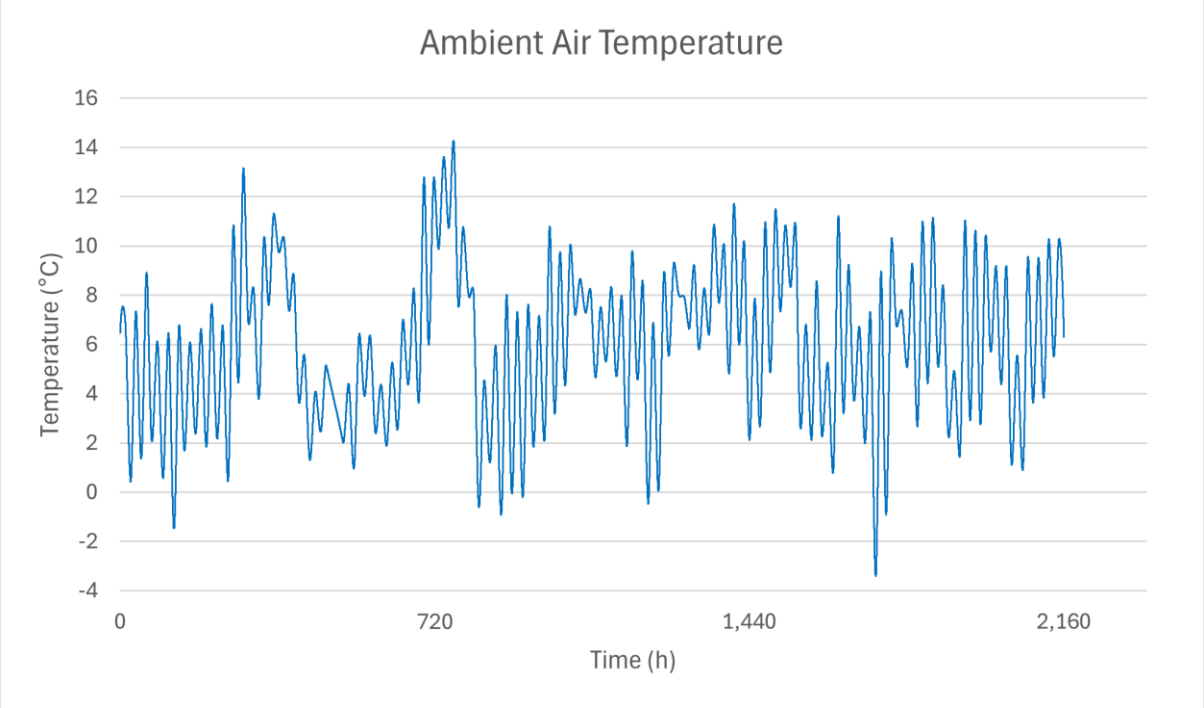

Figure 42: Ambient air temperature values for the simulation of the baseline flexible heat pump model.

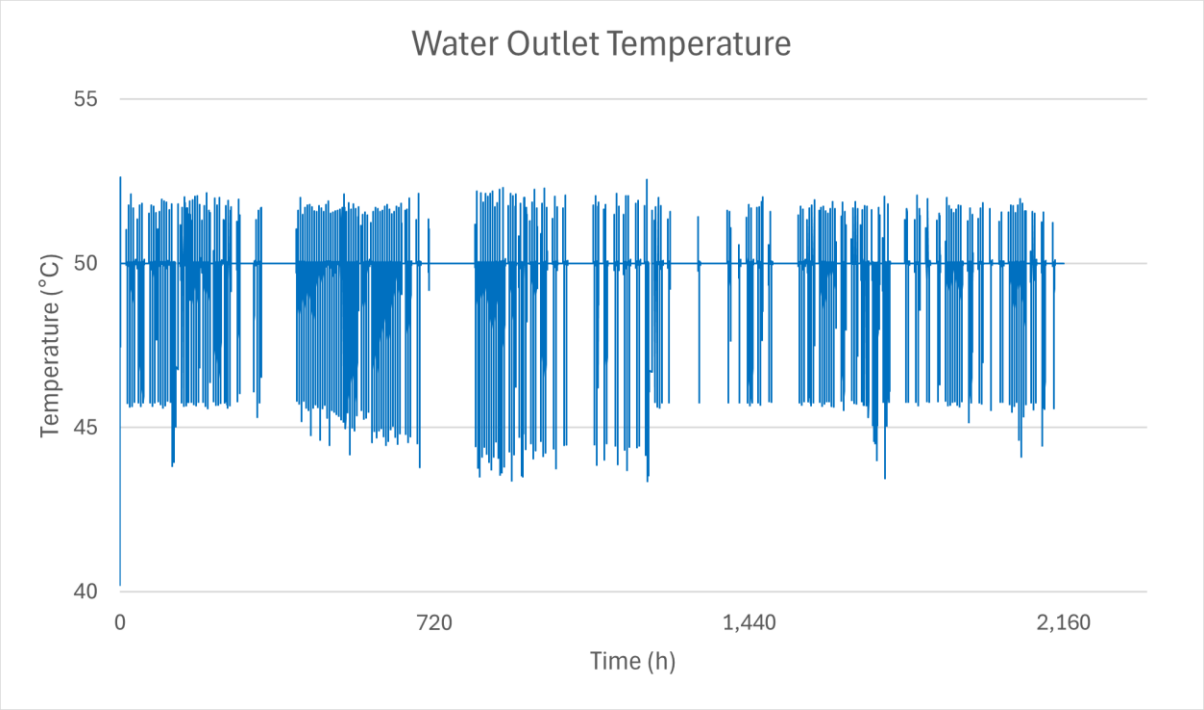

Figure 43: Water outlet temperature values for the simulation of the baseline flexible heat pump model.

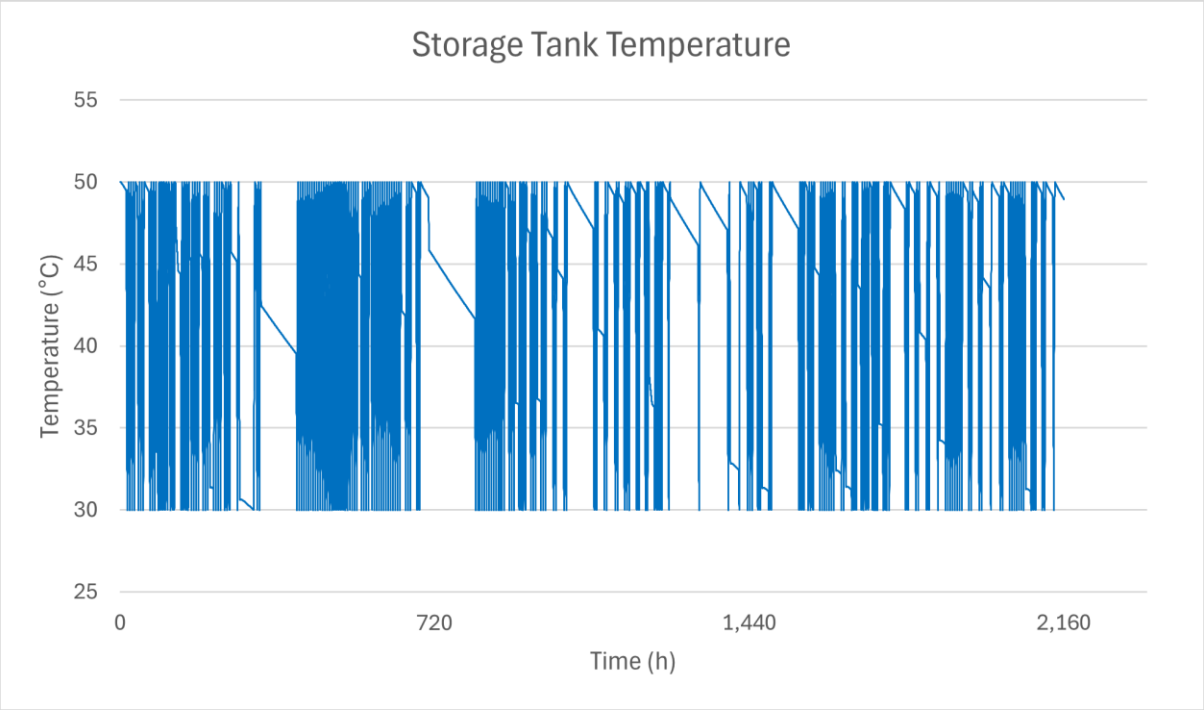

Figure 44: Storage tank temperature values for the simulation of the baseline flexible heat pump model.

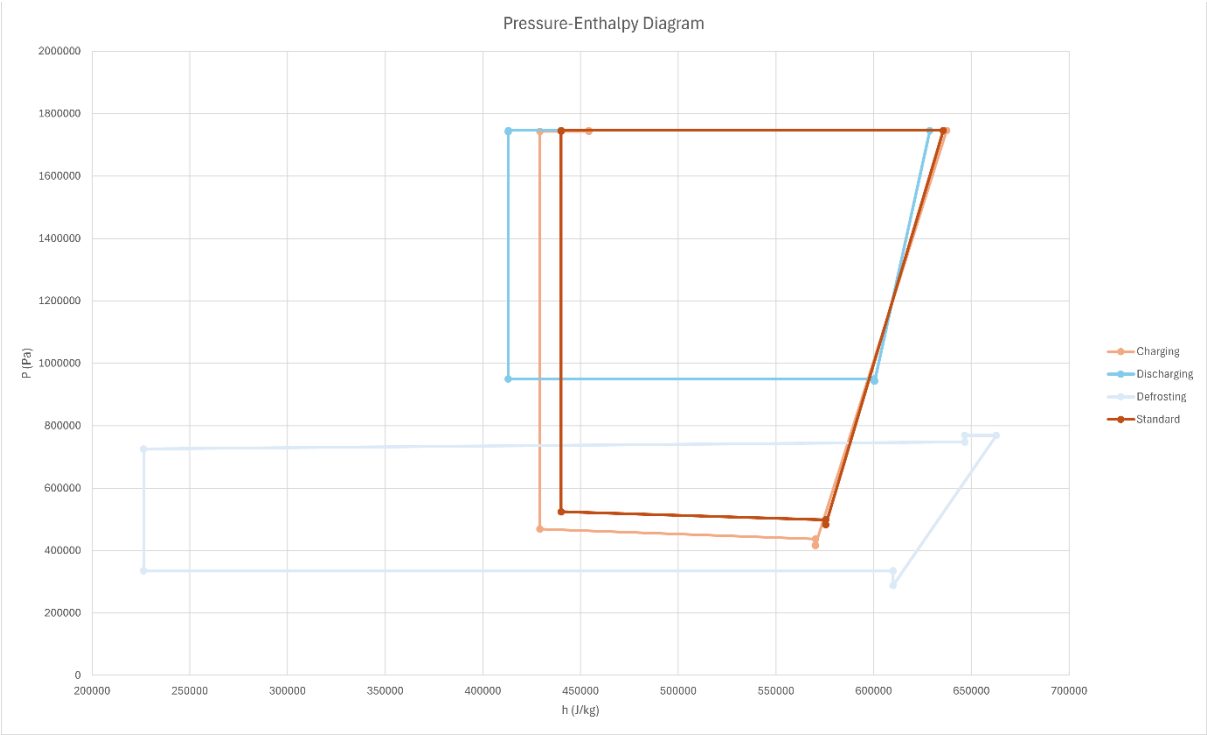

Figure 45: Pressure-enthalpy (p-h) diagram for the simulation of the baseline flexible heat pump model operating in the charging, discharging, defrosting and standard (charging while the storage tank is fully charged) modes.

4.3 Comparison to a conventional heat pump system

Figure 46 compares the coefficient of performance values of the flexible heat pump system to an equivalent standard heat pump system (modelled as a variation of the V2 model as shown in figure 10). These results are dynamic in nature and display the averaged long-term performance of the system. As the standard heat pump system is incapable of operating in either the discharging or defrosting mode, the system only has a single COP value for the charging mode equal to 3.43, which is also equal to the average COP of the system. As the flexible heat pump system is capable of operating in three different operational modes across the span of the 90 day simulation, three different COP values were obtained for this system, with one value being obtained for each mode utilised: charging, discharging and defrosting. These COP values were then compared to the singular COP value obtained for the standard system in order to assess the long-term performance of the two systems either incorporating or excluding thermal energy storage devices and how each operating mode affected the performance of the flexible system relative to that of the standard system. The average COP value for the flexible system's overall performance across all three modes was then also compared to the singular COP value of the standard system in order to establish how it

performed when operating across all three modes within the same time period, which would be its intended functionality in realistic domestic heating scenarios.

In comparison to the standard system, the flexible system performs noticeably worse while operating in the charging mode, with a COP value of 2.80. This results in a detrimental COP improvement value of -18.4%, as shown in figure 47. This reduction in performance may be due to the overall greater complexity of the flexible heat pump system and its thermal energy storage system. As the flexible system requires heat recovery from the refrigerant fluid exiting the condenser in order to charge the thermal energy storage tank, the thermal loads of the flexible system are greater than those of the standard system despite both systems fully meeting the primary heating demands of the end user. However, when comparing the discharging and defrosting mode COP values of the flexible system to the singular charging mode COP value of the standard system, the flexible heat pump system outperforms the standard system by a significant margin. The flexible system exhibits COP values of 5.98 and 4.11 for the discharging and defrosting modes respectively, with respective COP improvement values of 74.3% and 19.7% in comparison to the charging mode of the standard system. This improvement is due in part to the higher temperature of the heat source active during these modes (ie. the thermal energy storage tank), which is always considerably higher than the ambient air temperature present for the same timestep.

The average COP value of the flexible heat pump system across all three operational modes was 4.30 with a COP improvement value of 25.2%. While the charging mode COP value was lower than that of the standard system, the benefits from operating the flexible system in the discharging and defrosting modes offsets these negative effects on its overall performance, resulting in significant long-term improvements over the standard system. Therefore, as the average COP of the flexible heat pump system was greater than that of the equivalent standard heat pump system, the flexible system was deemed to be the superior heat pump model for domestic heating applications.

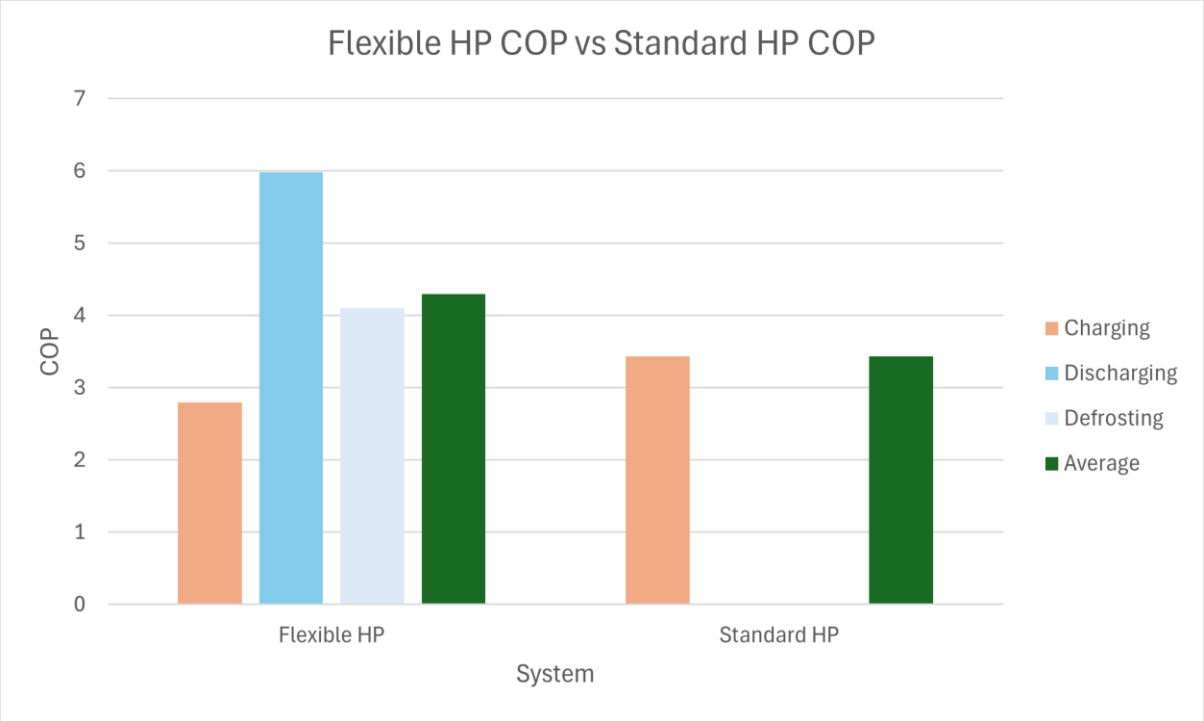

Figure 46: Results of the flexible heat pump system comparing the calculated COP values to those from an equivalent standard heat pump system.

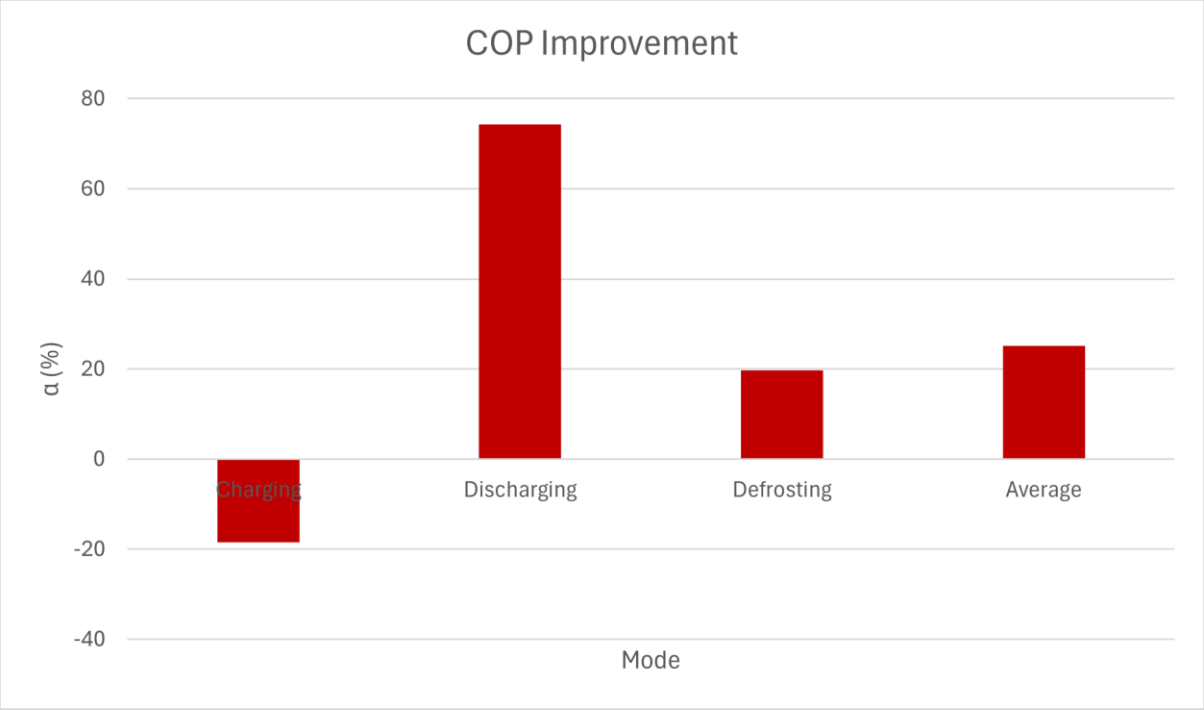

Figure 47: COP improvement values of the flexible heat pump system in relation to an equivalent standard heat pump system.

4.4 Varying the refrigerant fluid

Figure 48 compares the coefficient of performance values of the flexible heat pump system for three different refrigerant fluid choices. These results are dynamic in nature and display the averaged long-term performance of the system. In the charging mode, R1234ze obtained the highest COP value of 3.34, followed by R134a (3.17) and R290 (2.80). In the discharging mode, R290 obtained the highest COP value of 5.94, followed by R134a (5.84) and R1234ze (5.74). Similarly, in the defrosting mode, R290 obtained the highest COP value of 4.07, followed by R134a (3.64) and R1234ze (3.37). When comparing the average COP values, the system utilising R290 was found to be the most energy efficient overall, with an average COP value of 4.27, followed by R134a (4.22) and R1234ze (4.15).

In comparison to R134a, originally used in the flexible heat pump system prototype described by Yu et al. (2022) [10], the implementation of R290 resulted in an approximately 1.7% and 11.7% increase in the discharging and defrosting mode COP values respectively, with a 1.3% increase in the average COP value of the system as a whole. This would particularly benefit operation in cold climates where the continual charging and discharging of the thermal energy storage tank would be both frequent and in high demand, thus reducing the energy usage of the system and reducing operating costs for the end user. As such, R290 was identified as the most optimal refrigerant fluid choice for the flexible heat pump system out of the three potential options assessed in this study. For systems that primarily operate in the charging mode, either with or without charging the thermal energy storage tank, R1234ze may instead be utilised in the refrigerant loop as an acceptable substitute for R290. This change would result in an approximately 18.9% increase in the charging mode COP value with an expected (albeit minor) 3.3% reduction in the discharging mode COP value. Furthermore, the expected 17.1% reduction in the defrosting mode COP value in comparison to R290 could be avoided or eliminated entirely if the system was located within an environment that would not require the implementation of the defrosting mode. R134a can be considered as a midpoint option between R1234ze and R290, as it obtained the second highest COP values in all three operational modes, as well as the second highest average COP value overall. However, the implementation of R134a may become less common in future systems due to its higher global warming potential value and gradual phasing out in favour of greener alternatives.

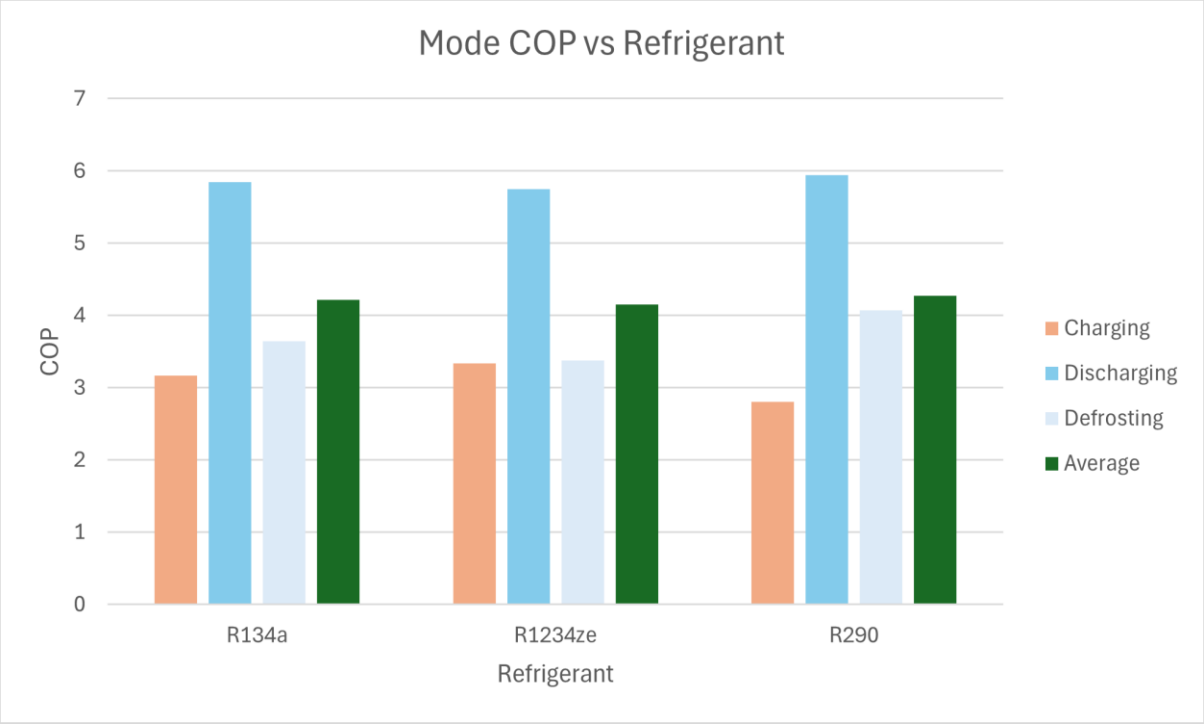

Figure 48: Results of the flexible heat pump system comparing the calculated COP values obtained for three different refrigerant fluid choices.

4.5 Varying the weather data location

Figure 49 compares the coefficient of performance values of the flexible heat pump system for ten different European climates. These results are dynamic in nature and display the averaged long-term performance of the system. As the model iteration of the system for Rome does not experience any weather patterns that were considered at any point to be "freezing" (ie. below 0°C), the COP value for the defrosting mode is equal to zero and was subsequently omitted from the calculation of average COP value for this location.

For the purposes of analysis and discussion, this set of ten model iterations were further subdivided into five smaller groups (ranked in order of effectiveness) based on their overall performance and how they were influenced by their individual weather profiles:

- **Group 1 (Edinburgh, Kirkwall & Aachen)**: Edinburgh, Kirkwall and Aachen were all considered to be the most optimal locations for the efficient performance of the flexible heat pump system, fully leveraging the flexible aspects of the system to their fullest potential. The average air temperature of each location ranged from 4.6°C (Aachen) to 5.4°C (Edinburgh), with a maximum air temperature ranging from 11.6°C

(Edinburgh) to 14.3°C (Kirkwall) and a minimum air temperature no lower than -4.8°C (Aachen). Furthermore, each location had the greatest number of datapoints within the "cold" air temperature regions out of the ten locations assessed, but also had a not-insignificant number of datapoints within the "hot" air temperature region. This allowed the system to properly charge the thermal energy storage tank during warmer periods for later use during colder periods that would otherwise harm its standard performance due to low ambient air temperatures. Periods in which the air temperature was considered to be "freezing" were most common observed for the system located in Aachen but were often spaced in between two "cold" temperature periods, creating situations in which the storage tank was used as a heat source for an extended period of time. This resulted in the highest COP values for the discharging and defrosting modes, ranging from 6.38 (Kirkwall) to 6.58 (Edinburgh) and 4.71 (Kirkwall) to 4.99 (Aachen) respectively. Additionally, these three locations exhibited the best average COP values overall, ranging from 4.56 (Kirkwall) to 4.68 (Edinburgh).

- **Group 2 (Glasgow, Liverpool & London)**: Glasgow, Liverpool and London were all considered to be suitable for the flexible heat pump system. The datapoints for these three locations tended towards a predominantly warmer climate, where the number of "hot" periods outweighed the combined number of "cold" and "freezing" periods, accounting for approximately 54-63% of the total winter heating season. This allowed for the storage tank to be charged under favourably warmer climate conditions, but the utilisation of this thermal charge for the purposes of acting as a heat source was more limited compared to those observed in group one. The charging mode COP values were some of the highest recorded, ranging from 2.80 (Glasgow) to 3.00 (London), whereas the discharging and defrosting mode COP values ranged from 5.58 (London) to 5.98 (Glasgow) and 3.51 (London) to 4.11 (Glasgow) respectively. Furthermore, the system located in Glasgow exhibited the best performance in the discharging and defrosting modes (as well as the highest average COP value for locations in groups two and three) due to its more balanced ratio between the time spent charging and discharging the thermal energy storage tank over the course of the winter heating season.
- **Group 3 (Berlin & Parma)**: Berlin and Parma were both considered to be suitable for the flexible heat pump system, but indicated some aspects that would somewhat hinder its performance. While initially appearing to be similar to the locations in group two, the datapoints for these two locations tended towards a predominantly colder climate, where the number of "freezing" periods were significantly greater than those

observed for the majority of the other locations. Furthermore, the charging mode COP values were some of the lowest recorded, with values of 3.7 and 4.6 for Berlin and Parma respectively. This indicated that the system was being forced to charge the storage tank during suboptimal cold or freezing conditions due to the greater number of "freezing" periods present during this time, significantly reducing its performance in comparison to the systems observed in groups one and two. Despite this, the discharging and defrosting mode COP values are still generally acceptable, ranging from 4.08 to 4.42 and 3.79 to 4.17 respectively, with Parma consistently performing better than Berlin due to its more favourable climate.

- **Group 4 (Rome)**: Rome exists within its own category due to the predominantly hot nature of its local climate, which partially hinders the operation of the flexible heat pump system. The average, maximum and minimum air temperatures were all found to be the highest out of the ten locations assessed, with values of 9.8°C, 20.2°C and 0.1°C respectively. The system primarily operated in the charging mode, as the number of datapoints in which the air temperature was considered to be "hot" was the highest out of the ten locations assessed, accounting for almost 69% of the total winter heating season. This caused the system to exhibit the highest COP value for the charging mode (3.48) out of all ten locations, as the warmer air temperature facilitated more efficient operation using the evaporator to extract heat from the surrounding air. The number of datapoints in which the air temperature was considered to be "cold" was also the joint-lowest out of all ten locations (alongside Parma), limiting the amount of time the storage tank was used as a heat source and resulting in the second lowest COP value for the discharging mode (4.85). Furthermore, the system never operates in the defrosting mode as the ambient air temperature never falls below 0°C, further limiting the usefulness of the thermal energy storage.
- **Group 5 (Kempten)**: Kempten exists within its own category due to the predominantly cold and freezing nature of its local climate, which greatly hinders the operation of the flexible heat pump system. The average and minimum air temperatures were found to be the lowest out of the ten locations assessed, with values of 1.3°C and -13.4°C respectively, whereas the maximum air temperature was found to be the third highest with a value of 16.8°C. However, this was offset by the significant number of datapoints within the "cold" or "freezing" air temperature regions, accounting for more than three quarters of the total winter heating season. This caused the flexible heat pump system to predominantly operate in the discharging or defrosting modes while charging the thermal energy storage tank under detrimental cold or freezing

conditions. This resulted in the lowest COP values for all three operational modes, with values of 1.42, 3.76 and 3.23 for charging, discharging and defrosting respectively, along with the lowest average COP value of 2.80. Despite this, the benefits of using the thermal energy storage tank as a heat source during cold winter periods are clearly identifiable, as the COP values for the discharging and defrosting modes exhibit a 265% and 227% increase in comparison to the COP value for the same system during the charging mode.

For the implementation of the flexible heat pump system, it is therefore recommended to focus primarily on locations with local climate conditions similar to those from groups one and two in order to guarantee high levels of performance with little to no changes in the pre-existing architecture of the system. Locations similar to those in group three may be included if minor changes to system parameters and components would enable the system to function at an acceptable level without suboptimal charging cycles, whereas groups four and five should be avoided wherever possible without significant adaptations.

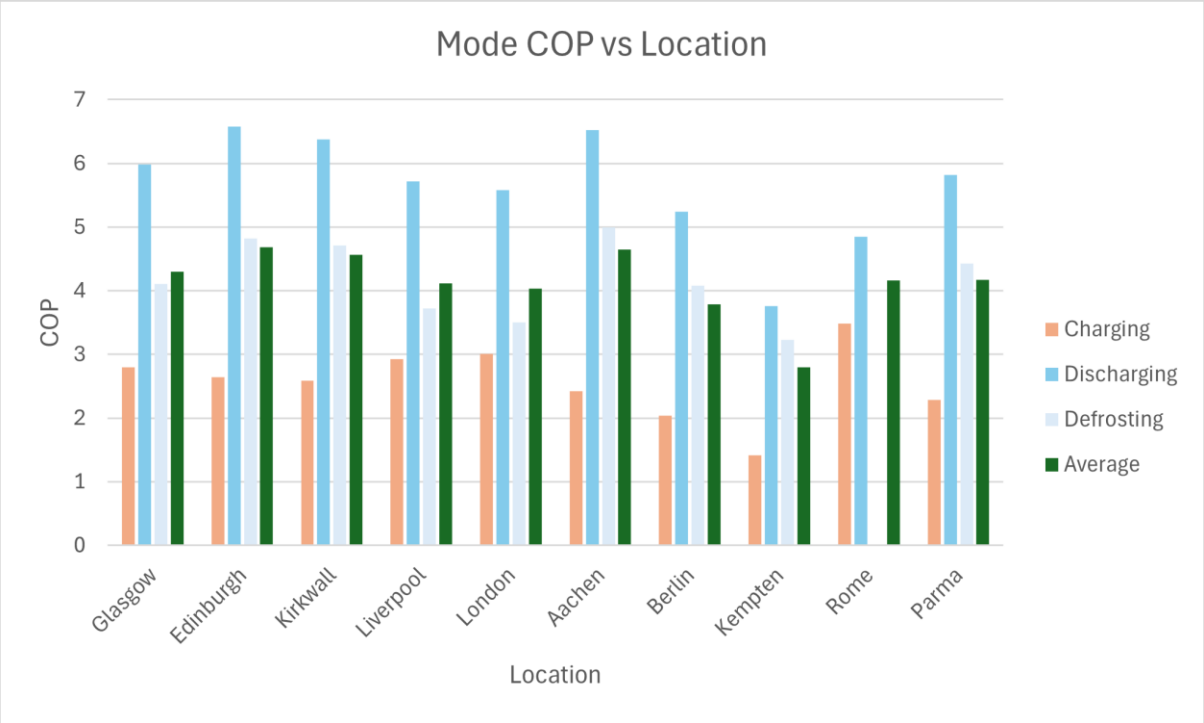

Figure 49: Results of the flexible heat pump system comparing the calculated COP values obtained for ten different European climates.

4.6 Varying the storage tank size

4.6.1 Overall performance

Figure 50 compares the coefficient of performance values of the flexible heat pump system for seven different storage tank sizes. These results are dynamic in nature and display the averaged long-term performance of the system. The COP values for all three operational modes, as well as the average COP values, are relatively consistent across all seven tank sizes assessed. In the charging mode, the COP values range from 2.75 (70l) to 2.80 (210l), with a variance of 1.8% between this set of iterations. In the discharging mode, the COP values range from 5.93 (300l) to 6.07 (170l), with a variance of 2.4%. In the defrosting mode, the COP values exhibit a slightly higher variance of 8.4%, ranging from 3.85 (70l) to 4.17 (170l). From these results, it can be observed that the most optimal performance of the thermal energy storage system was obtained when using either the 170l or 210l tank sizes, with the most suboptimal performance obtained when using either the smallest or largest tank sizes with internal volumes of 70l and 300l respectively.

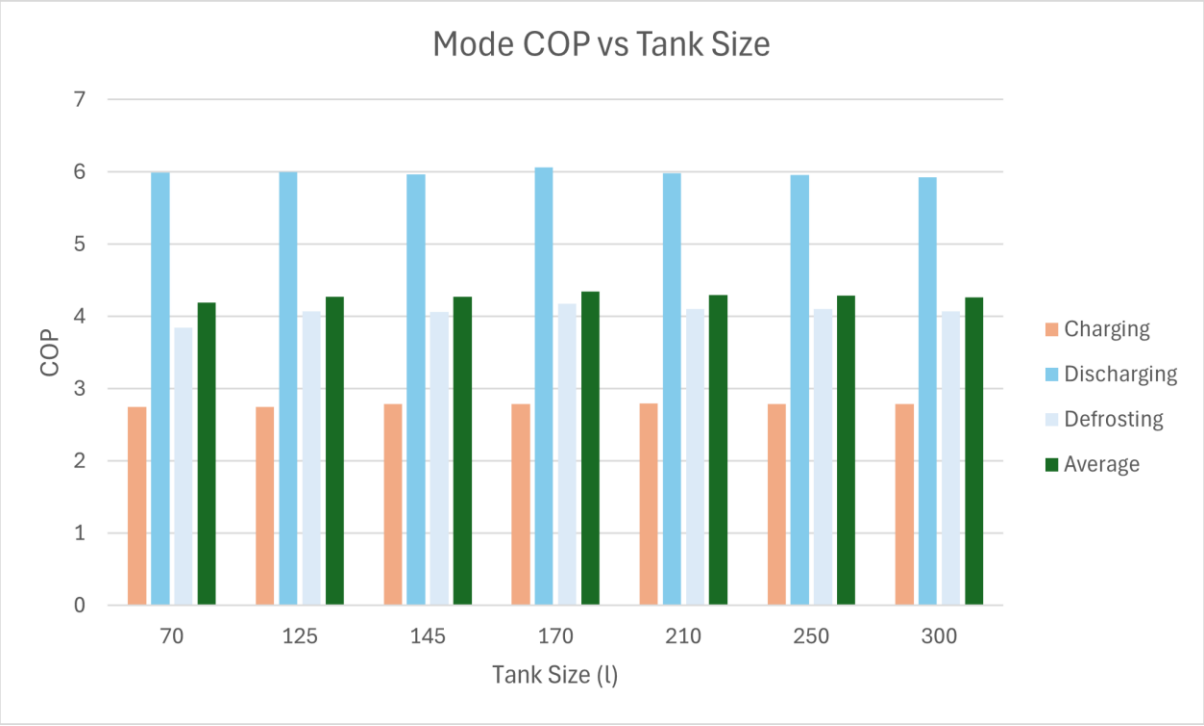

Figure 50: Results of the flexible heat pump system comparing the calculated COP values obtained for seven different storage tank sizes.

4.6.2 Charging, discharging and defrosting rates for each tank size

In order to thoroughly analyse the performance of the thermal energy storage system with regards to the size of the storage tank, a subset of these iterations focusing on the storage tank charging-discharging and charging-defrosting times for constant ambient air temperatures of 10°C and 0°C respectively were also carried out. For each simulation conducted, three instances of each operational mode (charging and either discharging or defrosting) were timed and subsequently averaged to obtain an average cycle time for each mode for each of the seven different storage tank sizes. These were then used to calculate the average time to complete one full charging-discharging or charging-defrosting cycle, as well as the operational time ratio β and the volumetric charging factor γ.

Figure 51 and 52 compare the average charging, discharging/defrosting and total cycle times of the thermal energy storage tank for different storage tank sizes at 10°C and 0°C ambient air temperatures respectively. As shown in the figures, the amount of time it takes to fully charge or discharge the thermal energy storage tank increases proportionally to the internal volume of the tank. At 10°C, the smallest tank size (70l) requires 0.79h to fully charge the storage tank in the charging mode and 0.85h to fully discharge it in the discharging mode, with an average time of 1.65h to complete one full charging-discharging cycle, while the largest tank size (300l) requires 3.43h to fully charge the storage tank in the charging mode and 3.60h to fully discharge it in the discharging mode, with an average time of 7.03h to complete one full charging-discharging cycle. At 0°C, the smallest tank size requires 0.86h to fully charge the storage tank in the charging mode and 0.30h to fully discharge it in the defrosting mode, with an average time of 1.16h to complete one full charging-defrosting cycle, while the largest tank size requires 3.73h to fully charge the storage tank in the charging mode and 1.24h to fully discharge it in the defrosting mode, with an average time of 4.97h to complete one full charging-defrosting cycle.

Figure 53 and 54 compare the operational time ratios of the thermal energy storage tank for different storage tank sizes at 10°C and 0°C ambient air temperatures respectively. As shown in the figures, the operational time ratios show slight variations between the seven different tank sizes, but vary significantly between the two different ambient air temperatures for the same tank size. At 10°C, the operational time ratios range from 1.08 (70l) to 1.05 (300l), whereas at 0°C the operational time ratios range from 0.35 (70l) to 0.33 (300l).

Figure 55 and 56 compare the volumetric charging factors for the charging and discharging cycles of the thermal energy storage tank for different storage tank sizes at 10°C and 0°C ambient air temperatures respectively. As shown in the figures, the volumetric charging factors for the system at 10°C show slight variations between the seven different tank sizes, while same values for the system at 0°C increase proportionally to the internal volume of the tank. At 10°C, the system with the smallest tank size (70l) charges and discharges the storage tank at a rate of 40.8 s/l and 43.9 s/l for the charging and discharging modes respectively, while the system with the largest tank size (300l) charges and discharges the storage tank at a rate of 41.2 s/l and 43.2 s/l for the same operational modes. At 0°C, the system with the smallest tank size charges and discharges the storage tank at a rate of 44.3 s/l and 15.4 s/l for the charging and defrosting modes respectively, while the system with the largest tank size charges and discharges the storage tank at a rate of 191.8 s/l and 63.8 s/l for the same operational modes.

As was initially predicted, increasing the size of the storage tank aids in allowing the thermal energy storage system to be used as a heat source in the discharging or defrosting modes for longer periods of time before requiring recharging, up to 322% and 314% longer for the 300l tank in comparison to the 70l tank operating at 10°C and 0°C respectively. This would provide significant long-term benefits to the end user if the charging time was calibrated so that it could be recharged consistently during warmer daytime periods for use during colder periods such as nighttime, while also minimising supply temperature fluctuations incurred due to mode switching. However, the system operating at a lower freezing air temperature suffered from overall poorer performance in comparison to the same system operating at an optimal hot air temperature. From the average cycle times and operational time ratios, it can be observed that the system operating at 0°C requires approximately three times longer to fully charge the thermal energy storage tank with regards to the amount of time required to fully discharge it while operating in the defrosting mode. Contrastingly, the system operating at 10°C fully charges the storage tank in approximately the same amount of time as the system operating at 0°C, but discharges it approximately 5-8% longer with regards to the amount of time required to fully charge it while operating in the charging mode. This behaviour was observed to be independent of the size and volume of the storage tank and can be explained by the number of thermal sinks active in the discharging mode, which is fewer than that in the defrosting mode (which requires the heating of both the condenser for domestic heating and the evaporator for external ice removal).

From the volumetric charging factors, it can be observed that the system experiences drastically reduced performance while charging large sizes of the thermal energy storage tank under freezing air temperatures. Under suboptimal conditions, the rate at which the 70l storage tank is charged is approximately equal to the charging rate of the 300l storage tank operating under optimal conditions, with minor variations between the other tank sizes operating at 10°C. For the larger tank sizes, the amount of time required to charge the equivalent of one litre of sensible storage material (in this case water) increases substantially with tank volume, ranging from 79% for the next largest tank size (125l) up to 333% for the largest tank size (300l). Therefore, under climate conditions that frequently tend towards freezing air temperatures, it is recommended to minimise the size and volume of the thermal energy storage tank in order to maximise the charging speed of the thermal energy storage system. Additionally, smaller tank sizes have the additional benefit of reducing the overall size and upfront costs of the flexible heat pump system during installation, which would be more advantageous to the end user short-term. However, backup heaters may also be required in the event that the system is unable to complete evaporator defrosting operations by itself.

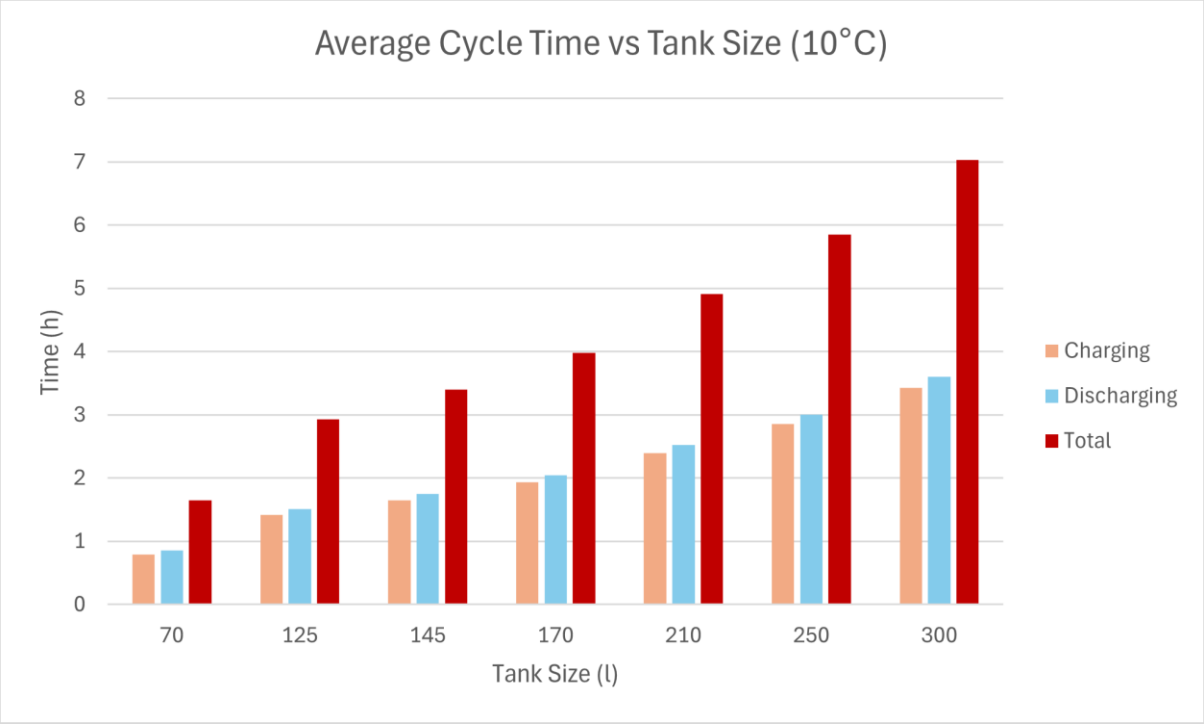

Figure 51: Average charging, discharging and total cycle times of the thermal energy storage tank for different storage tank sizes at 10°C ambient air temperature.

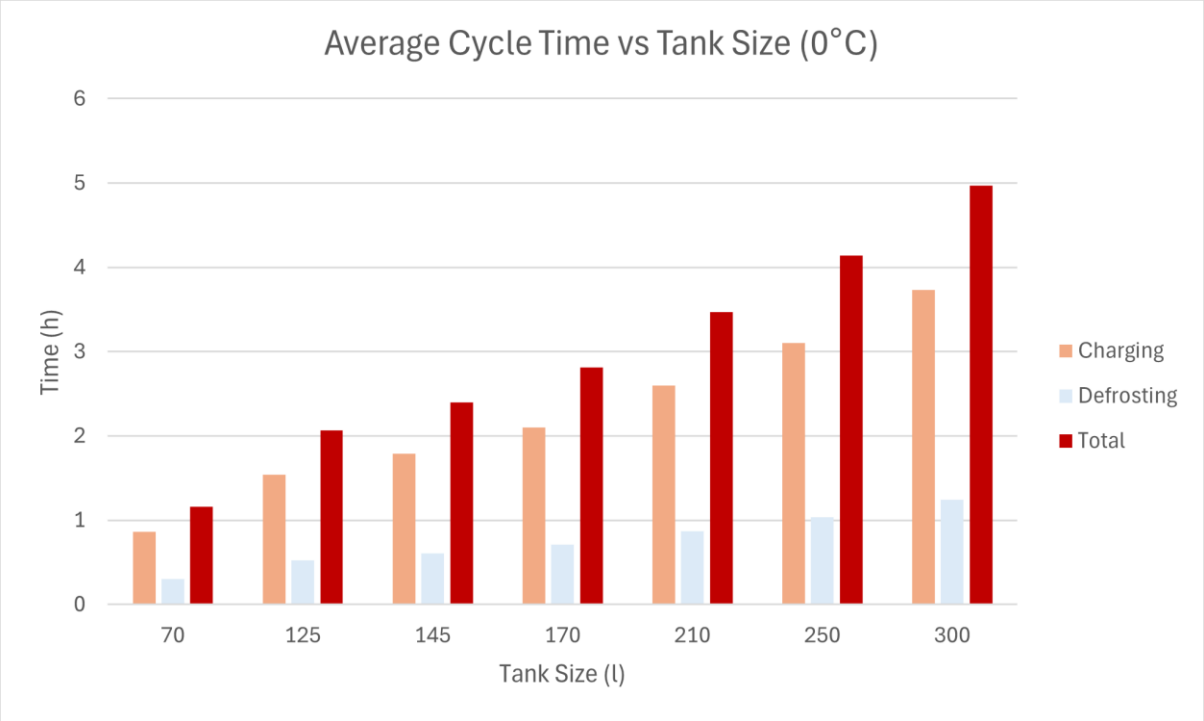

Figure 52: Average charging, defrosting and total cycle times of the thermal energy storage tank for different storage tank sizes at 0°C ambient air temperature.

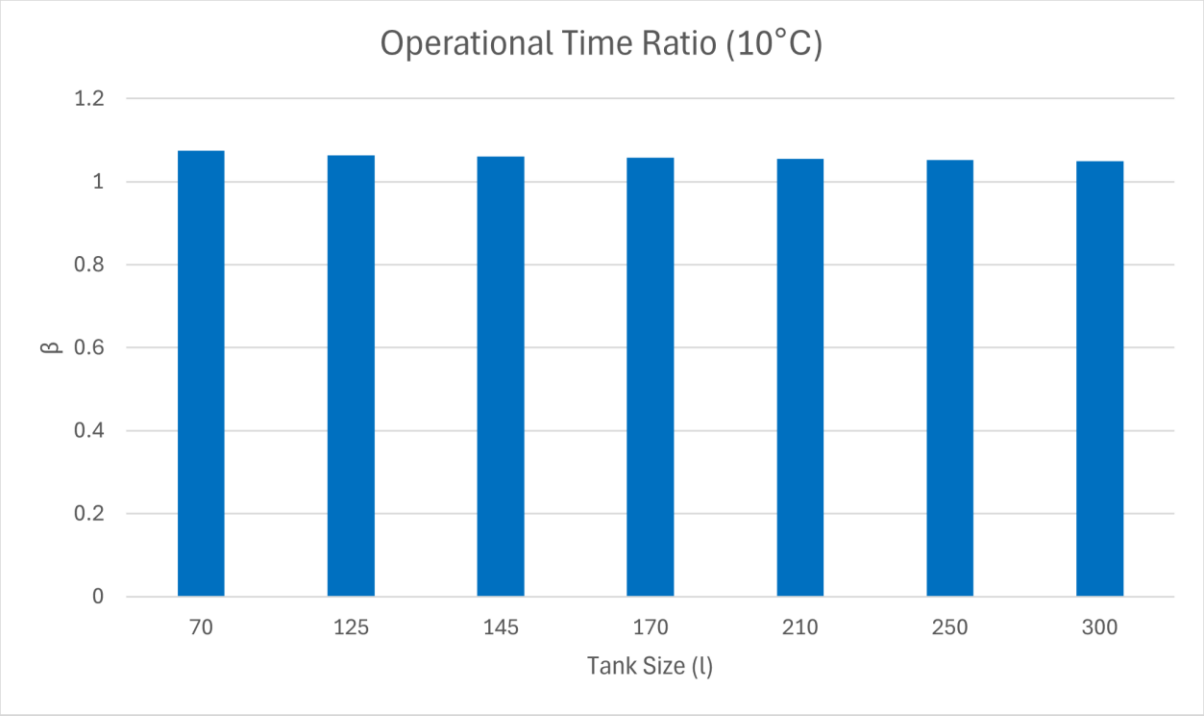

Figure 53: Operational time ratios of the thermal energy storage tank for different storage tank sizes at 10°C ambient air temperature.

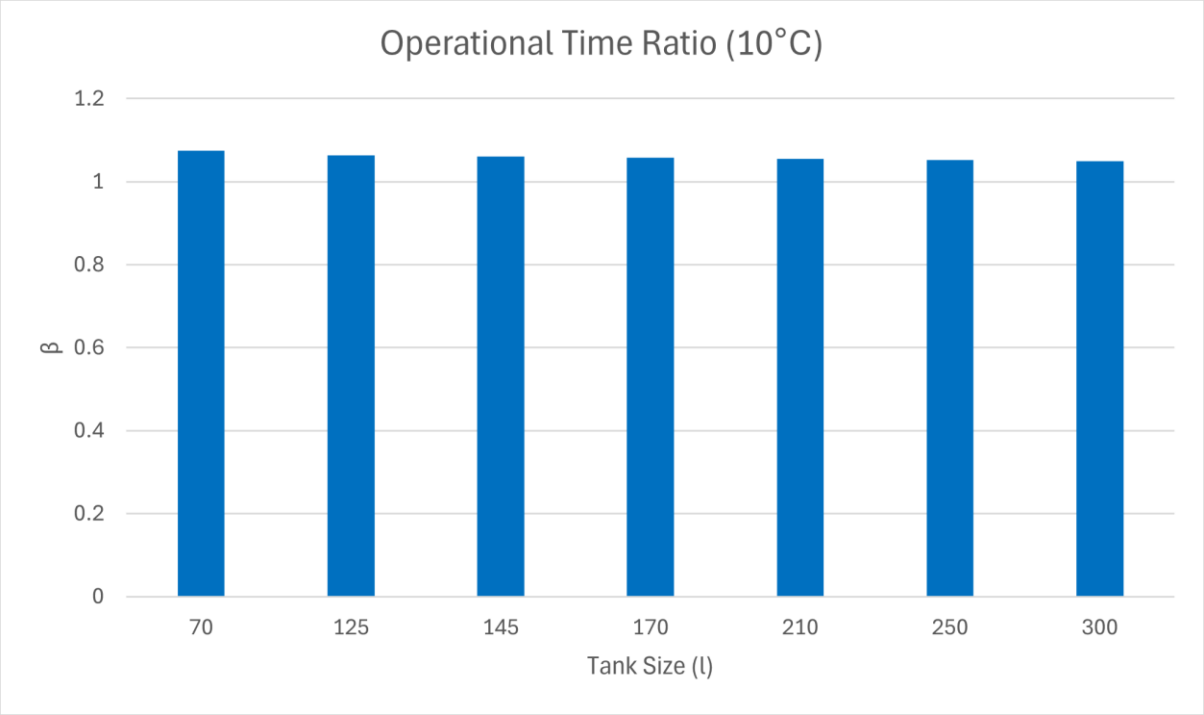

Figure 54: Operational time ratios of the thermal energy storage tank for different storage tank sizes at 0°C ambient air temperature.

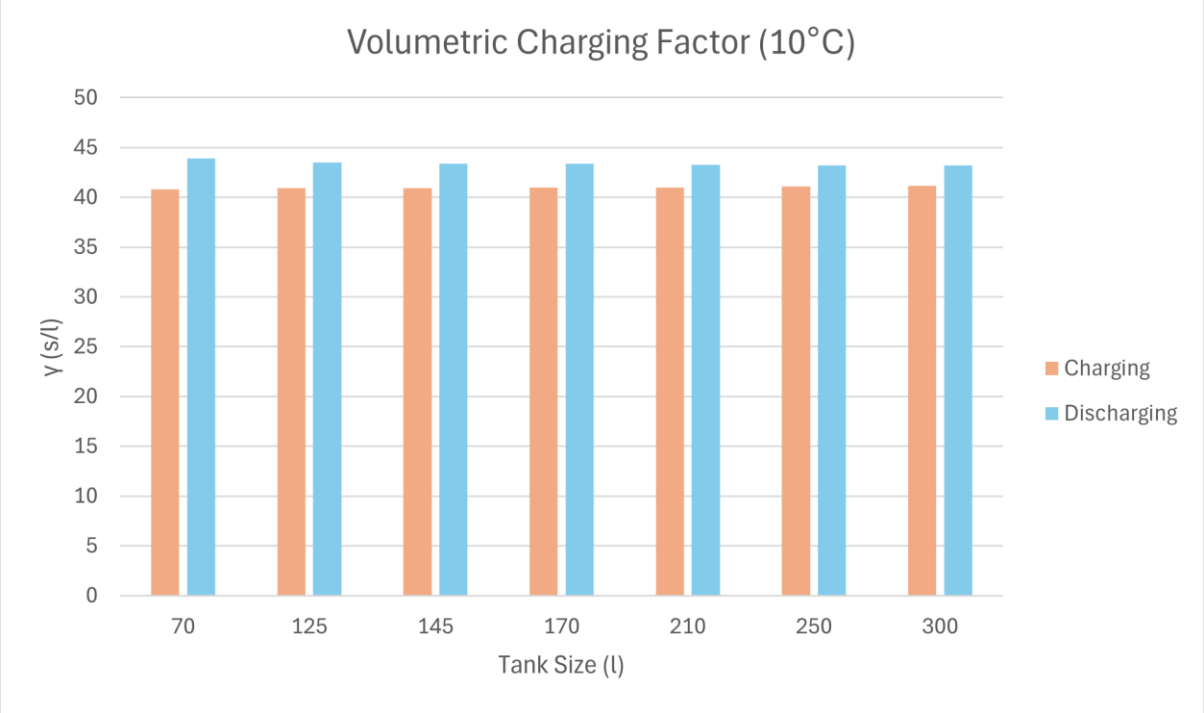

Figure 55: Volumetric charging factors for the charging and discharging cycles of the thermal energy storage tank for different storage tank sizes at 10°C ambient air temperature.

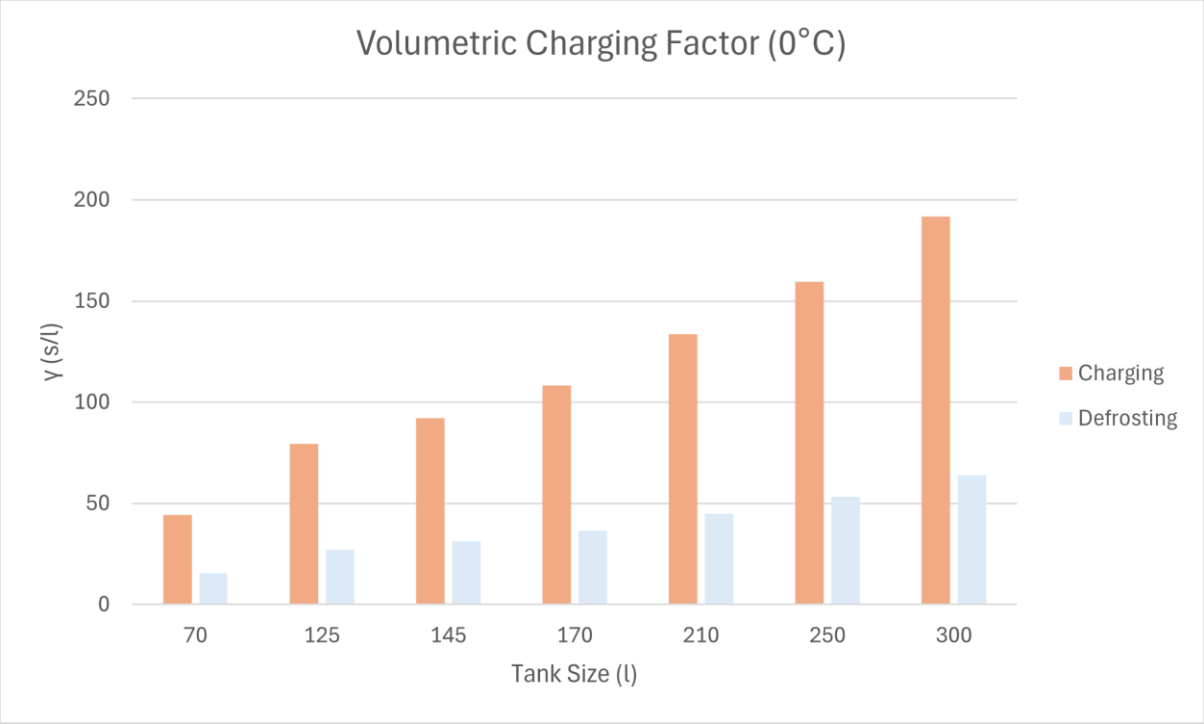

Figure 56: Volumetric charging factors for the charging and defrosting cycles of the thermal energy storage tank for different storage tank sizes at 0°C ambient air temperature.

4.7 Varying the hot/cold air temperature threshold

Figure 57 compares the coefficient of performance values of the flexible heat pump system for five different hot/cold air temperature thresholds for the operational mode switching control system. These results are dynamic in nature and display the averaged long-term performance of the system. Linear trends are observable for all five model iterations assessed: increasing the value of the hot/cold temperature threshold increases the discharging, defrosting and average COP values of the flexible heat pump system while reducing the COP value of the charging mode.

When the value of the hot/cold temperature threshold decreases, the region in which the ambient air temperature is considered to be “hot” increases, extending the overall time in which the flexible system operates in the charging mode (with or without charging the thermal energy storage tank). This results in a proportional increase to the COP value of the charging mode, ranging from 2.38 (8°C) to 3.01 (4°C). Additionally, a lower threshold temperature reduces the frequency of the mode switching fluctuations observed in the condenser outlet water temperature, allowing the system to provide a more consistent and stable supply temperature at the cost of reducing its flexible capabilities by limiting the

usage of the discharging mode. Similarly, increasing the value of the hot/cold temperature threshold increases the potential range of the “cold” temperature region, causing the system to operate in the discharging mode (or in the charging mode during suboptimal cold conditions) more often at the cost of requiring more frequent charging cycles to recharge the storage tank once fully depleted. This results in an increase in the discharging mode COP values, ranging from 4.79 (4°C) to 7.15 (8°C). This also results in a similar increase in the defrosting mode COP values, ranging from 2.73 (4°C) to 5.36 (8°C), as the frequent cycling of the thermal energy storage system results in more heat energy being stored in the storage tank upon initiating this mode, increasing its performance by extending its usage time and reducing the need to recharge the storage tank during detrimental freezing conditions. Furthermore, the average COP value for each model tends to be greater for higher values of the hot/cold temperature threshold, as the system uses the storage tank as a high temperature heat source for extended periods of time.

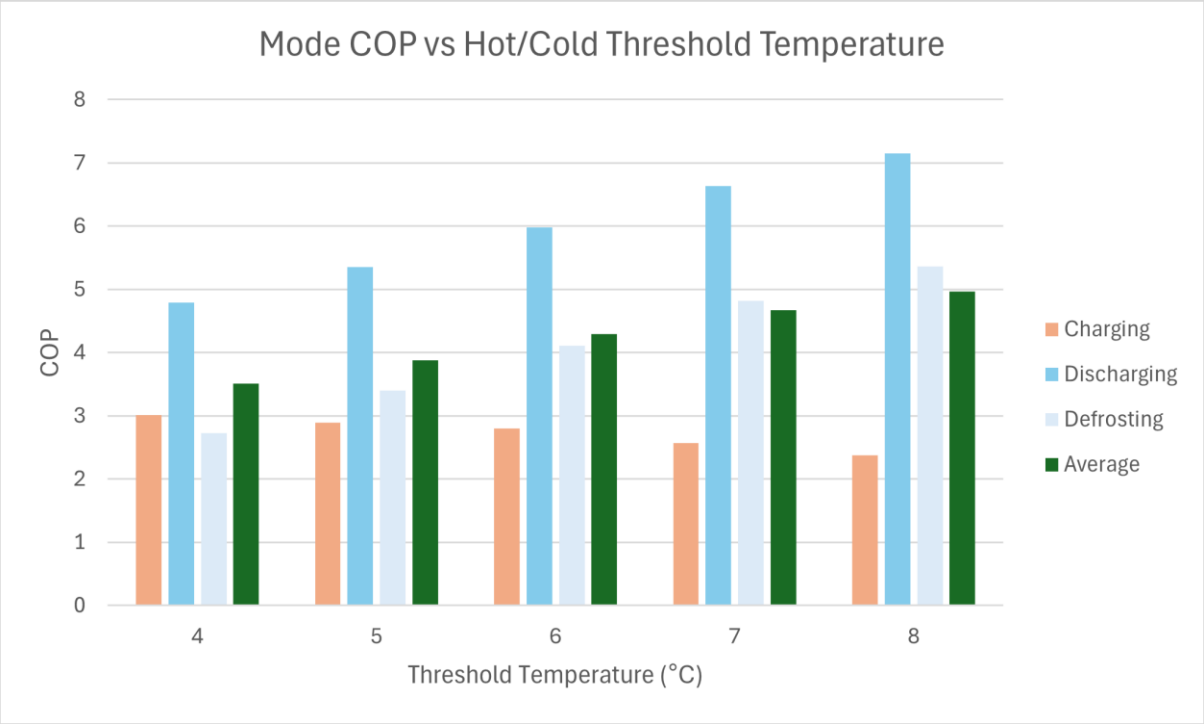

Figure 57: Results of the flexible heat pump system comparing the calculated COP values obtained for five different hot/cold air temperature thresholds for the operational mode switching control system.

4.8 Varying the max/min tank temperature thresholds

Figure 58 compares the coefficient of performance values of the flexible heat pump system for seven different sets of max/min temperature thresholds for the operational mode

switching control system. These results are dynamic in nature and display the averaged long-term performance of the system. In order to fairly compare the performance metrics of the seven model iterations, the desired condenser outlet water temperature setpoint for each iteration was increased to 60°C, with the condenser inlet (return) water temperature similarly being increased to 55°C. These adjustments allowed the system to meet the highest temperature demands found in iterations out with the scope of the default system configuration while resulting in minimal changes to the overall behaviours of the system.

For all seven model iterations assessed, the COP values for the charging mode were very consistent overall, with only a minor variation of approximately 2.5% between iterations. This was to be expected, as the performance of the flexible heat pump system during the charging mode was found to be independent of the size, volume and temperature range of the storage vessel itself. In comparison to the baseline iteration (30-50°C), the iterations that altered both the maximum and minimum tank temperature thresholds simultaneously (25-55°C and 20-60°C) performed better and almost identically to one another, resulting in improvements of up to 7.1% and 10.1% to the COP values of the discharging and defrosting modes respectively. For the iterations that only increased the maximum tank temperature threshold (30-55°C and 30-60°C), the improvements in comparison to the baseline iteration were even greater, resulting in improvements of up to 16.5% and 23.1% to the COP values of the discharging and defrosting modes respectively, with the best performance recorded for the maximum 60°C iteration. However, the iterations that only decreased the minimum tank temperature threshold (25-50°C and 20-50°C) resulted in poorer performance in comparison to the baseline iteration, resulting in COP values that were up to 8.1% and 11.5% lower for the discharging and defrosting modes respectively, with the worst performance recorded for the minimum 20°C iteration.

In general, air source heat pump systems exhibit better performance if the temperature difference between the available heat source (either the surrounding air or a thermal energy storage vessel) and the heat sink (typically an indoor environment) is minimised. By increasing the temperature of the thermal energy storage tank, less compressor work is required in order to elevate the refrigerant fluid to a higher temperature during the discharging and defrosting modes, thus improving their respective COP values. However, as the temperature of the storage tank gradually decreases over time and approaches the temperature of the ambient air surrounding the evaporator, the performance of the flexible system gradually decreases due to the greater temperature difference between the available heat source and the heat sink. This indicates that while increasing the maximum tank temperature threshold

(with or without also decreasing the minimum tank temperature threshold) results in improved performance over the baseline system, decreasing the minimum tank temperature threshold in isolation results in a reduction in the performance of the system. Therefore, in order to maximise the performance of the flexible heat pump system and the integrated thermal energy storage system, the temperature of the storage tank should be maximised and prolonged in order to ensure that a high temperature heat source is available for use during the discharging and defrosting modes. Furthermore, a long-term high temperature heat source could be ensured if latent thermal energy storage using phase change materials was implemented over the sensible water tank used in this study.

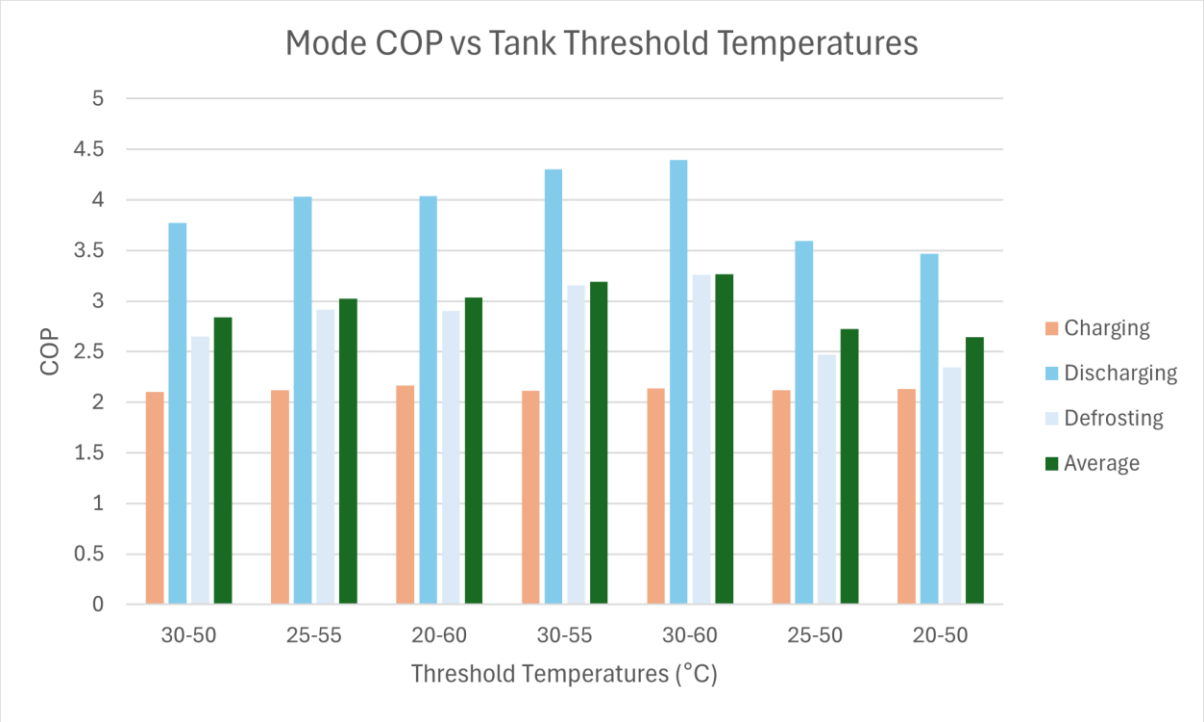

Figure 58: Results of the flexible heat pump system comparing the calculated COP values obtained for seven different sets of max/min tank temperature thresholds for the operational mode switching control system.

4.9 Potential safety concerns regarding the four-way valve

Figure 59 shows the fluid pressure values of the four-way valve for the simulation of the baseline flexible heat pump model. These values were taken for a selected period of time of 50,000s (or approximately 14 hours) in duration, covering three full charging and discharging cycles for ambient air temperatures ranging between 6.5°C and just above 0°C without entering the “freezing” temperature region. The four fluid ports were named based on their

positions and designations within Dymola: A (condenser outlet), B (subcooler inlet/outlet), C (evaporator inlet/outlet) and D (separator/compressor inlet). A breakdown of this figure covering the behaviours of each individual fluid port can be found in figure 60, and the position of the four-way valve over the same period of time can be found in figure 61.

Across all three operational modes, port A is included in the high pressure section of the flexible heat pump system. This port accepts high pressure refrigerant fluid exiting the condenser with a pressure of approximately 1,746 kPa. Similarly, port D is included in the low pressure section and expels low pressure refrigerant fluid exiting the heat source (either the evaporator or the subcooler) with a pressure of approximately 482 kPa. The pressure sections that ports A and D occupy, as well as their flow directions, remain constant throughout operation and represent the right half of the overall system architecture. The left half of the overall system architecture, including ports B and C, varies in pressure and flow direction depending on the position of the four-way valve and the redirection of the fluid flow entering from port A. In the charging mode, refrigerant fluid entering the valve from port A flows towards port B in order to facilitate heat recovery, whereas it flows towards port C in the discharging and defrosting modes in order to redirect it towards the evaporator (either bypassing or flowing through it respectively). In effect, the pressure sections that ports B and C occupy in the charging mode are swapped during the discharging and defrosting modes.

Starting from 50,000s, the flexible system steadily operates in the charging mode with fluid flowing from ports A-B in the high pressure section and from ports C-D in the low pressure section. At approximately 53,100s, the ambient air temperature drops below 6°C and the system transitions into the discharging mode, with fluid flowing from ports A-C in the high pressure section and from ports B-D in the low pressure section. At this moment of transition, the pressure of the refrigerant fluid through port C rapidly rises from 499 kPa to 1,746 kPa as it now accepts high pressure fluid flowing into it from port A. Additionally, the flow direction through port C becomes reversed and fluid mixing between two differing fluid phases (the superheated refrigerant exiting the condenser and the cooler liquid refrigerant previously exiting the expansion valve) occurs. This also occurs between ports B and D, wherein two different fluid phases mix and the flow direction through port B reverses. However, throughout this period of discharging, the fluid pressure through these ports first converges to an intermediary pressure of 1,442 kPa before gradually dropping to a value of 954 kPa over the course of 8,800s. It is predicted that if the thermal energy storage tank contained an infinite amount of heat energy such that the discharging mode could operate indefinitely, the pressure of the refrigerant fluid flowing through ports B and D would eventually settle back to

its initial value of approximately 482 kPa. At approximately 61,900s, the temperature of the thermal energy storage tank drops below 30°C and the system returns back to the charging mode. Similar to the behaviours previously observed in the discharging mode, the fluid pressure through ports A and B first converges to an intermediary pressure of 1,184 kPa before gradually rising back to its initial value of 1,746 kPa. Furthermore, the pressure of the refrigerant fluid through ports C and D rapidly falls to values of 363 kPa and 307 kPa respectively before gradually rising back to approximately 437 kPa. At approximately 70,900s, the system again returns to the discharging mode, where this behaviour then repeats periodically for the various conditions that trigger the mode switching functionalities of the system.

The potential issues regarding the refrigerant fluid flowing through the four-way valve (as well as through any adjacent components) are threefold. Firstly, the four-way valve must be selected so that the system is capable of managing the pressure changes that are incurred during mode switching operations. This behaviour is most notable in port C, which experiences a pressure change of approximately 1,383 kPa upon transitioning from the charging mode into the discharging mode (in addition to a change in flow direction), and this may cause the valve to rupture in the event that the pressure changes become too violent or extreme. Therefore, the four-way valve and all adjacent components and sections of piping must be rated to handle pressures of at least 1,750 kPa in order to ensure the system can function both effectively and safely. Secondly, fluid mixing between two or more different phases must be minimised in order to protect key components such as the compressor. The mixing of different fluid phases would directly harm the thermodynamic performance of the system, and components operating in the presence of an incompatible fluid phase would be subjected to potential wear or breakage. This may be corrected through the implementation of additional separator components connected before each port of the four-way valve, preventing incompatible fluid phases from entering key components at the cost of greater system complexity. Lastly, the aforementioned pressure changes and fluid mixing may lead to significant noise pollution in the form of loud banging noises that would occur upon initiating the transition between modes. This noise would be detrimental to both the end user and to the surrounding environment, and may become more frequent depending on the usage of the thermal energy storage tank. All three of these problems could be minimised or eliminated by first bringing the system to rest before initiating mode switching operations, however this would significantly reduce the overall performance and effectiveness of the system by limiting its ability provide a continuous heat supply for the end user.

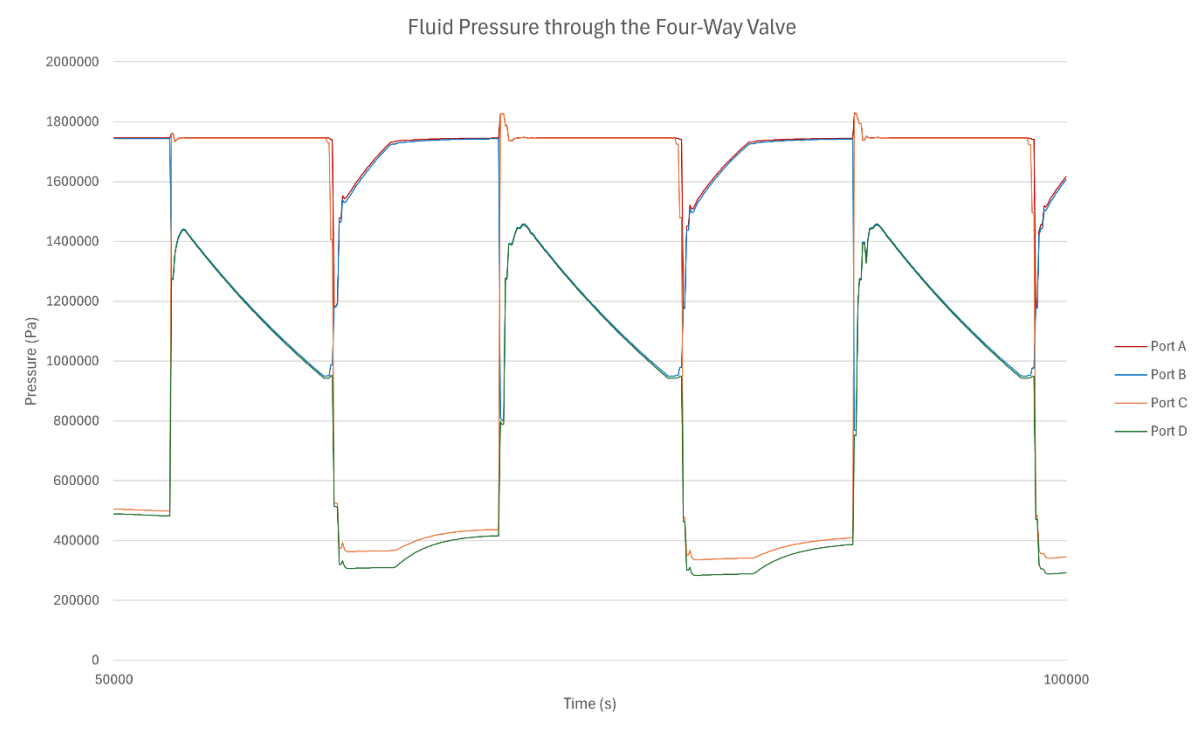

Figure 59: Fluid pressure values of the four-way valve for the simulation of the baseline flexible heat pump model.

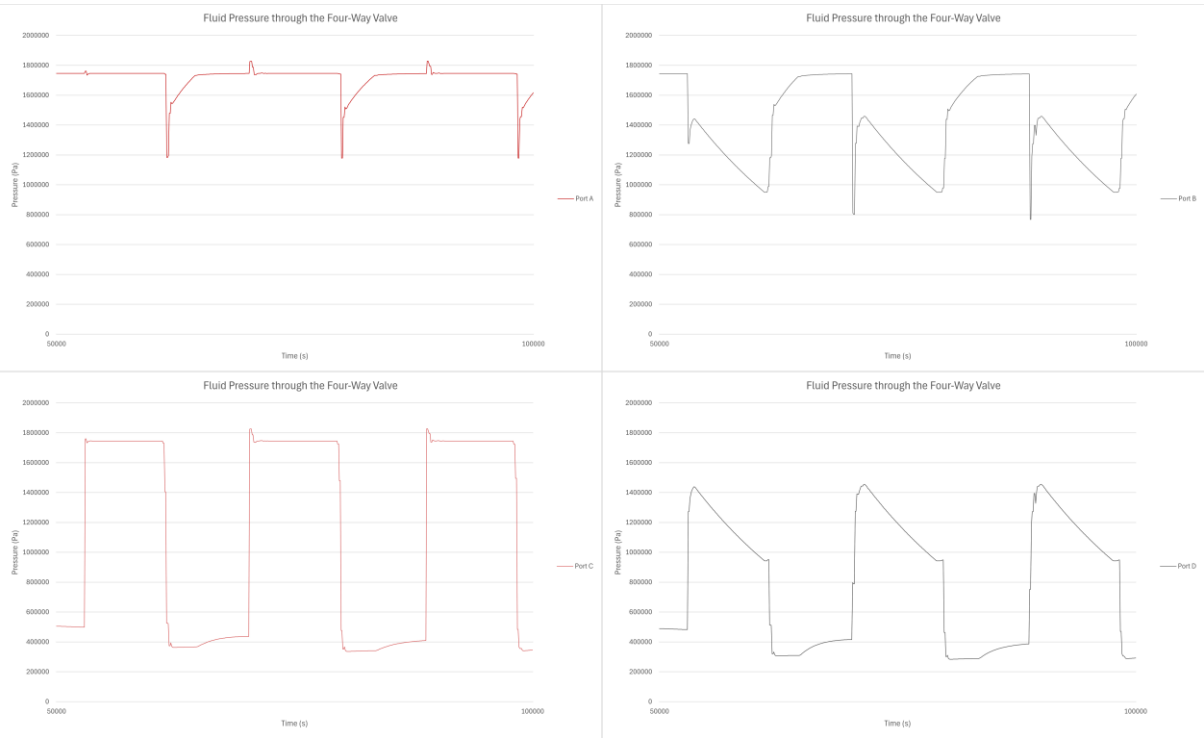

Figure 60: Fluid pressure values for all four ports of the four-way valve: A (top left), B (top right), C (bottom left) and D (bottom right).

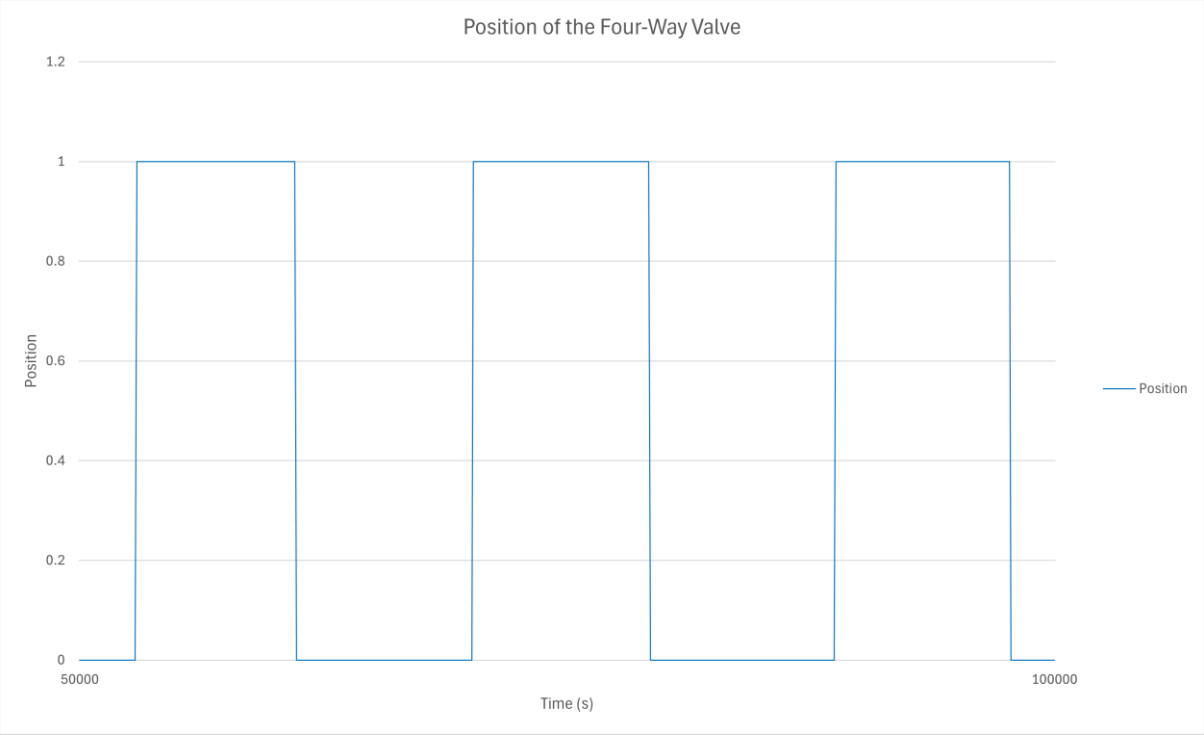

Figure 61: Position values of the four-way valve for the simulation of the baseline flexible heat pump model.

5 Conclusion

5.1 Main findings

In this thesis, a comprehensive simulation model of the flexible heat pump system, including integrated thermal energy storage systems and automatic mode switching functionalities, was constructed within the dynamic modelling and simulation environment Dymola, based on the Modelica language. A total of forty-nine iterations were simulated and analysed for various different working fluids, locations, components and component parameters in order to assess the optimal thermodynamic performance of the system and how it compares to non-flexible models. The main findings of this thesis can be summarised as follows:

- The overall performance of the flexible heat pump system demonstrates that it is sufficiently capable of providing the desired hot water supply temperature for the majority of its operational runtime. The inclusion of the thermal energy storage system within an Evans-Perkin vapour compression cycle was proven to increase the thermodynamic performance of the system, exhibiting an average performance improvement of 25.2% when compared to a conventional standard heat pump system of equivalent size and scale.
- In comparison to the original prototype system that utilised R134a as the working fluid, the flexible system utilising R290 exhibited improved performance in the discharging and defrosting modes, as well as the most optimal performance overall for the three potential options assessed. R1234ze was found to significantly improve the performance of the charging mode, with a minor reduction in the performance of the discharging mode. As such, both refrigerant fluids provide suitable, environmentally friendly alternatives to R134a.
- For the ten locations assessed, the local climates that had a sufficient balance of “hot” temperature periods to charge the storage tank and “cold” temperature periods to discharge the storage tank (primarily in the discharging mode) were found to result in the highest system performance. Weather profiles that limited the number of charging or discharging cycles were found to reduce its overall performance, with those featuring very little or near-constant discharging performing the worst overall.
- All seven tank sizes were found to be remarkably similar in terms of system performance but varied drastically in terms of their charging and discharging mechanics. Larger tank sizes were able to be used as a heat source for longer periods

of time before requiring recharging but required significantly more time to recharge once fully depleted. Similarly, smaller tank sizes could be charged faster but limited the amount of time that they could be discharged as a heat source and resulted in more frequent mode switching fluctuations in the hot water supply temperature. It was also observed that under freezing temperature conditions, the amount of time required to charge the equivalent of one litre of sensible storage material substantially increased with tank volume, up to 333% for the largest tank size assessed.

- For the iterations that varied the hot/cold air temperature threshold, it was found that increasing this threshold value increased the overall performance of the system by extending the range of temperatures in which the discharging mode is used, at the cost of reducing its performance in the charging mode. Decreasing this threshold value provided similar results, extending the temperature range of the charging mode but limiting the flexible capabilities of the discharging mode.
- For the iterations that varied the maximum/minimum tank temperature thresholds, it was found that increasing the maximum storage tank temperature resulted in significant improvements to the performance of the discharging and defrosting modes, up to 16.5% and 23.1% respectively for a maximum tank temperature of 60°C. However, decreasing the minimum tank temperature resulted in poorer performance compared to the default tank configuration, and as such is not recommended.
- Three potential issues regarding the pressure changes and fluid mixing behaviours of the refrigerant flowing through the four-way valve were identified and discussed. It was subsequently concluded that these issues could be minimised or eliminated through the implementation of specialised components or by bringing the system to rest before initiating mode switching operations, at the cost of greater system complexity or reducing its overall performance respectively.

5.2 Areas for future work

With regards to the currently ongoing research into the flexible heat pump system, the following areas show sufficient promise for further development and exploration:

- The implementation of a manual control scheme that overrides the automatic mode switching control scheme, used in the event that the end user wants the system to operate in a specific mode out with the standard control logic.
- Conduct a more thorough analysis into the characteristics of the charging mode, splitting its overall performance into four individual profiles for each of the four different charging behaviours as shown in table 12 (idle charging, optimal charging, suboptimal charging and detrimental charging).
- Expanding the input datasets to include information on the levels of occupancy (weekday working patterns, weekend activity, number of occupants, etc), dwelling size, number of heat delivery devices, levels of insulation, electricity usage, usage of domestic-scale renewable energy sources, and other relevant factors that would aid in improving the accuracy of the model.
- Recontextualising the potential performance and efficiency improvement benefits of the system by factoring in time-based electricity tariffs and electricity usage to calculate both the short- and long-term monetary savings that could be achieved.
- The implementation of water source or ground source heat pump arrangements, as well as additional heating methods through backup heating elements or solar photovoltaic panels.
- The implementation of latent phase change materials-based storage tank arrangements, primarily based on the altTank model iterations shown in figure 13 and 23.
- The implementation of transcritical vapour compression cycle arrangements using environmentally-friendly refrigerant fluids such as carbon dioxide (CO_2), with the focus on improving the performance of the flexible heat pump system operating in cold and freezing locations such as Kempten, Germany.

Appendices

Appendix 1 – Modelica code

Modelica code for the FlexHeatPump_V9 dynamic simulation model constructed within Dymola:

```
model FlexHeatPump_V9 "Fully calibrated flexible heat pump model"
  import ModelicaServices;

  inner TIL.SystemInformationManager sim(
    redeclare TILMedia.VLEFluidTypes.TILMedia_Propane vleFluidType1,
    redeclare TILMedia.GasTypes.TILMedia_MoistAir gasType1,
    redeclare TILMedia.LiquidTypes.TILMedia_Water liquidType1,
    generateEventsAtFlowReversalVLEFluid=false)
    annotation (Placement(transformation(extent={{110,70},{130,90}})));
  TIL.VLEFluidComponents.Compressors.EffCompressor compressor(
    use_mechanicalPort=true,
    nFixed=50,
    displacement=2.1e-5,
    volumetricEfficiency=1,
    isentropicEfficiency=1,
    effectiveIsentropicEfficiency=1)
    annotation (Placement(transformation(extent={{52,-8},{68,8}})));
  TIL.HeatExchangers.FinAndTube.GasVLEFluid.ParallelFlowHX evaporator(
    redeclare TIL.HeatExchangers.FinAndTube.Geometry.FinAndTubeGeometry
      hxGeometry(
      finnedTubeLength=0.406,
      nSerialTubes=3,
      serialTubeDistance(displayUnit="m") = 0.02159,
      nParallelTubes=16,
      parallelTubeDistance=0.02391,
      finThickness=0.00109,
      finPitch=0.00212,
      tubeInnerDiameter=0.009525,
      tubeWallThickness=0.000889,
      nTubeSideParallelHydraulicFlows=4),
    nCells=5,     pressureStateID=2,
    redeclare model TubeSideHeatTransferModel =
        TIL.HeatExchangers.FinAndTube.TransportPhenomena.TubeSideHeatTransfer.ConstantAlp
haA
        (constantAlphaA=2000),
    redeclare model TubeSidePressureDropModel =
        TIL.HeatExchangers.FinAndTube.TransportPhenomena.TubeSidePressureDrop.ZeroPressur
eDrop,
    redeclare model WallMaterial = TILMedia.SolidTypes.TILMedia_Copper,
    redeclare model WallHeatConductionModel =
        TIL.HeatExchangers.FinAndTube.TransportPhenomena.WallHeatTransfer.GeometryBasedCo
nduction,
    redeclare model FinMaterial = TILMedia.SolidTypes.TILMedia_Aluminum,
    redeclare model FinEfficiencyModel =
        TIL.HeatExchangers.FinAndTube.TransportPhenomena.FinEfficiency.ConstFinEfficiency
,
    redeclare model FinSideHeatTransferModel =
        TIL.HeatExchangers.FinAndTube.TransportPhenomena.FinSideHeatTransfer.ConstantAlph
aA
        (constantAlphaA=2000),
    redeclare model FinSidePressureDropModel =
        TIL.HeatExchangers.FinAndTube.TransportPhenomena.FinSidePressureDrop.ZeroPressure
Drop,
    initVLEFluid="constantEnthalpy",
    TInitialWall=279.35,
    fixedTInitialWall=false)
```

```
  annotation (Placement(transformation(extent={{-106,-54},{-134,-26}})));

TIL.VLEFluidComponents.Valves.OrificeValve expansionValve(
    use_effectiveFlowAreaInput=false, effectiveFlowAreaFixed=0.7e-6)
                                                          annotation (
    Placement(transformation(
      extent={{-8,-4},{8,4}},
      rotation=270,
      origin={-200,0})));
TIL.LiquidComponents.Boundaries.Boundary waterSink(
  boundaryType="m_flow", m_flowFixed=0.1)
  annotation (Placement(transformation(extent={{56,38},{64,58}})));
TIL.LiquidComponents.Boundaries.Boundary waterSource(boundaryType="p", TFixed=
      318.15)
  annotation (Placement(transformation(extent={{-64,38},{-56,58}})));
TIL.VLEFluidComponents.PressureStateElements.PressureState pressureState_Evap(
    pressureStateID=2)
  annotation (Placement(transformation(extent={{-156,-38},{-144,-26}})));
TIL.VLEFluidComponents.PressureStateElements.PressureState pressureState_Cond(
    pressureStateID=4)
  annotation (Placement(transformation(extent={{24,26},{36,38}})));
TIL.GasComponents.Boundaries.Boundary airSource(
  streamVariablesInputTypeConcentration="phi",
  use_temperatureInput=true,
  TFixed=283.15,
  phiFixed=5,                                                boundaryType=
      "p") annotation (Placement(transformation(extent={{-76,-58},{-84,-38}})));
TIL.GasComponents.Boundaries.Boundary airSink(
  streamVariablesInputTypeConcentration="phi",
  phiFixed=5,                                  boundaryType="m_flow",
    m_flowFixed=0.5)
  annotation (Placement(transformation(extent={{-204,-58},{-196,-38}})));
TIL.LiquidComponents.Sensors.Sensor_T sensor_T_w1(redeclare
    TIL.Utilities.Units.Conversions.Units.degC unit)
  annotation (Placement(transformation(extent={{-44,60},{-36,68}})));
TIL.LiquidComponents.Sensors.Sensor_T sensor_T_w2(redeclare
    TIL.Utilities.Units.Conversions.Units.degC unit)
  annotation (Placement(transformation(extent={{36,60},{44,68}})));
TIL.GasComponents.Sensors.Sensor_T sensor_T_a2(redeclare
    TIL.Utilities.Units.Conversions.Units.degC unit) annotation (Placement(
      transformation(
      extent={{-4,-4},{4,4}},
      rotation=180,
      origin={-180,-64})));
TIL.GasComponents.Sensors.Sensor_T sensor_T_a1(redeclare
    TIL.Utilities.Units.Conversions.Units.degC unit) annotation (Placement(
      transformation(
      extent={{-4,-4},{4,4}},
      rotation=180,
      origin={-100,-64})));

TIL.OtherComponents.Mechanical.RotatoryBoundary rotatoryBoundary(
  boundaryType="n",
  use_nInput=true,
  nFixed=50) annotation (Placement(transformation(extent={{84,-10},{76,10}})));
TIL.OtherComponents.Mechanical.Sensor_n sensor_n(redeclare
    TIL.Utilities.Units.Conversions.Units.rps unit)
  annotation (Placement(transformation(extent={{70,6},{78,14}})));
Modelica.Blocks.Sources.RealExpression cond_setpoint(y(unit="degC")=50)
  annotation (Placement(transformation(extent={{130,-10},{110,10}})));
TIL.OtherComponents.Controllers.PIController compressorController(
  controllerType="PI",
  k=6e-2,
  Ti=0.1,
  yMax=120,
  yMin=12,
  yInitial=25)
  annotation (Placement(transformation(extent={{106,6},{94,-6}})));
TIL.VLEFluidComponents.Separators.Separator separator(pressureStateID=3, V=
```

```
        0.6e-3)
    annotation (Placement(transformation(extent={{-6,-46},{6,-26}})));
  TIL.LiquidComponents.Sensors.Sensor_T sensor_T_s1(redeclare
      TIL.Utilities.Units.Conversions.Units.degC unit)
    annotation (Placement(transformation(extent={{-184,60},{-176,68}})));
  TIL.HeatExchangers.TubeAndTube.VLEFluidLiquid.ParallelFlowHX subcooler(
    redeclare TIL.HeatExchangers.TubeAndTube.Geometry.TubeAndTubeGeometry
      hxGeometry(
      length_a=0.6,
      nParallelTubes_a=70,
      innerDiameter_a=0.005,
      length_b=0.6,
      nParallelTubes_b=70,
      innerDiameter_b=0.005),
    nCells=5,
    pressureStateID=1,
    redeclare model HeatTransferModel_a =
        TIL.HeatExchangers.TubeAndTube.TransportPhenomena.TubeSideHeatTransfer.ConstantAl
phaA
        (constantAlphaA=2000),
    redeclare model PressureDropModel_a =
        TIL.HeatExchangers.TubeAndTube.TransportPhenomena.TubeSidePressureDrop.ZeroPressu
reDrop,
    redeclare model HeatTransferModel_b =
        TIL.HeatExchangers.TubeAndTube.TransportPhenomena.TubeSideHeatTransfer.ConstantAl
phaA
        (constantAlphaA=2000),
    redeclare model PressureDropModel_b =
        TIL.HeatExchangers.TubeAndTube.TransportPhenomena.TubeSidePressureDrop.ZeroPressu
reDrop,
    thermalResistanceInputType="R",
    thermalResistance=6e-5,
    heatCapacityInputType="m, solid",
    solidMass=6,
    redeclare model WallMaterial = TILMedia.SolidTypes.TILMedia_Copper,
    TInitialLiquid_b=tank.TInitial)
    annotation (Placement(transformation(extent={{-154,26},{-126,54}})));

  TIL.LiquidComponents.Sensors.Sensor_T sensor_T_s2(redeclare
      TIL.Utilities.Units.Conversions.Units.degC unit)
    annotation (Placement(transformation(extent={{-104,60},{-96,68}})));
  TIL.LiquidComponents.Pumps.SimplePump circulationPump(
    presetVariableType="m_flow",
    use_massFlowRateInput=true,
    m_flowFixed=0.1)
    annotation (Placement(transformation(extent={{-208,88},{-192,72}})));
  TIL.LiquidComponents.HydraulicCapacitors.ExpansionTank expansionTank(volume=
        0.002)
    annotation (Placement(transformation(extent={{-178,108},{-162,124}})));
  TIL.LiquidComponents.Volumes.Volume tank(
    nPorts=2,
    volume(displayUnit="l") = 0.21,
    enableHeatPort=true,
    TInitial=323.15)
    annotation (Placement(transformation(extent={{-114,114},{-106,130}})));
  TIL.OtherComponents.Thermal.HeatResistor heatResistor(
    inputType=TIL.Internals.ThermalResistanceType.CylinderGeometry,
                                                    thermalResistance=0.1,
    thermalConductivity=0.03,
    length=1.486,
    innerDiameter=0.579,
    thickness(displayUnit="m") = 0.06)
    "Heat transfer through the walls of the storage tank casing"
    annotation (Placement(transformation(extent={{-98,138},{-82,142}})));
  TIL.OtherComponents.Thermal.HeatCapacitor heatCapacitor(
    inputType="m, solid",
    solidMass=47,
    redeclare model WallMaterial = TILMedia.SolidTypes.TILMedia_StainlessSteel,
    TInitial=tank.TInitial)
```

```
  "Thermal mass of the storage tank casing"
  annotation (Placement(transformation(extent={{-76,128},{-64,140}})));

TIL.OtherComponents.Thermal.ConvectiveResistor convectiveResistor(
    flowVelocityFixed=0.1, redeclare model HeatTransferModel =
      TIL.OtherComponents.Thermal.HeatTransfer.CylinderForcedConvectionCrossFlow)
                          "Heat convection to the ambient air"
  annotation (Placement(transformation(extent={{-58,138},{-42,142}})));
TIL.OtherComponents.Thermal.HeatBoundary heatBoundary(TFixed=283.15)
  annotation (Placement(transformation(extent={{-34,134},{-26,146}})));
TIL.VLEFluidComponents.PressureStateElements.PressureState pressureState_Sub(
    pressureStateID=1)
  annotation (Placement(transformation(extent={{-176,26},{-164,38}})));
TIL.VLEFluidComponents.PressureStateElements.PressureState pressureState_Sep(
    pressureStateID=3)
  annotation (Placement(transformation(extent={{24,-38},{36,-26}})));
TIL.VLEFluidComponents.Valves.FourWayValve fourWayValve(redeclare package
    MediaConfiguration = TIL.Utilities.MediaConfigurationForMixtures)
                                                        annotation (Placement(
      transformation(
      extent={{-8,-8},{8,8}},
      rotation=270,
      origin={-70,28})));
TIL.VLEFluidComponents.Valves.DirectionalControlValve directionalControlValve(
  use_switchingPositionInput=true,
  switchingPositionFixed=0,
  includeDefaultSummary=true)
  annotation (Placement(transformation(extent={{-148,-4},{-132,8}})));

TIL.VLEFluidComponents.Valves.DirectionalControlValve directionalControlValveAlt(
  use_switchingPositionInput=true,
  switchingPositionFixed=0,
  includeDefaultSummary=true) annotation (Placement(transformation(
      extent={{8,-6},{-8,6}},
      rotation=90,
      origin={-172,-20})));
TIL.OtherComponents.Thermal.Sensor_T sensor_T(redeclare
    TIL.Utilities.Units.Conversions.Units.degC unit) annotation (Placement(
      transformation(
      extent={{-4,-4},{4,4}},
      rotation=90,
      origin={-126,140})));
Modelica.Blocks.Sources.RealExpression tank_midpoint(y(unit="degC")=40)
  annotation (Placement(transformation(extent={{-370,90},{-350,110}})));
Modelica.Blocks.Logical.OnOffController onOffController(bandwidth=20,
    pre_y_start=true)
  annotation (Placement(transformation(extent={{-330,84},{-310,104}})));
Modelica.Blocks.Math.BooleanToReal booleanToReal(realTrue=0.1, realFalse=0)
  annotation (Placement(transformation(extent={{-300,84},{-280,104}})));
Modelica.Blocks.Continuous.FirstOrder firstOrder(T=0.5)
  annotation (Placement(transformation(extent={{-270,84},{-250,104}})));
Modelica.Blocks.Logical.Switch pumpSwitch
  annotation (Placement(transformation(extent={{-238,96},{-218,76}})));
Modelica.Blocks.Sources.RealExpression pump_flow(y(unit="kg/s")=0.1)
  annotation (Placement(transformation(extent={{-370,68},{-350,88}})));
Components.BooleanRangeSwitch booleanRangeSwitch2(
  rangeUpper(unit="degC")=6,
  rangeLower(unit="degC")=0,
  outputUpper=false,
  outputMiddle=true,
  outputLower=false)
  annotation (Placement(transformation(extent={{-330,-58},{-310,-38}})));
Components.BooleanRangeSwitch booleanRangeSwitch1(
  rangeUpper(unit="degC")=6,
  rangeLower(unit="degC")=0,
  outputUpper=false,
  outputMiddle=true,
  outputLower=true)
  annotation (Placement(transformation(extent={{-330,-4},{-310,16}})));
```

```
  Modelica.Blocks.Math.BooleanToReal booleanToRealValve(realTrue=1, realFalse=0)
    annotation (Placement(transformation(extent={{-240,-50},{-220,-30}})));
  Components.BooleanRelaySwitch                  booleanRelaySwitch(
    rangeUpper(unit="degC")=50,
    rangeLower(unit="degC")=30,
    outputUpper=true,
    outputLower=false,
    yInitial=false)
          annotation (Placement(transformation(extent={{-330,40},{-310,60}})));
  Modelica.Blocks.Logical.And and1
    annotation (Placement(transformation(extent={{-280,4},{-260,24}})));
  Modelica.Blocks.Logical.And and2
    annotation (Placement(transformation(extent={{-280,-50},{-260,-30}})));
  Modelica.Blocks.Sources.CombiTimeTable ambient_temperature(
    table=dataSource.getRealArray2D(181, 2),
    smoothness=Modelica.Blocks.Types.Smoothness.ContinuousDerivative,
    extrapolation=Modelica.Blocks.Types.Extrapolation.Periodic)
    "Temperature of the ambient air"
    annotation (Placement(transformation(extent={{-20,-64},{-40,-44}})));
  inner parameter ExternData.CSVFile dataSource(fileName=
        ModelicaServices.ExternalReferences.loadResource(
        "modelica://FlexHeatPump_Dyn/Data/Met Office weather data/tasmaxmin_hadukgrid_uk_
1km_day_20211201-20220228.csv"))
    annotation (Placement(transformation(extent={{110,-64},{130,-44}})));
  Modelica.Blocks.Math.UnitConversions.From_degC from_degC
    annotation (Placement(transformation(extent={{-50,-64},{-70,-44}})));
  TIL.HeatExchangers.Plate.VLEFluidLiquid.ParallelFlowHX condenser(
    hxGeometry(
      numberOfPlates=70,
      length=0.278,
      width=0.0762,
      phi=31,
      wallThickness=0.75e-3,
      patternAmplitude=2e-3,
      patternWaveLength=12.6e-3),
    nCells=5,
    pressureStateID=4,
    redeclare model HeatTransferModel_a =
        TIL.HeatExchangers.Plate.TransportPhenomena.HeatTransfer.ConstantAlphaA
        (constantAlphaA=2000),
    redeclare model PressureDropModel_a =
        TIL.HeatExchangers.Plate.TransportPhenomena.PressureDrop.ZeroPressureDrop,
    redeclare model HeatTransferModel_b =
        TIL.HeatExchangers.Plate.TransportPhenomena.HeatTransfer.ConstantAlphaA
        (constantAlphaA=2000),
    redeclare model PressureDropModel_b =
        TIL.HeatExchangers.Plate.TransportPhenomena.PressureDrop.ZeroPressureDrop,
    redeclare model WallMaterial = TILMedia.SolidTypes.TILMedia_StainlessSteel,
    redeclare model WallHeatConductionModel =
        TIL.HeatExchangers.Plate.TransportPhenomena.WallHeatTransfer.GeometryBasedConduct
ion,
    TInitialLiquid_b=waterSource.TFixed)
    annotation (Placement(transformation(extent={{-14,26},{14,54}})));

  TIL.VLEFluidComponents.Sensors.Sensor_T sensor_T_r1(redeclare
      TIL.Utilities.Units.Conversions.Units.degC unit) annotation (Placement(
        transformation(
        extent={{-4,-4},{4,4}},
        rotation=270,
        origin={68,-20})));
  TIL.VLEFluidComponents.Sensors.Sensor_T sensor_T_r2(redeclare
      TIL.Utilities.Units.Conversions.Units.degC unit) annotation (Placement(
        transformation(
        extent={{-4,-4},{4,4}},
        rotation=270,
        origin={68,28})));
  TIL.VLEFluidComponents.Sensors.Sensor_T sensor_T_r3(redeclare
      TIL.Utilities.Units.Conversions.Units.degC unit) annotation (Placement(
        transformation(
```

```
        extent={{-4,-4},{4,4}},
        rotation=0,
        origin={-44,40})));
  TIL.VLEFluidComponents.Sensors.StatePoint statePoint1(stateViewerIndex=1)
    annotation (Placement(transformation(
        extent={{-4,-4},{4,4}},
        rotation=270,
        origin={68,-28})));
  TIL.VLEFluidComponents.Sensors.StatePoint statePoint2(stateViewerIndex=2)
    annotation (Placement(transformation(
        extent={{-4,-4},{4,4}},
        rotation=270,
        origin={68,20})));
  TIL.VLEFluidComponents.Sensors.StatePoint statePoint3(stateViewerIndex=3)
    annotation (Placement(transformation(
        extent={{-4,-4},{4,4}},
        rotation=0,
        origin={-36,40})));
  TIL.VLEFluidComponents.Sensors.Sensor_T sensor_T_r4(redeclare
      TIL.Utilities.Units.Conversions.Units.degC unit) annotation (Placement(
        transformation(
        extent={{-4,-4},{4,4}},
        rotation=0,
        origin={-104,40})));
  TIL.VLEFluidComponents.Sensors.StatePoint statePoint4(stateViewerIndex=4)
    annotation (Placement(transformation(
        extent={{-4,-4},{4,4}},
        rotation=0,
        origin={-96,40})));
  TIL.VLEFluidComponents.Sensors.Sensor_T sensor_T_r5(redeclare
      TIL.Utilities.Units.Conversions.Units.degC unit) annotation (Placement(
        transformation(
        extent={{-4,-4},{4,4}},
        rotation=90,
        origin={-208,20})));
  TIL.VLEFluidComponents.Sensors.StatePoint statePoint5(stateViewerIndex=5)
    annotation (Placement(transformation(
        extent={{-4,-4},{4,4}},
        rotation=90,
        origin={-208,28})));
  TIL.VLEFluidComponents.Sensors.Sensor_T sensor_T_r6(redeclare
      TIL.Utilities.Units.Conversions.Units.degC unit) annotation (Placement(
        transformation(
        extent={{-4,-4},{4,4}},
        rotation=180,
        origin={-186,-28})));
  TIL.VLEFluidComponents.Sensors.StatePoint statePoint6(stateViewerIndex=6)
    annotation (Placement(transformation(
        extent={{-4,-4},{4,4}},
        rotation=180,
        origin={-194,-28})));
  TIL.VLEFluidComponents.Sensors.StatePoint statePoint7(stateViewerIndex=7)
    annotation (Placement(transformation(
        extent={{-4,-4},{4,4}},
        rotation=180,
        origin={-104,16})));
  TIL.VLEFluidComponents.Sensors.Sensor_T sensor_T_r7(redeclare
      TIL.Utilities.Units.Conversions.Units.degC unit) annotation (Placement(
        transformation(
        extent={{-4,-4},{4,4}},
        rotation=180,
        origin={-96,16})));
  TIL.VLEFluidComponents.Sensors.StatePoint statePoint8(stateViewerIndex=8)
    annotation (Placement(transformation(
        extent={{-4,-4},{4,4}},
        rotation=90,
        origin={-58,-20})));
  TIL.VLEFluidComponents.Sensors.Sensor_T sensor_T_r8(redeclare
      TIL.Utilities.Units.Conversions.Units.degC unit) annotation (Placement(
```

```
        transformation(
        extent={{-4,-4},{4,4}},
        rotation=90,
        origin={-58,-28})));
  TIL.VLEFluidComponents.PressureStateElements.PressureState pressureState5(
      pressureStateID=5)
    annotation (Placement(transformation(extent={{-168,-2},{-164,2}})));
  TIL.VLEFluidComponents.Tubes.Tube tube1(pressureStateID=5, redeclare model
      TubeSideHeatTransferModel =
        TIL.VLEFluidComponents.Tubes.TransportPhenomena.HeatTransfer.ConstantAlpha
        (constantAlpha=0.01))
    annotation (Placement(transformation(extent={{-162,-2},{-150,2}})));
  TIL.VLEFluidComponents.PressureStateElements.PressureState pressureState6(
      pressureStateID=6)
    annotation (Placement(transformation(extent={{-126,22},{-122,26}})));
  TIL.VLEFluidComponents.Tubes.Tube tube2(pressureStateID=6, redeclare model
      TubeSideHeatTransferModel =
        TIL.VLEFluidComponents.Tubes.TransportPhenomena.HeatTransfer.ConstantAlpha
        (constantAlpha=0.01))
    annotation (Placement(transformation(extent={{-120,22},{-108,26}})));
equation

  connect(pressureState_Cond.portA, compressor.portB) annotation (Line(
      points={{36,32},{60,32},{60,8}},
      color={153,204,0},
      thickness=0.5));
  connect(sensor_T_w2.port, waterSink.port) annotation (Line(
      points={{40,60},{40,48},{60,48}},
      color={0,170,238},
      thickness=0.5));
  connect(airSink.port, evaporator.portB_gas) annotation (Line(
      points={{-200,-48},{-134,-48}},
      color={255,153,0},
      thickness=0.5));
  connect(sensor_T_a2.port, evaporator.portB_gas) annotation (Line(
      points={{-180,-60},{-180,-48},{-134,-48}},
      color={255,153,0},
      thickness=0.5));
  connect(evaporator.portA_gas, airSource.port) annotation (Line(
      points={{-106,-48},{-80,-48}},
      color={255,153,0},
      thickness=0.5));
  connect(sensor_T_a1.port, airSource.port) annotation (Line(
      points={{-100,-60},{-100,-48},{-80,-48}},
      color={255,153,0},
      thickness=0.5));
  connect(pressureState_Evap.portA, evaporator.portB_vle) annotation (Line(
      points={{-144,-32},{-134,-32}},
      color={153,204,0},
      thickness=0.5));
  connect(compressor.rotatoryFlange, rotatoryBoundary.rotatoryFlange)
    annotation (Line(
      points={{68,0},{80,0}},
      color={135,135,135},
      thickness=0.5));
  connect(sensor_n.port, rotatoryBoundary.rotatoryFlange) annotation (Line(
      points={{74,6},{74,0},{80,0}},
      color={135,135,135},
      thickness=0.5));
  connect(cond_setpoint.y, compressorController.u_s)
    annotation (Line(points={{109,0},{105.6,0}}, color={0,0,127}));
  connect(compressorController.y, rotatoryBoundary.n_in)
    annotation (Line(points={{93.6,0},{84,0}}, color={0,0,127}));
  connect(sensor_T_w2.sensorValue, compressorController.u_m) annotation (Line(
        points={{40,66},{40,80},{100,80},{100,5.8}}, color={0,0,127}));
  connect(sensor_T_s1.port, subcooler.portA_b) annotation (Line(
      points={{-180,60},{-180,48},{-154,48}},
      color={0,170,238},
      thickness=0.5));
```

```
  connect(expansionTank.portA, circulationPump.portA) annotation (Line(
      points={{-178,112},{-200,112},{-200,88}},
      color={0,170,238},
      thickness=0.5));
  connect(circulationPump.portB, subcooler.portA_b) annotation (Line(
      points={{-200,72},{-200,48},{-154,48}},
      color={0,170,238},
      thickness=0.5));
  connect(subcooler.portB_b, sensor_T_s2.port) annotation (Line(
      points={{-126,48},{-100,48},{-100,60}},
      color={0,170,238},
      thickness=0.5));
  connect(expansionTank.portB, tank.portArray[1]) annotation (Line(
      points={{-162,112},{-110,112},{-110,113.75}},
      color={0,170,238},
      thickness=0.5));
  connect(tank.portArray[2], sensor_T_s2.port) annotation (Line(
      points={{-110,114.25},{-110,112},{-80,112},{-80,48},{-100,48},{-100,60}},
      color={0,170,238},
      thickness=0.5));

  connect(heatResistor.heatPortB, heatCapacitor.heatPort) annotation (Line(
      points={{-82,140},{-70,140}},
      color={204,0,0},
      thickness=0.5));
  connect(convectiveResistor.heatPortA, heatCapacitor.heatPort) annotation (
      Line(
      points={{-58,140},{-70,140}},
      color={204,0,0},
      thickness=0.5));
  connect(convectiveResistor.heatPortB, heatBoundary.heatPort) annotation (Line(
      points={{-42,140},{-30,140}},
      color={204,0,0},
      thickness=0.5));
  connect(expansionValve.portA, pressureState_Sub.portB) annotation (Line(
      points={{-200,8},{-200,32},{-176,32}},
      color={153,204,0},
      thickness=0.5));
  connect(pressureState_Sub.portA, subcooler.portA_a) annotation (Line(
      points={{-164,32},{-154,32}},
      color={153,204,0},
      thickness=0.5));
  connect(separator.portGas, pressureState_Sep.portB) annotation (Line(
      points={{5,-32},{24,-32}},
      color={153,204,0},
      thickness=0.5));
  connect(pressureState_Sep.portA, compressor.portA) annotation (Line(
      points={{36,-32},{60,-32},{60,-8}},
      color={153,204,0},
      thickness=0.5));
  connect(subcooler.portB_a, fourWayValve.portB) annotation (Line(
      points={{-126,32},{-78,32}},
      color={153,204,0},
      thickness=0.5));
  connect(fourWayValve.portD, separator.portInlet) annotation (Line(
      points={{-62,24},{-50,24},{-50,-32},{-5,-32}},
      color={153,204,0},
      thickness=0.5));
  connect(directionalControlValve.portB, evaporator.portA_vle) annotation (Line(
      points={{-132,0},{-90,0},{-90,-32},{-106,-32}},
      color={153,204,0},
      thickness=0.5));
  connect(heatResistor.heatPortA, tank.heatPort) annotation (Line(
      points={{-98,140},{-110,140},{-110,128}},
      color={204,0,0},
      thickness=0.5));
  connect(directionalControlValveAlt.portB, pressureState_Evap.portB)
    annotation (Line(
      points={{-170,-28},{-170,-32},{-156,-32}},
```

```
    color={153,204,0},
    thickness=0.5));
connect(sensor_T.port, tank.heatPort) annotation (Line(
    points={{-122,140},{-110,140},{-110,128}},
    color={204,0,0},
    thickness=0.5));
connect(sensor_T.sensorValue, onOffController.u) annotation (Line(points={{-128,
      140},{-340,140},{-340,88},{-332,88}},      color={0,0,127}));
connect(tank_midpoint.y, onOffController.reference)
  annotation (Line(points={{-349,100},{-332,100}},
                                                  color={0,0,127}));
connect(onOffController.y, booleanToReal.u)
  annotation (Line(points={{-309,94},{-302,94}}, color={255,0,255}));
connect(booleanToReal.y, firstOrder.u)
  annotation (Line(points={{-279,94},{-272,94}}, color={0,0,127}));
connect(pump_flow.y, pumpSwitch.u1)
  annotation (Line(points={{-349,78},{-240,78}}, color={0,0,127}));
connect(firstOrder.y, pumpSwitch.u3)
  annotation (Line(points={{-249,94},{-240,94}}, color={0,0,127}));
connect(circulationPump.m_flow_in, pumpSwitch.y)
  annotation (Line(points={{-210,86},{-217,86}}, color={0,0,127}));
connect(booleanRangeSwitch2.u, sensor_T_a1.sensorValue) annotation (Line(
    points={{-332,-48},{-340,-48},{-340,-80},{-100,-80},{-100,-66}}, color=
      {0,0,127}));
connect(booleanRangeSwitch1.u, sensor_T_a1.sensorValue) annotation (Line(
    points={{-332,6},{-340,6},{-340,-80},{-100,-80},{-100,-66}}, color={0,0,
      127}));
connect(booleanRelaySwitch.u, sensor_T.sensorValue) annotation (Line(points={
      {-332,50},{-340,50},{-340,140},{-128,140}}, color={0,0,127}));
connect(booleanRangeSwitch1.y, and1.u2)
  annotation (Line(points={{-309,6},{-282,6}}, color={255,0,255}));
connect(and1.y, fourWayValve.crossedConnection_in)
  annotation (Line(points={{-259,14},{-70,14},{-70,19}}, color={255,0,255}));
connect(booleanRangeSwitch2.y, and2.u2)
  annotation (Line(points={{-309,-48},{-282,-48}}, color={255,0,255}));
connect(and2.y, booleanToRealValve.u)
  annotation (Line(points={{-259,-40},{-242,-40}}, color={255,0,255}));
connect(directionalControlValve.switchingPosition_in, booleanToRealValve.y)
  annotation (Line(points={{-140,-4.6},{-140,-40},{-219,-40}}, color={0,0,127}));
connect(directionalControlValveAlt.switchingPosition_in, booleanToRealValve.y)
  annotation (Line(points={{-165.4,-20},{-140,-20},{-140,-40},{-219,-40}},
    color={0,0,127}));
connect(pumpSwitch.u2, and1.y) annotation (Line(points={{-240,86},{-246,86},{
      -246,14},{-259,14}}, color={255,0,255}));
connect(booleanRelaySwitch.y, and1.u1) annotation (Line(points={{-309,50},{
      -292,50},{-292,14},{-282,14}}, color={255,0,255}));
connect(and2.u1, booleanRelaySwitch.y) annotation (Line(points={{-282,-40},{
      -292,-40},{-292,50},{-309,50}}, color={255,0,255}));
connect(airSource.T_in, from_degC.y)
  annotation (Line(points={{-76,-54},{-71,-54}}, color={0,0,127}));
connect(from_degC.u, ambient_temperature.y[1])
  annotation (Line(points={{-48,-54},{-41,-54}}, color={0,0,127}));
connect(expansionValve.portB, directionalControlValveAlt.portA) annotation (
    Line(
    points={{-200,-8},{-200,-20},{-178,-20}},
    color={153,204,0},
    thickness=0.5));
connect(waterSource.port, condenser.portA_b) annotation (Line(
    points={{-60,48},{-14,48}},
    color={0,170,238},
    thickness=0.5));
connect(sensor_T_w1.port, condenser.portA_b) annotation (Line(
    points={{-40,60},{-40,48},{-14,48}},
    color={0,170,238},
    thickness=0.5));
connect(condenser.portB_b, waterSink.port) annotation (Line(
    points={{14,48},{60,48}},
    color={0,170,238},
    thickness=0.5));
```

```
connect(condenser.portB_a, pressureState_Cond.portB) annotation (Line(
    points={{14,32},{24,32}},
    color={153,204,0},
    thickness=0.5));
connect(fourWayValve.portA, condenser.portA_a) annotation (Line(
    points={{-62,32},{-14,32}},
    color={153,204,0},
    thickness=0.5));
connect(sensor_T_r1.port, compressor.portA) annotation (Line(
    points={{64,-20},{60,-20},{60,-8}},
    color={153,204,0},
    thickness=0.5));
connect(sensor_T_r2.port, compressor.portB) annotation (Line(
    points={{64,28},{60,28},{60,8}},
    color={153,204,0},
    thickness=0.5));
connect(sensor_T_r3.port, condenser.portA_a) annotation (Line(
    points={{-44,36},{-44,32},{-14,32}},
    color={153,204,0},
    thickness=0.5));
connect(statePoint1.sensorPort, compressor.portA) annotation (Line(
    points={{64,-28},{60,-28},{60,-8}},
    color={153,204,0},
    thickness=0.5));
connect(statePoint2.sensorPort, compressor.portB) annotation (Line(
    points={{64,20},{60,20},{60,8}},
    color={153,204,0},
    thickness=0.5));
connect(statePoint3.sensorPort, condenser.portA_a) annotation (Line(
    points={{-36,36},{-36,32},{-14,32}},
    color={153,204,0},
    thickness=0.5));
connect(sensor_T_r4.port, fourWayValve.portB) annotation (Line(
    points={{-104,36},{-104,32},{-78,32}},
    color={153,204,0},
    thickness=0.5));
connect(statePoint4.sensorPort, fourWayValve.portB) annotation (Line(
    points={{-96,36},{-96,32},{-78,32}},
    color={153,204,0},
    thickness=0.5));
connect(statePoint5.sensorPort, pressureState_Sub.portB) annotation (Line(
    points={{-204,28},{-200,28},{-200,32},{-176,32}},
    color={153,204,0},
    thickness=0.5));
connect(sensor_T_r5.port, pressureState_Sub.portB) annotation (Line(
    points={{-204,20},{-200,20},{-200,32},{-176,32}},
    color={153,204,0},
    thickness=0.5));
connect(statePoint6.sensorPort, directionalControlValveAlt.portA) annotation (
   Line(
    points={{-194,-24},{-194,-20},{-178,-20}},
    color={153,204,0},
    thickness=0.5));
connect(sensor_T_r6.port, directionalControlValveAlt.portA) annotation (Line(
    points={{-186,-24},{-186,-20},{-178,-20}},
    color={153,204,0},
    thickness=0.5));
connect(statePoint7.sensorPort, fourWayValve.portC) annotation (Line(
    points={{-104,20},{-104,24},{-78,24}},
    color={153,204,0},
    thickness=0.5));
connect(sensor_T_r7.port, fourWayValve.portC) annotation (Line(
    points={{-96,20},{-96,24},{-78,24}},
    color={153,204,0},
    thickness=0.5));
connect(statePoint8.sensorPort, separator.portInlet) annotation (Line(
    points={{-54,-20},{-50,-20},{-50,-32},{-5,-32}},
    color={153,204,0},
    thickness=0.5));
```

```
  connect(sensor_T_r8.port, separator.portInlet) annotation (Line(
      points={{-54,-28},{-50,-28},{-50,-32},{-5,-32}},
      color={153,204,0},
      thickness=0.5));
  connect(pressureState5.portB, directionalControlValveAlt.portC) annotation (
      Line(
      points={{-168,0},{-170,0},{-170,-12}},
      color={153,204,0},
      thickness=0.5));
  connect(pressureState5.portA, tube1.portA) annotation (Line(
      points={{-164,0},{-162,0}},
      color={153,204,0},
      thickness=0.5));
  connect(tube1.portB, directionalControlValve.portC) annotation (Line(
      points={{-150,0},{-148,0}},
      color={153,204,0},
      thickness=0.5));
  connect(tube2.portB, fourWayValve.portC) annotation (Line(
      points={{-108,24},{-78,24}},
      color={153,204,0},
      thickness=0.5));
  connect(pressureState6.portA, tube2.portA) annotation (Line(
      points={{-122,24},{-120,24}},
      color={153,204,0},
      thickness=0.5));
  connect(pressureState6.portB, directionalControlValve.portA) annotation (Line(
      points={{-126,24},{-140,24},{-140,8}},
      color={153,204,0},
      thickness=0.5));
  annotation (Icon(coordinateSystem(preserveAspectRatio=false, extent={{-380,
          -100},{140,160}})),                                    Diagram(
        coordinateSystem(preserveAspectRatio=false, extent={{-380,-100},{140,
          160}})),
    experiment(
      StopTime=7776000,
      __Dymola_NumberOfIntervals=77760,
      __Dymola_Algorithm="Radau"));
end FlexHeatPump_V9;
```

Appendix 2 – Weather profiles

Historical weather profiles of ambient air temperature values for ten European locations recorded between December 2021 and February 2022:

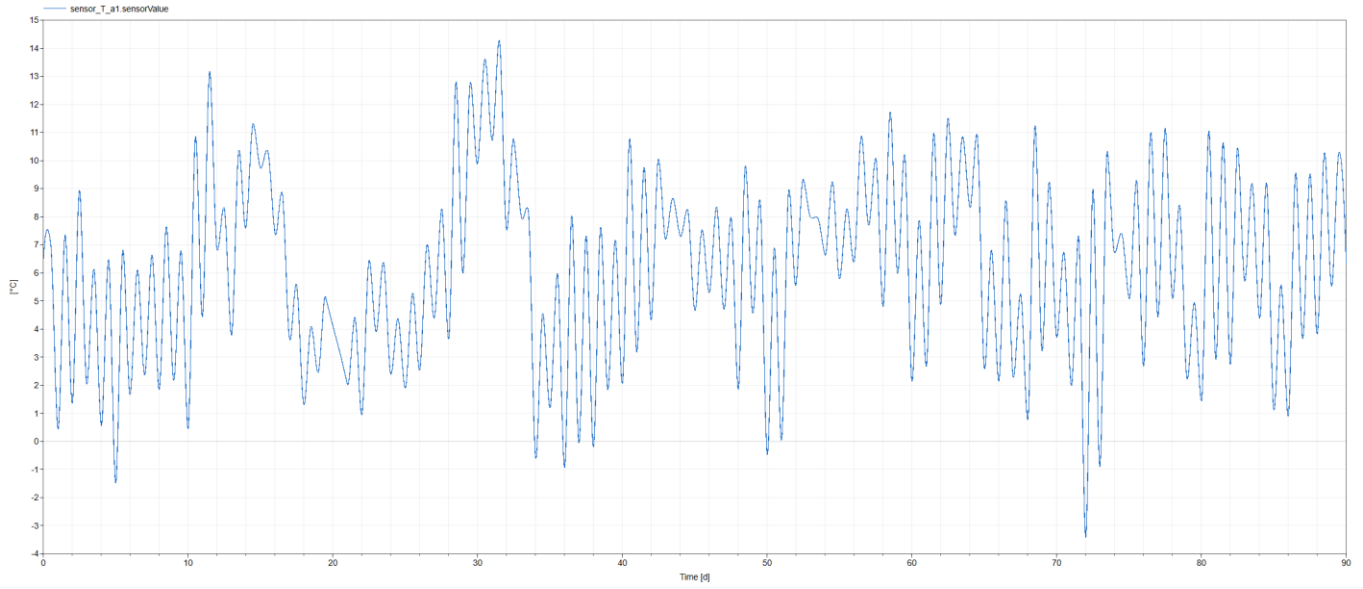

Weather profile for Glasgow, Scotland (Scotland West).

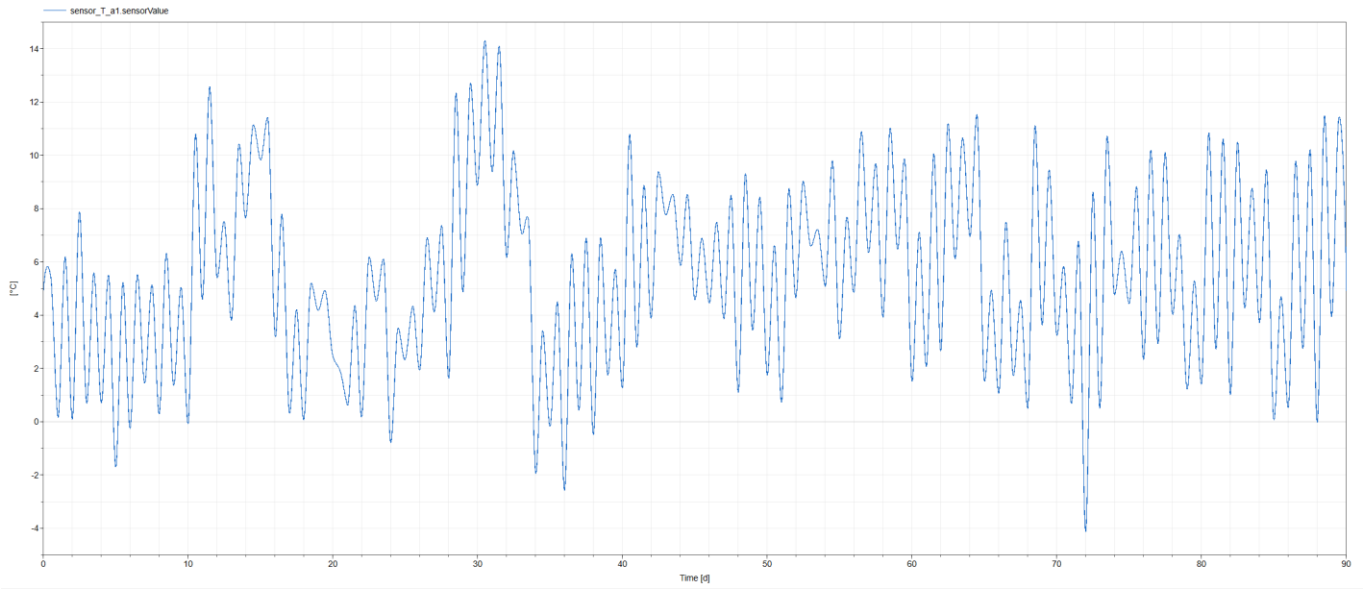

Weather profile for Edinburgh, Scotland (Scotland East).

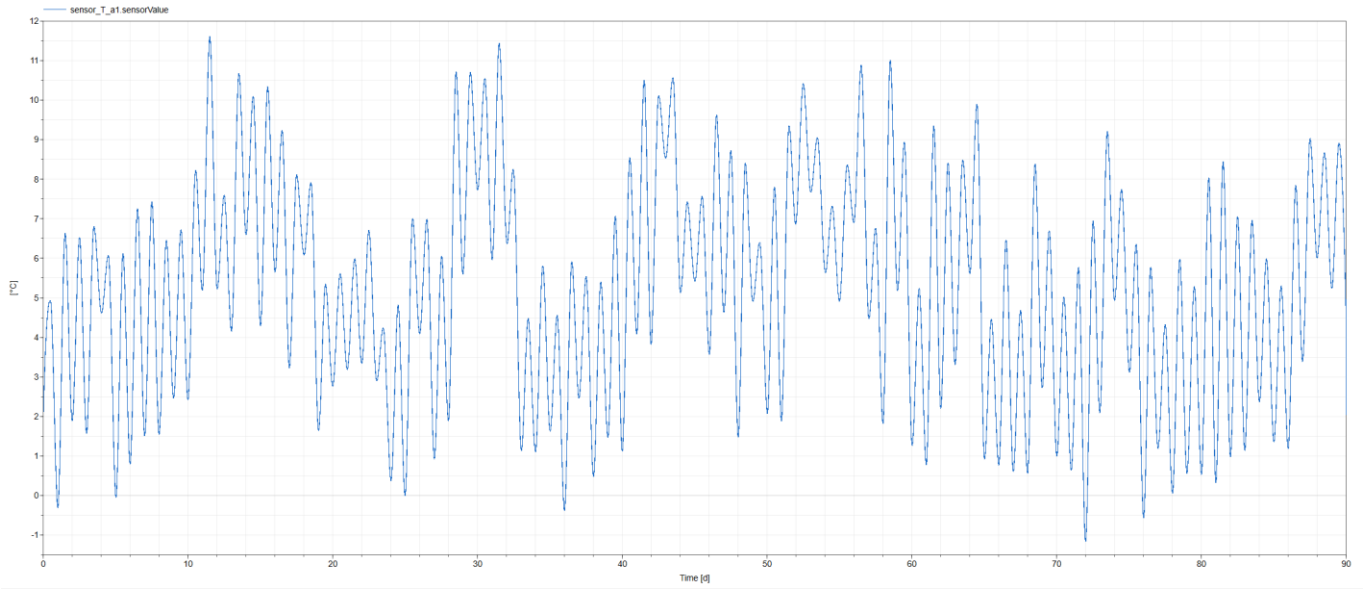

Weather profile for Kirkwall, Scotland (Scotland North).

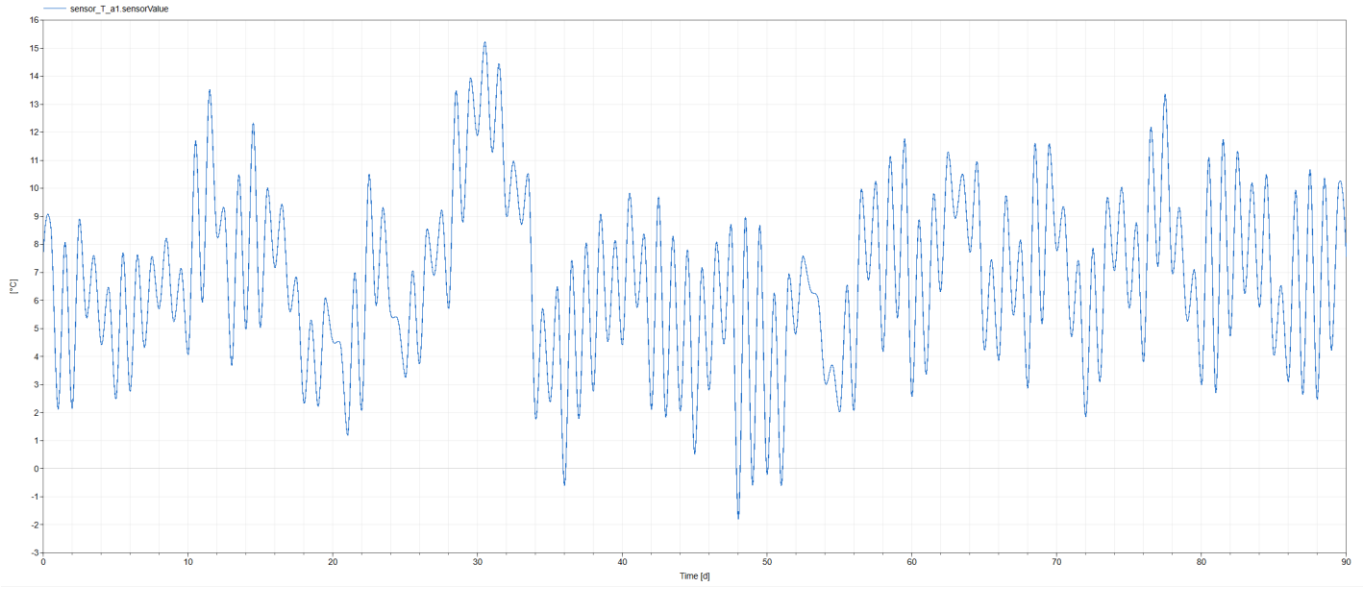

Weather profile for Liverpool, England (England Northwest).

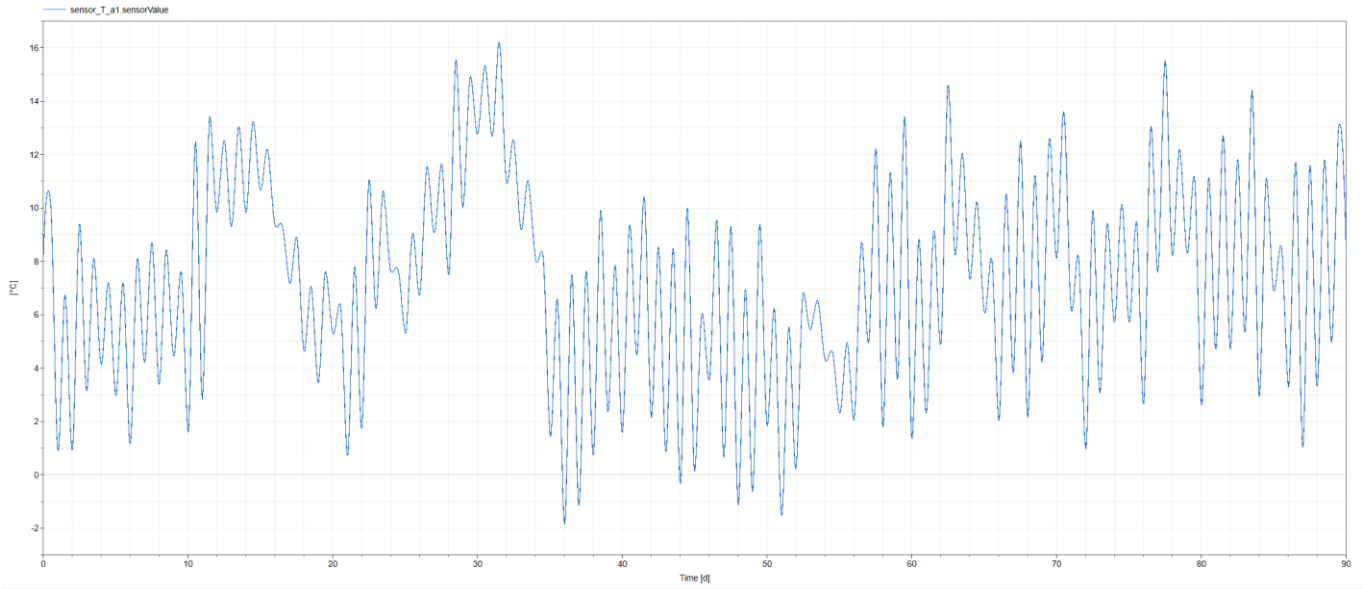

Weather profile for London, England (England Southeast).

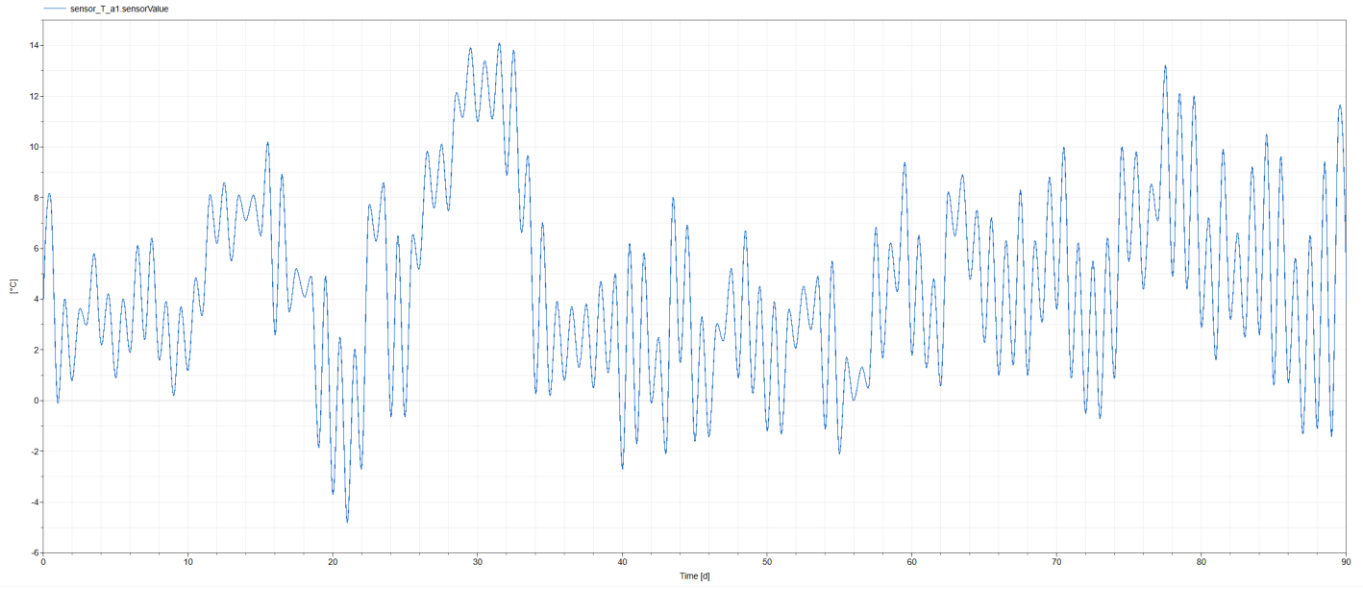

Weather profile for Aachen, Germany (Germany West).

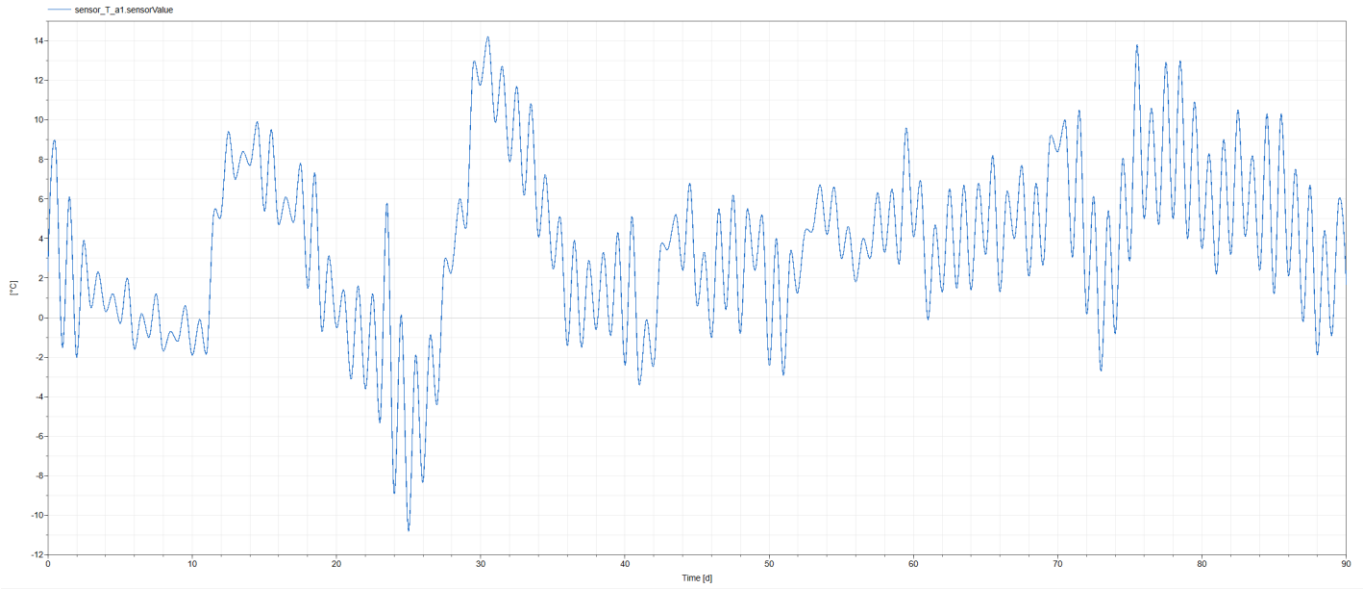

Weather profile for Berlin, Germany (Germany East).

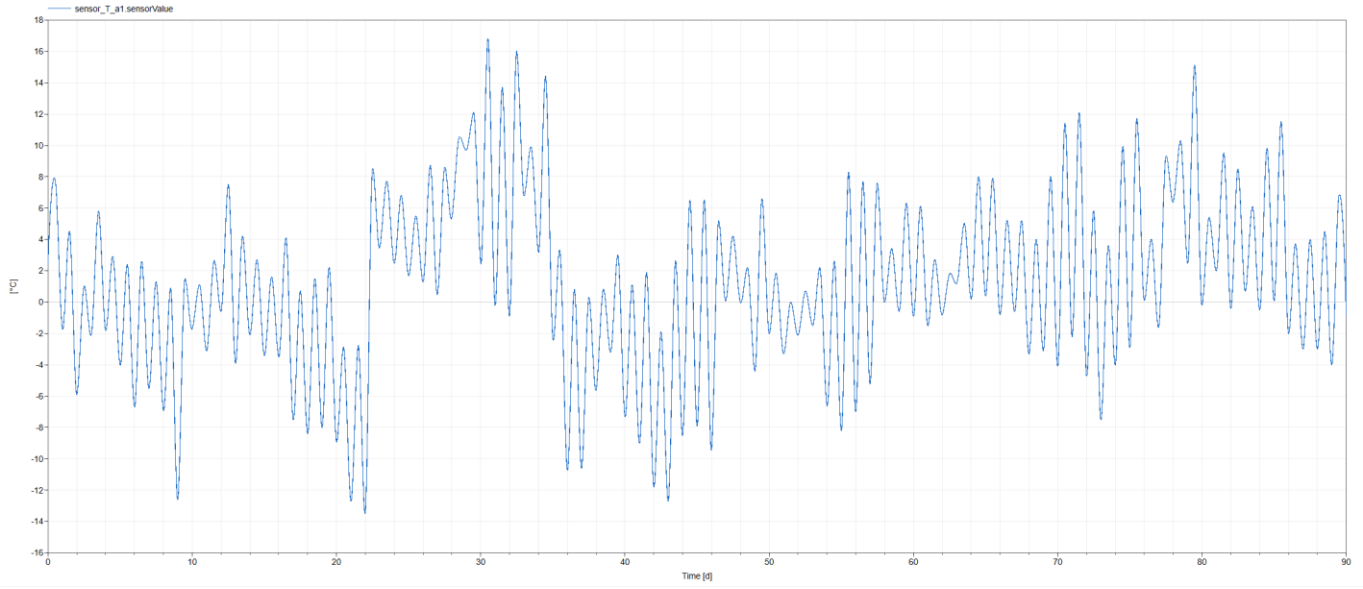

Weather profile for Kempten, Germany (Germany South).

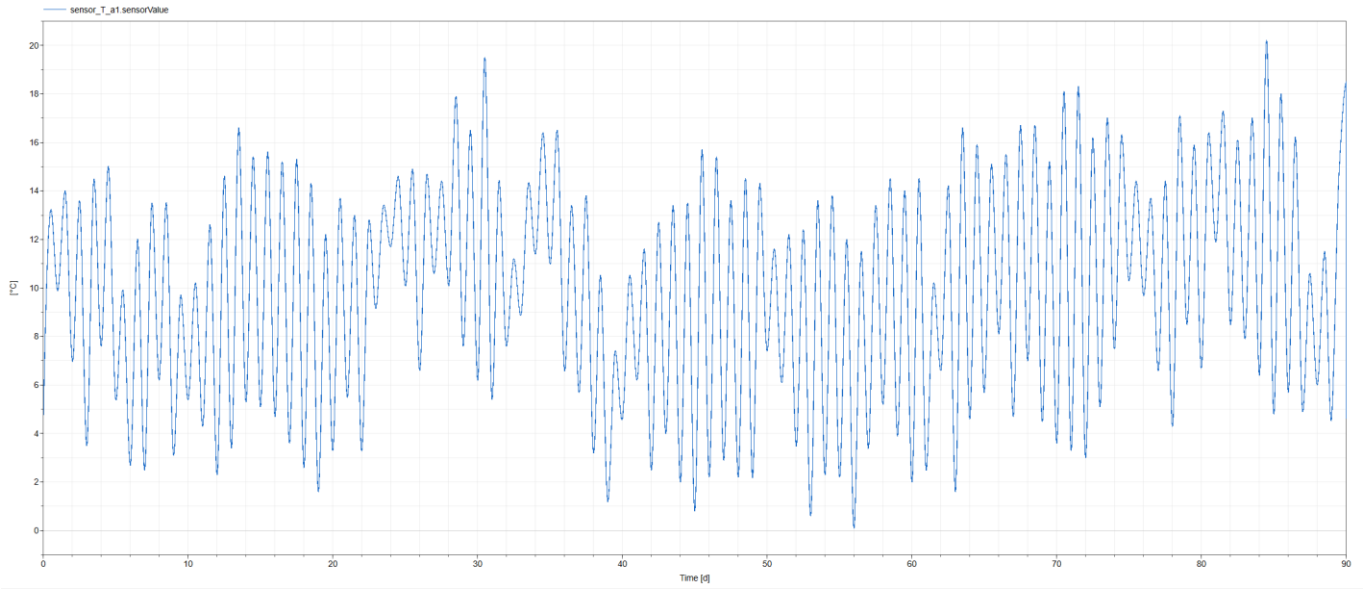

Weather profile for Rome, Italy (Italy West).

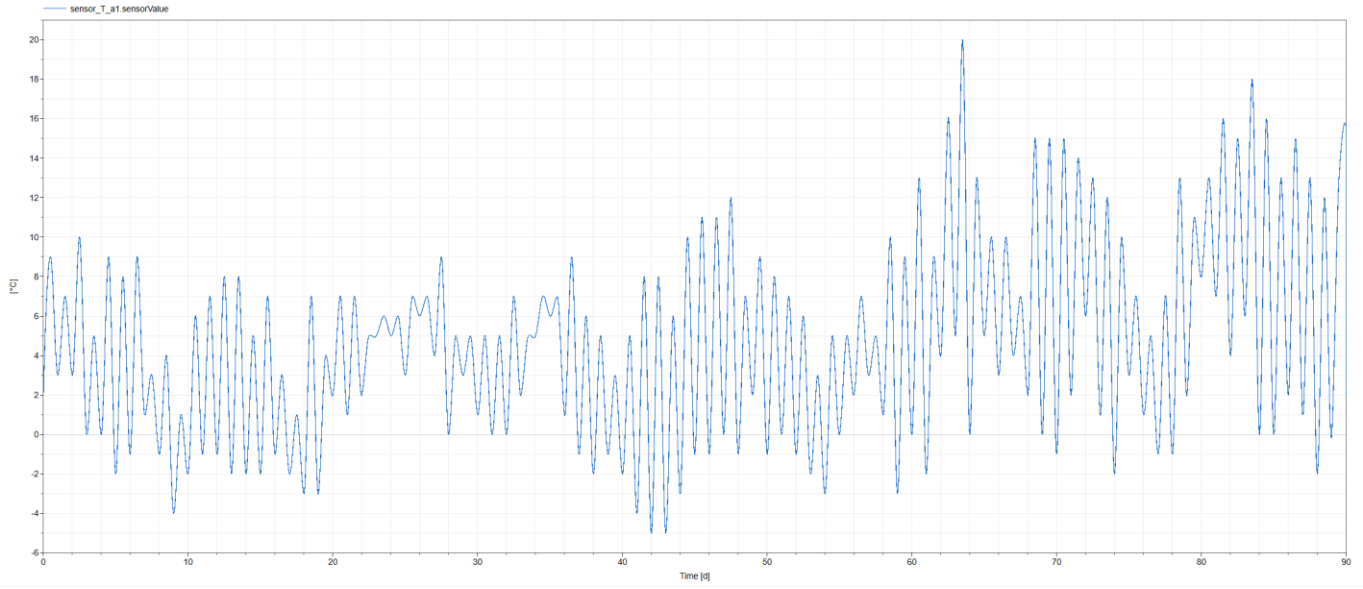

Weather profile for Parma, Italy (Italy North).

List of References

1. Agency, I.E. *Heat Pumps*. 2024; Available from: https://www.iea.org/energy-system/buildings/heat-pumps.
2. Ji, S., et al., *Application and Analysis of Air-Source Heat Pump Heat Supply System in Cold Areas*. Journal of Physics: Conference Series, 2022. **2186**(1). DOI: 10.1088/1742-6596/2186/1/012017.
3. Bertsch, S.S. and E.A. Groll, *Two-stage air-source heat pump for residential heating and cooling applications in northern U.S. climates*. International Journal of Refrigeration, 2008. **31**(7): p. 1282-1292. DOI: 10.1016/j.ijrefrig.2008.01.006.
4. Qu, M., et al., *Thermal energy storage based (TES-based) reverse cycle defrosting control strategy optimization for a cascade air source heat pump*. Energy and Buildings, 2020. **219**. DOI: 10.1016/j.enbuild.2020.110014.
5. Carroll, P., M. Chesser, and P. Lyons, *Air Source Heat Pumps field studies: A systematic literature review*. Renewable and Sustainable Energy Reviews, 2020. **134**. DOI: 10.1016/j.rser.2020.110275.
6. Li, Y., N. Zhang, and Z. Ding, *Investigation on the energy performance of using air-source heat pump to charge PCM storage tank*. Journal of Energy Storage, 2020. **28**. DOI: 10.1016/j.est.2020.101270.
7. Millar, Burnside, and Yu, *An Investigation into the Limitations of Low Temperature District Heating on Traditional Tenement Buildings in Scotland*. Energies, 2019. **12**(13). DOI: 10.3390/en12132603.
8. Ermel, C., et al., *Thermal storage integrated into air-source heat pumps to leverage building electrification: A systematic literature review*. Applied Thermal Engineering, 2022. **215**. DOI: 10.1016/j.applthermaleng.2022.118975.
9. Jin, X., et al., *Energy and economic performance of the heat pump integrated with latent heat thermal energy storage for peak demand shifting*. Applied Thermal Engineering, 2023. **218**. DOI: 10.1016/j.applthermaleng.2022.119337.
10. Roquet, M. and P. Dewallef, *A Model for Integrated Design of District Heating Networks*, in *37th International Conference on Efficiency, Cost, Optimization, Simulation and Environmental Impact of Energy Systems (ECOS 2024)*. 2024. p. 275-286. DOI: 10.52202/077185-0024.
11. Conte, R., et al., *The advantage of running a direct expansion CO2 heat pump with solar-and-air simultaneous heat sources: experimental and numerical investigation*. Applied Energy, 2024. **369**. DOI: 10.1016/j.apenergy.2024.123478.
12. Wang, W., Y. Li, and B. Hu, *Real-time efficiency optimization of a cascade heat pump system via multivariable extremum seeking*. Applied Thermal Engineering, 2020. **176**. DOI: 10.1016/j.applthermaleng.2020.115399.
13. Cui, C., et al., *Multi-variable extreme seeking control for efficient operation of sub-cooler vapor injection trans-critical CO2 heat pump water heater*. Applied Thermal Engineering, 2021. **184**. DOI: 10.1016/j.applthermaleng.2020.116261.
14. Rasmussen, B.P. and B. Shenoy, *Dynamic modeling for vapor compression systems—Part II: Simulation tutorial*. HVAC&R Research, 2012. **18**(5): p. 956-973. DOI: 10.1080/10789669.2011.582917.
15. Yu, Z., et al., *A flexible heat pump cycle for heat recovery*. Communications Engineering, 2022. **1**(1). DOI: 10.1038/s44172-022-00018-3.
16. Yu, Z., *A heat pump system*. 2022.
17. Essadik, M., et al., *A multi-valve flexible heat pump system with latent thermal energy storage for defrosting operation*. Energy and Buildings, 2024. **321**. DOI: 10.1016/j.enbuild.2024.114656.

18. Gou, X., et al., *Research on a Household Dual Heat Source Heat Pump Water Heater with Preheater Based on ASPEN PLUS*. Energies, 2016. **9**(12). DOI: 10.3390/en9121026.
19. Yang, L., et al., *Simulation and Economic Research of Circulating Cooling Water Waste Heat and Water Resource Recovery System*. Energies, 2021. **14**(9). DOI: 10.3390/en14092496.
20. Fritzson, P. and V. Engelson, *Modelica — A unified object-oriented language for system modeling and simulation*, in *ECOOP'98 — Object-Oriented Programming*. 1998. p. 67-90. DOI: https://doi.org/10.1007/BFb0054087.
21. Fritzson, P., *Modelica - A cyber-physical modeling language and the OpenModelica environment*, in *2011 7th International Wireless Communications and Mobile Computing Conference*. 2011. p. 1648-1653. DOI: 10.1109/iwcmc.2011.5982782.
22. Hinkelman, K., et al., *Modelica-based modeling and simulation of district cooling systems: A case study*. Applied Energy, 2022. **311**. DOI: 10.1016/j.apenergy.2022.118654.
23. Mattsson, S.E. and H. Elmqvist, *Modelica - An International Effort to Design the Next Generation Modeling Language*. IFAC Proceedings Volumes, 1997. **30**(4): p. 151-155. DOI: 10.1016/s1474-6670(17)43628-7.
24. Evens, M., A. Mugnini, and A. Arteconi, *Design energy flexibility characterisation of a heat pump and thermal energy storage in a Comfort and Climate Box*. Applied Thermal Engineering, 2022. **216**. DOI: 10.1016/j.applthermaleng.2022.119154.
25. Feghali, J.E., et al., *Electrical Grid Flexibility via Heat Pump and Thermal Storage Control*. IFAC-PapersOnLine, 2022. **55**(11): p. 84-89. DOI: 10.1016/j.ifacol.2022.08.053.
26. Abugabbara, M., et al., *Modelica-based simulations of decentralised substations to support decarbonisation of district heating and cooling*. Energy Reports, 2021. **7**: p. 465-472. DOI: 10.1016/j.egyr.2021.08.081.
27. Chamoun, M., et al., *Modelica-based modeling and simulation of a twin screw compressor for heat pump applications*. Applied Thermal Engineering, 2013. **58**(1-2): p. 479-489. DOI: 10.1016/j.applthermaleng.2013.04.020.
28. Ahrens, M.U., et al., *Numerical investigation of an oil-free liquid-injected screw compressor with ammonia-water as refrigerant for high temperature heat pump applications*. Applied Thermal Engineering, 2023. **219**. DOI: 10.1016/j.applthermaleng.2022.119425.
29. Systemes, D. *DYMOLA Systems Engineering: Multi-Engineering Modeling and Simulation based on Modelica and FMI*. Available from: https://www.3ds.com/products-services/catia/products/dymola/.
30. OpenModelica. *OpenModelica*. 2023; Available from: https://www.openmodelica.org/.
31. Adamson, K.-M., et al., *High-temperature and transcritical heat pump cycles and advancements: A review*. Renewable and Sustainable Energy Reviews, 2022. **167**. DOI: 10.1016/j.rser.2022.112798.
32. Programme, U.E. *The Montreal Protocol on Substances that Deplete the Ozone Layer*. Available from: https://www.unep.org/ozonaction/who-we-are/about-montreal-protocol.
33. Song, Y., et al., *Advanced development and application of transcritical CO2 refrigeration and heat pump technology—A review*. Energy Reports, 2022. **8**: p. 7840-7869. DOI: 10.1016/j.egyr.2022.05.233.
34. Tan, Z., et al., *Energy and economic performance comparison of heat pump and power cycle in low grade waste heat recovery*. Energy, 2022. **260**. DOI: 10.1016/j.energy.2022.125149.
35. Tan, Z., X. Feng, and Y. Wang, *Performance comparison of different heat pumps in low-temperature waste heat recovery*. Renewable and Sustainable Energy Reviews, 2021. **152**. DOI: 10.1016/j.rser.2021.111634.

36. Zhao, Z., et al., *Research on the Performance on Frost-Free Air Source Heat Pump with Waste Heat Desorption.* Journal of Physics: Conference Series, 2022. **2329**(1). DOI: 10.1088/1742-6596/2329/1/012029.
37. Agency, I.E. *Heat Pumps*. 2022; Available from: https://www.iea.org/reports/heat-pumps.
38. Wang, Z., et al., *Experimental investigation and seasonal performance assessment of a frost-free ASHP system with radiant floor heating.* Energy and Buildings, 2018. **179**: p. 200-212. DOI: 10.1016/j.enbuild.2018.09.019.
39. Wei, P., et al., *Frost suppression performance of an air source heat pump using sensible heat from indoor air to preheat outdoor air.* Building Services Engineering Research and Technology, 2023. **44**(5): p. 537-555. DOI: 10.1177/01436244231188708.
40. Spirito, G., et al., *Energy mapping and district heating as effective tools to decarbonize a city: Analysis of a case study in Northern Italy.* Energy Reports, 2021. **7**: p. 254-262. DOI: 10.1016/j.egyr.2021.08.147.
41. Gaur, A.S., D.Z. Fitiwi, and J. Curtis, *Heat pumps and our low-carbon future: A comprehensive review.* Energy Research & Social Science, 2021. **71**. DOI: 10.1016/j.erss.2020.101764.
42. Todorov, O., et al., *A method and analysis of aquifer thermal energy storage (ATES) system for district heating and cooling: A case study in Finland.* Sustainable Cities and Society, 2020. **53**. DOI: 10.1016/j.scs.2019.101977.
43. Scholliers, N., et al., *Identification of key factors for the sustainable integration of high-temperature aquifer thermal energy storage systems in district heating networks.* Smart Energy, 2024. **13**. DOI: 10.1016/j.segy.2024.100134.
44. Osterman, E. and U. Stritih, *Review on compression heat pump systems with thermal energy storage for heating and cooling of buildings.* Journal of Energy Storage, 2021. **39**. DOI: 10.1016/j.est.2021.102569.
45. Vasilyev, G.P., et al., *Geothermal heat pump systems in cold regions: efficiency improvement by use of ambient air.* IOP Conference Series: Earth and Environmental Science, 2019. **367**(1). DOI: 10.1088/1755-1315/367/1/012010.
46. Sazon, T.A. and H. Nikpey, *Modeling and investigation of the performance of a solar-assisted ground-coupled CO2 heat pump for space and water heating.* Applied Thermal Engineering, 2024. **236**. DOI: 10.1016/j.applthermaleng.2023.121546.
47. Zhu, N., et al., *Recent research and applications of ground source heat pump integrated with thermal energy storage systems: A review.* Applied Thermal Engineering, 2014. **71**(1): p. 142-151. DOI: 10.1016/j.applthermaleng.2014.06.040.
48. Sangi, R. and D. Müller, *Dynamic modelling and simulation of a slinky-coil horizontal ground heat exchanger using Modelica.* Journal of Building Engineering, 2018. **16**: p. 159-168. DOI: 10.1016/j.jobe.2018.01.005.
49. Wei, W., et al., *Optimal Borehole Energy Storage Charging Strategy in a Low Carbon Space Heat System.* IEEE Access, 2018. **6**: p. 76176-76186. DOI: 10.1109/access.2018.2883798.
50. Ekmekci, E., et al., *Very high temperature BTES: A potential for operationally cost-free and emission-free heating.* Applied Energy, 2024. **360**. DOI: 10.1016/j.apenergy.2024.122859.
51. Zhang, Q., et al., *Techno-economic analysis of a biogas-fueled micro gas turbine cogeneration system with seasonal thermal energy storage.* Energy Conversion and Management, 2023. **292**. DOI: 10.1016/j.enconman.2023.117407.
52. Liang, C.-h., et al., *Study on the performance of a solar assisted air source heat pump system for building heating.* Energy and Buildings, 2011. **43**(9): p. 2188-2196. DOI: 10.1016/j.enbuild.2011.04.028.
53. Chen, Y., et al., *Dynamic modeling of solar-assisted ground source heat pump using Modelica.* Applied Thermal Engineering, 2021. **196**. DOI: 10.1016/j.applthermaleng.2021.117324.

54. Abdelsalam, M.Y., et al., *Hybrid thermal energy storage with phase change materials for solar domestic hot water applications: Direct versus indirect heat exchange systems.* Renewable Energy, 2020. **147**: p. 77-88. DOI: 10.1016/j.renene.2019.08.121.
55. Sazon, T.A., Q. Zhang, and H. Nikpey, *Multi-Objective Optimization of a Solar-Assisted Ground-Source CO2 Heat Pump System for Space and Water Heating Using the Taguchi Method and Utility Concept*, in *36th International Conference on Efficiency, Cost, Optimization, Simulation and Environmental Impact of Energy Systems (ECOS 2023)*. 2023. p. 769-780. DOI: 10.52202/069564-0070.
56. Kazem, H.A., et al., *A systematic review of photovoltaic/thermal applications in heat pumps systems.* Solar Energy, 2024. **269**. DOI: 10.1016/j.solener.2023.112299.
57. Bai, J., et al., *Experimental study on high temperature heat pump system with a double heat source cascade.* Thermal Science, 2023. **27**(3 Part A): p. 1845-1853. DOI: 10.2298/tsci2303845b.
58. Wang, Z., et al., *Experimental investigation on thermal characteristics of transcritical CO2 heat pump unit combined with thermal energy storage for residential heating.* Applied Thermal Engineering, 2020. **165**. DOI: 10.1016/j.applthermaleng.2019.114505.
59. Wang, Z., et al., *Performance investigation of a transcritical CO2 heat pump combined with the terminal of radiator and floor radiant coil for space heating in different climates, China.* Journal of Building Engineering, 2021. **44**. DOI: 10.1016/j.jobe.2021.102927.
60. Zhang, D., et al., *Performance study of transcritical CO2 heat pump integrated with ejector and latent thermal energy storage for space heating.* Energy Conversion and Management, 2022. **268**. DOI: 10.1016/j.enconman.2022.115979.
61. Wang, Z., et al., *Study on performance evaluation of CO2 heat pump system integrated with thermal energy storage for space heating.* Energy Procedia, 2019. **158**: p. 1380-1387. DOI: 10.1016/j.egypro.2019.01.338.
62. Javanshir, N., et al., *Abandoning peat in a city district heat system with wind power, heat pumps, and heat storage.* Energy Reports, 2022. **8**: p. 3051-3062. DOI: 10.1016/j.egyr.2022.02.064.
63. Rehman, O.A., et al., *Numerical and Experimental Analysis of a Low-GWP Heat Pump Coupled to Electrical and Thermal Energy Storage to Increase the Share of Renewables across Europe.* Sustainability, 2023. **15**(6). DOI: 10.3390/su15064973.
64. Rotas, R., et al., *Dynamic Simulation and Performance Enhancement Analysis of a Renewable Driven Trigeneration System.* Energies, 2022. **15**(10). DOI: 10.3390/en15103688.
65. Descamps, M.N., et al., *Performance assessment of a multi-source heat production system with storage for district heating*, in *Energy Procedia*. 2018. p. 390-399. DOI: 10.1016/j.egypro.2018.08.203.
66. Zanetti, E., et al., *Experimental and numerical analysis of a CO2 dual-source heat pump with PVT evaporators for residential heating applications.* Applied Thermal Engineering, 2023. **233**. DOI: 10.1016/j.applthermaleng.2023.121165.
67. Jradi, M., C. Veje, and B.N. Jørgensen, *Performance analysis of a soil-based thermal energy storage system using solar-driven air-source heat pump for Danish buildings sector.* Applied Thermal Engineering, 2017. **114**: p. 360-373. DOI: 10.1016/j.applthermaleng.2016.12.005.
68. Violidakis, I., et al., *Dynamic modeling and energy analysis of renewable heating and electricity systems at residential buildings using phase change material based heat storage technologies.* Journal of Energy Storage, 2020. **32**. DOI: 10.1016/j.est.2020.101942.
69. Wang, W., et al., *Performance improvement of air-source heat pump heating system with variable water temperature difference.* Applied Thermal Engineering, 2022. **210**. DOI: 10.1016/j.applthermaleng.2022.118366.

70. Arteconi, A., N.J. Hewitt, and F. Polonara, *Domestic demand-side management (DSM): Role of heat pumps and thermal energy storage (TES) systems.* Applied Thermal Engineering, 2013. **51**(1-2): p. 155-165. DOI: 10.1016/j.applthermaleng.2012.09.023.
71. Arteconi, A., N.J. Hewitt, and F. Polonara, *State of the art of thermal storage for demand-side management.* Applied Energy, 2012. **93**: p. 371-389. DOI: 10.1016/j.apenergy.2011.12.045.
72. Huang, R., et al., *Evaluation of phase change thermal storage in a cascade heat pump.* Applied Energy, 2024. **359**. DOI: 10.1016/j.apenergy.2024.122654.
73. Inkeri, E., T. Tynjälä, and M. Nikku, *Numerical modeling of latent heat thermal energy storage integrated with heat pump for domestic hot water production.* Applied Thermal Engineering, 2022. **214**. DOI: 10.1016/j.applthermaleng.2022.118819.
74. Agyenim, F. and N. Hewitt, *The development of a finned phase change material (PCM) storage system to take advantage of off-peak electricity tariff for improvement in cost of heat pump operation.* Energy and Buildings, 2010. **42**(9): p. 1552-1560. DOI: 10.1016/j.enbuild.2010.03.027.
75. Lu, S., et al., *Performance study and heating simulation on novel latent heat thermal energy storage device suit for air source heat pump.* Journal of Energy Storage, 2023. **65**. DOI: 10.1016/j.est.2023.107259.
76. Lin, Y., et al., *Performance investigation on an air source heat pump system with latent heat thermal energy storage.* Energy, 2022. **239**. DOI: 10.1016/j.energy.2021.121898.
77. Wang, Y., et al., *Energy and exergy analysis of a novel dual-source heat pump system with integrated phase change energy storage.* Renewable Energy, 2024. **222**. DOI: 10.1016/j.renene.2023.119905.
78. Cabrol, L. and P. Rowley, *Towards low carbon homes – A simulation analysis of building-integrated air-source heat pump systems.* Energy and Buildings, 2012. **48**: p. 127-136. DOI: 10.1016/j.enbuild.2012.01.019.
79. Zhou, C., et al., *A Review of the Performance Improvement Methods of Phase Change Materials: Application for the Heat Pump Heating System.* Energies, 2023. **16**(6). DOI: 10.3390/en16062676.
80. Hirmiz, R., et al., *Performance of heat pump integrated phase change material thermal storage for electric load shifting in building demand side management.* Energy and Buildings, 2019. **190**: p. 103-118. DOI: 10.1016/j.enbuild.2019.02.026.
81. Kelly, N.J., P.G. Tuohy, and A.D. Hawkes, *Performance assessment of tariff-based air source heat pump load shifting in a UK detached dwelling featuring phase change-enhanced buffering.* Applied Thermal Engineering, 2014. **71**(2): p. 809-820. DOI: 10.1016/j.applthermaleng.2013.12.019.
82. Yıldız, Ç., et al., *An experimental study on a solar-assisted heat pump incorporated with PCM based thermal energy storage unit.* Energy, 2023. **278**. DOI: 10.1016/j.energy.2023.128035.
83. Olympios, A.V., et al., *Operational optimisation of an air-source heat pump system with thermal energy storage for domestic applications.* Energy Conversion and Management, 2022. **273**. DOI: 10.1016/j.enconman.2022.116426.
84. Kocher, J.D., et al., *Thermal battery cost scaling analysis: minimizing the cost per kW h.* Energy & Environmental Science, 2024. **17**(6): p. 2206-2218. DOI: 10.1039/d3ee03594h.
85. Bloess, A., W.-P. Schill, and A. Zerrahn, *Power-to-heat for renewable energy integration: A review of technologies, modeling approaches, and flexibility potentials.* Applied Energy, 2018. **212**: p. 1611-1626. DOI: 10.1016/j.apenergy.2017.12.073.
86. Hedegaard, K. and O. Balyk, *Energy system investment model incorporating heat pumps with thermal storage in buildings and buffer tanks.* Energy, 2013. **63**: p. 356-365. DOI: 10.1016/j.energy.2013.09.061.

87. Hedegaard, K., et al., *Wind power integration using individual heat pumps – Analysis of different heat storage options.* Energy, 2012. **47**(1): p. 284-293. DOI: 10.1016/j.energy.2012.09.030.
88. Reynders, G., T. Nuytten, and D. Saelens, *Potential of structural thermal mass for demand-side management in dwellings.* Building and Environment, 2013. **64**: p. 187-199. DOI: 10.1016/j.buildenv.2013.03.010.
89. Wang, Y., J. Wang, and W. He, *Development of efficient, flexible and affordable heat pumps for supporting heat and power decarbonisation in the UK and beyond: Review and perspectives.* Renewable and Sustainable Energy Reviews, 2022. **154**. DOI: 10.1016/j.rser.2021.111747.
90. Technica, C. *Thermal Systems Library & TIL Suite*. Available from: https://www.claytex.com/products/dymola/model-libraries/thermal-systems-library/.
91. GmbH, T.-T. *TIL Suite*. 2023; Available from: https://www.tlk-thermo.com/en/software/til-suite.
92. Thomas, B. and W. Dietmar, *Efficient Parameterization of Modelica Models*, in *Proceedings of 14th Modelica Conference 2021, Linköping, Sweden, September 20-24, 2021*. 2021. p. 141-146. DOI: 10.3384/ecp21181141.
93. libraries, M.r.-p. *ExternData GitHub Repository*. 2015; Available from: https://github.com/modelica-3rdparty/ExternData.
94. VEVOR, *User Manual - VEVOR Heat Exchanger Model:C16×16*. 2025.
95. SWEP, *Product Sheet - SWEP B8LAS*. 2022.
96. Solutions, A.C., *Data Sheet - Compressor hermetic rotary GMCC EDTN210D32EFZ*. 2025.
97. Sadia, H., *Data Sheet - Heatrae Sadia Megaflo Eco Indirect*. 2025.
98. Hollis, D., et al., *HadUK-Grid—A new UK dataset of gridded climate observations.* Geoscience Data Journal, 2019. **6**(2): p. 151-159. DOI: 10.1002/gdj3.78.
99. Hollis, D., et al., *HadUK-Grid Gridded Climate Observations on a 1km grid over the UK, v1.3.0.ceda (1836-2023)*, M. Office, Editor. 2024: CEDA Archive. DOI: https://doi.org/10.5285/b963ead70580451aa7455782224479d5.
100. Agency, E.S. *ESA SNAP*. Available from: https://step.esa.int/main/toolboxes/snap/.
101. Wetterdienst, D. *DWD - Deutscher Wetterdienst*. 2025; Available from: https://www.dwd.de/EN/Home/home_node.html.
102. Climatici, S.N.p.l.E.e.D.d.D. *SCIA - National System for the Processing and Dissemination of Climate Data*. 2025; Available from: https://scia.isprambiente.it/.
103. Wetterdienst, D., *CDC Daily station observations of temperature at 2 m above ground*, D. Wetterdienst, Editor. 2025: CDC Climate Data Center.
104. Climatici, S.N.p.l.E.e.D.d.D., *SCIA Daily regional station observations of temperature*, S.N.p.l.E.e.D.d.D. Climatici, Editor. 2025: Sistema Nazionale per l'Elaborazione e Diffusione di Dati Climatici.
105. Lyu, W., et al., *Influence of the water tank size and air source heat pump size on the energy saving potential of the energy storage heating system.* Journal of Energy Storage, 2022. **55**. DOI: 10.1016/j.est.2022.105542.